AD640945

AD

USAAVLABS TECHNICAL REPORT 66-53

AN ANALYTICAL STUDY OF FACTORS INFLUENCING THE LONGITUDINAL STABILITY OF TILT-WING VTOL AIRCRAFT

By

G. Beppu

H. C. Curtiss, Jr.

CLEARINGHOUSE
FOR FEDERAL SCIENTIFIC AND
TECHNICAL INFORMATION

Hardcopy	Microfiche	
$4.00	$0.75	108 pp

ARCHIVE COPY

Code 1

July 1966

U. S. ARMY AVIATION MATERIEL LABORATORIES
FORT EUSTIS, VIRGINIA

CONTRACT DA 44-177-AMC-8(T)
PRINCETON UNIVERSITY
PRINCETON, NEW JERSEY

Distribution of this document is unlimited

DDC
RECEIVED
OCT 31 1966
C

DEPARTMENT OF THE ARMY
U. S. ARMY AVIATION MATERIEL LABORATORIES
FORT EUSTIS, VIRGINIA 23604

This report has been reviewed by this Command and is considered to be technically sound. This work, which was performed under Contract DA 44-177-AMC-8(T), was undertaken to develop an analytical method for predicting the longitudinal stability characteristics and to compare these results with experimental data from a four-propeller tilt-wing V/STOL aircraft tested on the Princeton Dynamic Model Track.

Task 1P125901A14233
Contract DA 44-177-AMC-8(T)
USAAVLABS Technical Report 66-53
July 1966

AN ANALYTICAL STUDY OF FACTORS INFLUENCING THE LONGITUDINAL STABILITY OF TILT-WING VTOL AIRCRAFT

Report No. 756

by

G. Beppu and H. C. Curtiss, Jr.

Prepared by

Department of Aerospace and Mechanical Sciences
Princeton University
Princeton, New Jersey

for

U. S. ARMY AVIATION MATERIEL LABORATORIES
FORT EUSTIS, VIRGINIA

Distribution of this document is unlimited

SUMMARY

An analytical method for predicting the stability characteristics of tilt-wing VTOL aircraft in the transition speed range is presented. Sample calculations based on an assumed tilt-wing VTOL transport configuration of the XC-142A class with double slotted flaps are given.

Particular emphasis is placed on the sensitivity of the results to various assumptions made in the analysis. The contributions of the various aircraft components and the aerodynamic interactions of the components to the stability derivatives are discussed, as well as the changes in the characteristic modes of motion of the vehicle that result from variations in the stability derivatives.

The trim conditions of the vehicle are shown to be quite sensitive to the prediction of the flap characteristics.

A limited comparison of the calculated results with experimental data obtained from a dynamic model of the XC-142A, which is somewhat dissimilar from the assumed configuration, is presented. This comparison indicates that the trends of the stability derivatives are correctly predicted. The agreement between theory and experiment is good in hovering; however, as the wing incidence is reduced, the difference between theory and experiment becomes quite large.

FOREWORD

This research was performed by the Department of Aerospace and Mechanical Sciences, Princeton University, under the sponsorship of the United States Army Aviation Materiel Laboratories Contract DA 44-177-AMC-8(T), with financial support from the United States Navy, Bureau of Weapons, and the United States Air Force Flight Dynamics Laboratory of the Research and Technology Division. The research was monitored by Mr. William E. Sickles of the United States Army Aviation Materiel Laboratories.

The research was conducted by G. Beppu and Assistant Professor H. C. Curtiss, Jr., of Princeton University.

TABLE OF CONTENTS

LIST OF FIGURES

LIST OF SYMBOLS

A	Propeller disc area (189 square feet)
A_T	Tail rotor disc area (50.2 square feet)
AR	Wing aspect ratio (8.53)
a	Propeller blade lift curve slope (5.73 per radian)
a.c.	Aerodynamic center
b	Number of blades (4)
b_w	Wing span (67.5 feet)
c	Blade chord (feet)
c.g.	Center of gravity
C_{D_o}	Drag coefficient at zero lift
C_{D,S_o}	Drag coefficient at zero lift, based on the slipstream velocity
$C_{L,S_{\alpha_e}}$	Wing lift curve slope in slipstream, based on slipstream velocity and effective angle of attack (per radian)
C_{L_α}	Wing lift curve slope in a uniform free stream (per radian)
$C_{L_{\alpha_T}}$	Lift curve slope of horizontal tail (per radian)
C_{L_T}	Lift coefficient of horizontal tail
C_T	Thrust coefficient, $C_T = \dfrac{T}{\rho \pi R^2 (\Omega R)^2}$
$C_{T,S}$	Thrust coefficient, $C_{T,S} = \dfrac{T/A}{q + T/A}$
D_f	Fuselage drag parallel to free stream (pounds)
D_s	Wing drag, parallel to slipstream velocity (pounds)

D_T Drag of horizontal tail (pounds)

f Equivalent flat plate area of fuselage (5.0 square feet)

H Inplane force of the propeller (pounds)

I Moment of inertia of the airplane about Y-axis (100,000 slug-feet squared)

i_t Horizontal tail incidence angle, measured from fuselage reference line (radians)

i_w Wing incidence, measured from fuselage reference line (radians or degrees)

K Correction factor for wing lift curve slope in slipstream (0.5)

K_f Fuselage moment factor (0.83)

L_s Wing lift, perpendicular to slipstream velocity, V_R (pounds)

L_T Horizontal tail lift (pounds)

$\ell_H, \ell_{HT}, \ell_{TR}, \ell_{OP}, \ell_P, \ell_{OW}, \ell_W$ Various geometric distances from center of gravity (Figure A-1b) (feet)

M Pitching moment, nose up positive (foot-pounds)

M_f Fuselage pitching moment (foot-pounds)

M_T Downwash reduction factor, nondimensional (Equation 16)

M_{ID} Propeller pitching moment due to inflow distribution arising from a pitching velocity (foot-pounds)

M_{PD} Propeller pitching moment due to induced velocity distribution across propeller disc (foot-pounds)

$M_u, M_w, M_{\dot{\theta}}$ Stability derivatives

$$M_u = \frac{1}{I}\frac{\partial M}{\partial u}, \qquad M_w = \frac{1}{I}\frac{\partial M}{\partial w}, \qquad M_{\dot{\theta}} = \frac{1}{I}\frac{\partial M}{\partial \dot{\theta}}$$

m Mass of airplane (slugs)

N	Number of propellers (4)
q	Free stream dynamic pressure (pounds per square foot)
r	Radius of blade element from axis of rotation (feet)
R	Propeller radius (7.75 feet)
R_T	Tail rotor radius (4 feet)
S	Wing area (534 square feet)
S_T	Horizontal tail area (140 square feet)
T	Propeller thrust (pounds)
T_T	Tail rotor thrust (pounds)
u	Horizontal velocity perturbation (feet per second)
V	Flight velocity (feet per second)
V_R	Slipstream velocity (feet per second)
v	Propeller induced velocity (feet per second)
v_o	Average value of propeller induced velocity (feet per second)
v_1	Slope of propeller induced velocity with nondimensional radius (Equation 3) (feet per second)
v_T	Tail rotor induced velocity (feet per second)
W	Gross weight of aircraft (37,350 pounds)
w	Vertical velocity, downward motion of the aircraft is positive (feet per second)
X	Longitudinal force, positive forward (pounds)
X_f	Longitudinal force due to fuselage, positive forward (pounds)
X_u, X_w	Stability derivatives

$$X_u = \frac{1}{m}\frac{\partial X}{\partial u} \quad , \qquad X_w = \frac{1}{m}\frac{\partial X}{\partial w}$$

Z Vertical force, positive downward (pounds)

Z_u, Z_w Stability derivatives

$$Z_u = \frac{1}{m}\frac{\partial Z}{\partial u} \quad , \quad Z_w = \frac{1}{m}\frac{\partial Z}{\partial w}$$

α Angle of attack of the fuselage (radians or degrees)

α_o Angle of attack for zero lift of the wing (radians or degrees)

α_e Effective wing angle of attack in slipstream (Equation 11) (radians)

δ_f Flap deflection angle (radians or degrees)

δ Blade section profile drag coefficient of the propeller (0.016)

δ_T Blade section profile drag coefficient of the tail rotor (0.016)

ϵ Downwash angle (radians)

ϵ_P Propeller downwash angle at tail, $\epsilon_p = (i_w + \alpha - \alpha_e)$ (radians)

ϵ_T Downwash angle at the tail rotor due to horizontal tail lift (radians)

θ Aircraft pitch angle, positive nose up (radians)

$\theta_{0.75R}$ Propeller blade pitch angle at 0.75R (radians)

$\theta_{0.75R_T}$ Tail rotor blade pitch angle at 0.75R (radians)

λ_i Nondimensional induced velocity of the propeller $\lambda_i = \frac{v}{\Omega R}$ (always positive)

λ_{i_T} Nondimensional induced velocity of the tail rotor $\lambda_{i_T} = \left(\frac{v}{\Omega R}\right)_T$ (always positive)

μ Nondimensional velocity parallel to the propeller plane

$$\mu = \frac{V \sin(i_w + \alpha)}{\Omega R} \text{ or, using Equation 11, } \mu = \frac{V_R \sin \alpha_e}{\Omega R}$$

μ_T Nondimensional velocity parallel to the plane of the tail rotor

$$\mu_T = \frac{V \cos \alpha}{(\Omega R)_T}$$

ν Nondimensional velocity perpendicular to the propeller plane $\nu = \dfrac{V \cos(i_w + \alpha)}{\Omega R}$

ν_T Nondimensional velocity perpendicular to the plane of the tail rotor $\nu_T = \dfrac{V \sin \alpha}{(\Omega R)_T}$

σ Solidity of main propeller $\sigma = \dfrac{bc}{\pi R}$, (0.153)

σ_T Solidity of the tail rotor (0.124)

ρ Air density (slugs per cubic foot)

Ω Rotational velocity of the propeller (129 radians per second)

Ω_T Rotational velocity of the tail rotor (363.4 radians per second)

ξ $\xi = \sqrt{(\lambda_i + \nu)^2 + \mu^2}$ nondimensional velocity at propeller plane

Ψ Propeller blade azimuth angle (measured from downwind position)

η_T Tail efficiency factor $\left(\dfrac{q_T}{q}\right)$

ADDITIONAL NOTATION

$( )_{HT}$ Horizontal tail

$( )_T$ Tail rotor

$(\dot{})$ Derivative with respect to time

$( )_o$ Initial value

BLANK PAGE

INTRODUCTION

The analytical prediction of the stability and control characteristics of tilt-wing VTOL aircraft at high wing incidences with correspondingly low forward speeds presents a number of difficulties. The first is the algebraic complexity of the expressions obtained for the stability derivatives, arising from the numerous components and aerodynamic interactions that contribute to the aerodynamic forces acting on the vehicle. A second and more important difficulty is associated with the lack of suitable aerodynamic data available on the various components for stability and control analysis. In addition, the nature of the flow fields involved makes theoretical results difficult to apply since simple closed-form expressions are generally not available.

The algebraic complexity may be circumvented by the use of high-speed digital computing equipment. However, the importance of the sensitivity of the results of an analysis to various assumptions made during the course of the analysis becomes clouded by the length of the analytical expressions used.

The objective of this study is to clarify the aerodynamic interactions entering into the stability calculations and to determine their significance to the prediction of the stability characteristics of the aircraft.

The approach presented here is analytical. A simplified mathematical model of the propeller and the wing-slipstream interaction is used to predict the trim conditions and the stability derivatives of an assumed tilt-wing VTOL. The results are compared where possible with experimental data taken on a 0.10 scale dynamic model of the XC-142A. The experiments were conducted on the Princeton Dynamic Model Track. The test set-up and the model are described in Appendix A.

The major contributions to each stability derivative are analyzed, and the significant effects are discussed for level flight trim conditions.

The report consists of the following parts. In the section entitled Method of Analysis and Assumptions, the mathematical models used for the various components of the vehicle and the assumptions involved are described. In the next section, the trim calculations are discussed, and in particular the importance of accurately predicting the aerodynamic characteristics of flaps is discussed. The next section discusses the stability derivatives themselves and the important contributing factors to the stability derivatives. Then, the sensitivity of the modes of motion of the vehicle to variations in the stability derivatives is discussed. Finally, a comparison of the analytical results with experimental data is discussed.

METHOD OF ANALYSIS AND ASSUMPTIONS

Other methods of approach to tilt-wing stability and control are presented in References 1, 2 and 3. References 1 and 2 are based primarily on experimental data, and only certain aspects of the problem are treated analytically. The analysis presented in Reference 3 is quite similar to that presented in this report but with two exceptions. The airplane configuration investigated in Reference 3 had flapping propellers, while in this investigation a conventional (rigid) propeller is considered. In addition, in Reference 3, a rather extreme analytical model was taken for the wing characteristics to include the effects of wing stall. In the following, it is assumed that the use of flaps prevents wing stall and no variation in wing lift curve slope with effective wing angle of attack is included. This should not be an important limitation on the analysis since large areas of separated flow on the wing must be avoided in this type of aircraft in order to obtain satisfactory flying qualities (Reference 9).

The sample calculations in this report are based on a typical four-propeller tilt-wing VTOL configuration. The physical parameters of the vehicle are given in Appendix A. Simplifying assumptions are used wherever possible, and are discussed in detail in the following sections.

PROPELLER FORCES AND MOMENTS

The propeller forces and moments are treated by methods that are similar to those used for the helicopter rotor in stability and control investigations (Reference 11, chapter 20, and Reference 13). The primary assumptions are:

1. The average value of the induced velocity at the propeller plane is given by momentum theory (Reference 10, page 185) and is expressed as follows:

$$\lambda_i = \frac{v_o}{\Omega R} = \frac{C_T}{2\sqrt{(\lambda_i + \nu)^2 + \mu^2}} = \frac{C_T}{2\xi} \qquad (1)$$

The mass flow influenced by the propeller is based on the resultant velocity at the rotor plane (Reference 10). The inplane component of the free-stream velocity, μ, is retained in this analysis rather than neglected as in References 2 and 7. The validity of neglecting this component of velocity at the rotor plane depends upon the "wing incidence/forward speed" relationship (References 1 and 2). Neglect of this component will significantly influence the propeller derivatives at high wing incidences, if the relative forward speed is high.

2. The propeller induced velocity is assumed to be uniform in a plane perpendicular to the direction of motion and to increase linearly from the leading edge of the propeller disc to the trailing edge in the fashion given by Reference 8, that is,

$$v = v_o + v_1 \left(\frac{r}{R}\right) \cos \Psi \tag{2}$$

where

$$v_1 = v_o \frac{V \sin(i_w + \alpha)}{V \cos(i_w + \alpha) + v_o} \tag{3}$$

and v_o is obtained from Equation (1).

While this is a rough approximation to the actual induced velocity variation across the propeller disc, this variation is the source of the propeller pitching moments. Uniform induced velocity will result in zero propeller pitching moments in conflict with experimental data. See, for example, Reference 7.

3. The propeller blades are assumed to be infinitely rigid in bending and torsion.

4. It is assumed that the effects of twist and taper of the blades may be taken into account by use of an equivalent pitch angle and weighted solidity (Reference 10, page 86). The blade pitch angle used in the following formulae is taken to be that at 75-percent radius.

5. The influence of the presence of the wing on the propellers and mutual interference between propellers is neglected. Limited experimental data indicate that the presence of the wing may have a strong influence on the propeller (Reference 7); however, there is not sufficient information to estimate the importance of this effect. It would be expected that interference between propellers may be important in computing lateral stability derivatives, but not in longitudinal calculations.

While the above assumptions yield a highly simplified model of the actual propeller and may not be satisfactory for performance estimation or computation of propeller blade stresses, unpublished calculations by one of the authors indicate that the basic trends of propeller aerodynamics are adequately represented for stability and control investigations.

On the basis of these assumptions, blade element equations may be developed to evaluate propeller thrust, inplane force, and pitching moment. The

results of Reference 10, pages 190 and 198, may be used for calculating thrust and inplane force. The flapping terms in the inplane force expression are set equal to zero.

$$T = \rho \pi R^2 (\Omega R)^2 \frac{a\sigma}{2} \left[\frac{\theta_{0.75R}}{3} \left(1 + \frac{3}{2}\mu^2\right) - \frac{\lambda_i + \nu}{2} \right] \tag{4}$$

$$H = \rho \pi R^2 (\Omega R)^2 \frac{a\sigma}{2} \left[\frac{\delta}{2a} + \frac{(\lambda_i + \nu)}{2} \theta_{0.75R} \right] \mu \tag{5}$$

The expression for propeller pitching moment due to the variation in induced velocity across the disc may be obtained from Reference 17 as

$$(M)_{PD} = \frac{b}{16} \rho \Omega c a R^3 v_1 \tag{6}$$

To compute the propeller pitching moment due to a pitching velocity about the propeller hub, the change in inflow distribution arising from this velocity is taken into account. The induced velocity is assumed to be independent of pitching velocity. Physically, it is clear that there would be a redistribution of induced velocity due to the change in load distribution as a result of angular motion. This induced velocity variation would act to reduce the rotor damping as compared to the value based on constant induced velocity. Therefore, a somewhat larger value of damping will be obtained than would be present. However, as seen in the following, the propeller angular damping contribution is small and so the significance of any errors incurred would be small. Then the theoretical expression for the contribution of the propeller to the pitch damping becomes

$$\left(\frac{\partial M}{\partial \dot{\theta}}\right)_{ID} = - \frac{\rho a \sigma \pi}{16} \Omega R^5 \tag{7}$$

For pitching moment trim at low speeds, the example airplane has a tail rotor. The contributions to the stability derivatives from the tail rotor are computed using the same assumptions as for the propellers. The downwash from the wing and horizontal tail is included in computation of the inflow velocity, λ_T, of the tail rotor.

$$\lambda_T = \frac{1}{(\Omega R)_T} \left[- V \sin \alpha + \epsilon V + \epsilon_T V + \dot{\theta} \ell_{TR} \right] \tag{8}$$

where

$$\epsilon_T = \frac{2C_{L_{\alpha_T}}}{\pi A} (\alpha + i_T - \epsilon) \tag{9}$$

The inplane force and pitching moment of the tail rotor are neglected.

WING LIFT AND DRAG

The wing lift and drag are computed taking into account what are considered to be the first-order effects of the presence of the propeller slipstream. On the example airplane, the wing is entirely immersed in the slipstream. The following assumptions regarding the nature and influence of the slipstream are made:

1. The slipstream velocity is computed on the basis of a uniform propeller induced velocity far downstream $2v_o$. This is considered reasonable since the contraction of the slipstream takes place a short distance downstream of the disc (Reference 19). However, certain of the derivatives computed in the following are sensitive to this assumption, and it may be desirable to use a value somewhat less than 2 to account for the contraction and downstream dissipation of the slipstream.

2. The effects of slipstream rotation are neglected. While slipstream rotation may have a significant effect on spanwise load distribution on the wing (Reference 1), it is assumed that its influence on the longitudinal stability characteristics will not be important unless large areas of separated flow result.

   This assumption is implicit in the usual method of data presentation where it is assumed that the aerodynamic forces on a wing-propeller combination are only a function of α and $C_{T,S}$ (References 7 and 18 for example). That is, the slipstream rotation depends upon the torque of the propeller and thus both on advance ratio and blade angle. Thus, there is little or no aerodynamic data to verify the validity of this assumption. Experiments should be conducted at different combinations of blade angle and advance ratio that produce the same propeller thrust at different levels of torque to determine the importance of slipstream rotation.

3. The effects of the finite extent of the slipstream flow are taken into account by a reduction in the wing lift curve slope. It is shown in Reference 15 that the finite extent of the slipstream will reduce the lift curve slope of the wing based on slipstream velocity, compared to its value in a stream of infinite extent of the same velocity.

   A simplified approach such as presented, for example, in Reference 5, is considered satisfactory for stability and control calculations. An approach such as developed in Reference 14 is too complex for use here. The approximation suggested in Reference 2 appears to be incorrect since it assumes that there is no change in wing downwash field and only a change in the mass flow influenced by the wing.

However, if there is no change in the downwash behind the wing, then from the viewpoint of vortex theory there would be no change in wing lift, contradicting the momentum theory result. It is important to note that momentum theory cannot be used alone and must be combined with a sectional approach to obtain a defined answer. A more recent analysis, presented in Reference 16, also seems to be incorrect and therefore will not be used. In this reference, the boundary conditions on the problem are not properly satisfied.

Therefore, since precise theoretical results are not particularly satisfactory, it is considered that a semiempirical approach to the problem that agrees with the various limiting cases involved is the best alternative. As a result, it is assumed that the lift curve slope of the wing based on resultant velocity in the slipstream may be expressed in terms of the lift curve slope of the wing in a uniform flow C_{L_α} as

$$C_{L,S_{\alpha_e}} = C_{L_\alpha}\left[(1 - K) + K\frac{V\cos(i_w + \alpha - \alpha_e)}{V_R}\right] \qquad (10)$$

K is an empirical factor that may be adjusted to match the low-speed wing characteristics when experimental data are available. It is assumed that the variation in lift curve slope depends upon the ratio of the component of the free-stream velocity parallel to the slipstream velocity $[V\cos(i_w + \alpha - \alpha_e)]$. In hovering then, when V approaches zero, the wing lift curve slope is

$$C_{L,S_{\alpha_e}} = C_{L_\alpha}(1 - K)$$

and in high-speed forward flight, when $V_R \cong V\cos(i_w + \alpha - \alpha_e)$,

$$C_{L,S_{\alpha_e}} = C_{L_\alpha}$$

The empirical constant K depends in a complex way upon the wing geometry, the propeller geometry, and the immersed aspect ratio, as well as other factors. To obtain good agreement between the experimental and theoretical values of the speed stability (M_u) in hover, a value of $K = 0.5$ was selected. This expression will be discussed further in the section on stability derivatives.

4. The angle of attack of the wing in the slipstream α_e is

assumed to be given by the vector sum of fully developed induced velocity produced by the propeller, $2v$, and the free-stream velocity, V (References 1, 2, 3 and Figure A-1). This particular aspect of the wing slipstream problem has not been considered theoretically in detail in this report or in other analyses. That is, all of the above analyses have investigated, precisely speaking, the change in the lift of a wing immersed in a slipstream when the wing geometric angle of attack in the slipstream is changed, rather than that due to a change in the direction or magnitude of the external flow. It is implied that these two sources of angle of attack changes are equivalent. Therefore, the above assumption is made in absence of a better approach. As a result, the effective wing angle of attack is taken to be

$$\alpha_e = \tan^{-1} \frac{V \sin(i_w + \alpha)}{V \cos(i_w + \alpha) + 2v_o} = \sin^{-1} \frac{V \sin(i_w + \alpha)}{V_R} \qquad (11)$$

and the following expressions are used for wing lift and drag.

$$L_s = \tfrac{1}{2} \rho V_R^2 S C_{L,S_{\alpha_e}} (\alpha_o + \alpha_e) \qquad (12)$$

$$D_s = \tfrac{1}{2} \rho V_R^2 S \left[C_{D,S_o} + \frac{C_{L,S_{\alpha_e}}}{\pi AR} (\alpha_o + \alpha_e)^2 \right] \qquad (13)$$

The lift is taken perpendicular to the slipstream velocity V_R and the drag parallel to V_R. For simplicity, the drag is computed on the basis of an elliptically loaded wing, while in the actual case the loading may be far from elliptical.

Thus the propeller induced flow has been idealized to a uniform tubular flow of velocity $2v_o$ that is added vectorially to the free stream. The wing is assumed to be completely immersed in this flow and only the finite size of the slipstream is taken into account in the computation of wing lift and drag. These assumptions imply that the design and relative location of the propeller on the wing have no influence on the wing lift.

HORIZONTAL TAIL

The horizontal tail lift is calculated on the basis of a simplified approximation to wing downwash assuming an elliptically loaded wing, that is,

$$L_T = \frac{1}{2} \rho V^2 S_T C_{L_{\alpha_T}} \eta_T \left(\alpha + i_T - \epsilon - \epsilon_R + \frac{\ell_{TH} \dot{\theta}}{V} \right) \qquad (14)$$

It is assumed that the downwash velocity is the same inside and outside the slipstream. The following expression is then obtained for the downwash angle outside the slipstream

$$\epsilon = \frac{2}{\pi A} C_{L,S_{\alpha_e}} (1 - M_T^2) \frac{V_R}{V} (\alpha_o + \alpha_e) \qquad (15)$$

The downwash reduction factor, M_T, accounts for the location of the horizontal tail with respect to the wing trailing vortex system. If the distance of the horizontal tail above the wing wake is small compared to the semispan of the wing, then M_T may be expressed as

$$M_T \cong \frac{\ell_{HT} \tan(i_w - \alpha_e) + \ell_H}{\frac{b_w}{2}} \qquad (16)$$

The tail efficiency η_T is assumed to be one ($\eta_T = 1.0$) because of a lack of experimental data. To obtain accurate information on the downwash, experiments are necessary, and Equations (14) through (16) are used only to obtain an estimate of the tail contributions. Note that experiments should include a measurement of the velocity at the tail to determine η_T, as well as measurement of the downwash angles.

WING FLAP CHARACTERISTICS

The wing flap characteristics used are shown in Figure 37. The changes in C_{D_o} and α_o are included directly in Equations (12) and (13) for wing lift and drag. The pitching moment due to flap deflection is assumed to be proportional to slipstream velocity squared, and independent of the ratio of slipstream velocity to free-stream velocity. While there would be an apparent camber change due to the finite extent of the slipstream (Reference 15), this effect is assumed to be small in the absence of experimental data.

FUSELAGE PITCHING MOMENT AND DRAG

Again, for lack of experimental data, the fuselage pitching moment characteristics are computed on the basis of slender body theory (Reference 11, page 64) using the following equation:

$$M_f = 2(\text{Vol})_f K_f q \alpha \qquad (17)$$

The fuselage drag is expressed in terms of an equivalent flat plate drag area f (Reference 10, page 221) as

$$D_f = q\, f \tag{18}$$

This equivalent flat plate area is assumed to be independent of angle of attack and is taken to be 5.0 square feet. The frontal area of the fuselage is 92 square feet and the fineness ratio is 5.3. Assuming that the fuselage is a streamline body, from Reference 21, page 6-19, Figure 25, a drag coefficient based on frontal area of 0.054 is obtained, giving the above value of f. Experimental data are necessary to obtain a better estimate of the fuselage characteristics.

Further experimental data are desirable to obtain better estimates of the two parameters η_T and K. Since the analysis indicates that the speed stability (M_u) is dominated by the wing contribution in hover, it is considered that the empirical factor K may be estimated reasonably well by use of test results near hover. Wake surveys are desirable to obtain substantiation of the assumed value of η_T, and the value of one should be considered only as a rough estimate.

DISCUSSION OF RESULTS

TRIM CONDITIONS

The force equations for level flight equilibrium, parallel and perpendicular to the propeller shaft (Figure A-1) are

$$T + L_s \sin \alpha_e + D_s \cos \alpha_e + D_f \cos i_w = W \sin i_w \qquad (19)$$

$$L_s \cos \alpha_e + D_s \sin \alpha_e + D_f \sin i_w + H = W \cos i_w \qquad (20)$$

It is assumed that forces produced by the horizontal tail and the tail rotor do not influence the balance of forces significantly, so that Equations (19) and (20) may be solved for the flight condition. The moment equation will determine the longitudinal control setting necessary for pitching moment trim.

The quantities on the left-hand side of Equations (19) and (20) are functions of the following variables, in addition to the airplane geometry:

$\theta_{0.75R}$ - propeller blade angle (radians)

V - flight velocity (feet per second)

Ω - propeller rotational speed (radians per second)

δ_f - flap deflection (radians or degrees)

v - propeller induced velocity (feet per second)

α - aircraft angle of attack (radians or degrees)

i_w - wing incidence angle (radians or degrees)

The momentum equation relates propeller thrust to induced velocity. As a result, there are three equations [(1), (19) and (20)] with seven unknowns. The wing incidence, flap deflection (flap deflection as a function of wing incidence is shown in Figure A-2), propeller rotational speed, and aircraft angle of attack (zero) are specified. Then the propeller blade angle, trim velocity, and propeller induced velocity can be determined. The results of this calculation are shown in Figures 1 and 3 as a function of wing incidence angle. Figure 2 presents propeller thrust and wing lift as a function of incidence angle. The slipstream velocity and the effective wing angle of attack are shown in Figures 4 and 5.

In order to obtain an estimate of the manner in which various assumptions enter into the equilibrium calculations, a first-order approximation to Equations (19) and (20) may be obtained by neglecting all left-hand terms except thrust in Equation (19), and the wing lift in Equation (20):

$$T \cong W \sin i_w \tag{19a}$$

$$L_s \cos \alpha_e \cong W \cos i_w \tag{20a}$$

It can be seen from Figure 2 that Equation (19a) gives a very good approximation to the thrust required for equilibrium.

The wing lift in terms of flight variables is given by Equation (12) and α_e by Equation (11). Assuming that effective wing angle of attack is small, Equation (20a) may be expressed as

$$L_s = \frac{\rho}{2} V_R^2 S C_{L_\alpha} \left[(1 - K) + K \frac{V \cos(i_w+\alpha-\alpha_e)}{V_R}\right]\left[\alpha_o + \frac{V \sin(i_w+\alpha)}{V_R}\right] \cong \frac{W \cos i_w}{\cos \alpha_e} \tag{20b}$$

Since the slipstream velocity, V_R, is roughly constant through transition (Figure 4), Equation (20b) may be viewed as primarily determining the relationship between flight velocity and wing incidence angle. At a given wing incidence, changing α_o by deflecting a flap will have a strong influence on the trim velocity of the aircraft.

The influence of flap effectiveness $\frac{\partial \alpha_o}{\partial \delta_f}$ on trim velocity is shown in Figure 1. A plus or minus 33 1/3-percent change in flap effectiveness causes a large variation in the relationship between wing incidence and flight velocity as shown. No variation occurs at wing incidence higher than 80° because the flap is not deflected (Figure A-2).

The variation of slipstream velocity with wing incidence is comparatively small because as the flight speed increases, the induced velocity decreases (Figure 3), resulting in a slowly varying slipstream velocity. Calculation of the slipstream velocity is not particularly sensitive to flap effectiveness (Figure 4).

The effective wing angle of attack, α_e, particularly the maximum value, is sensitive to flap effectiveness (Figure 5), as expected from the above discussion. Thus, the flap may be viewed as a means of controlling the effective wing angle of attack as seen from Equation (20b). The variation

of the parameters in the expression for the effective wing angle of attack is such that a maximum value of α_e occurs at a wing incidence of approximately 25°.

The pitching moment acting on the airplane with no tail rotor thrust and no horizontal tail lift is shown in Figure 6. The important contributions to the pitching moment acting on the airplane from the various components are also shown. The moments arising from wing lift and propeller thrust vary with wing incidence because of changes in the magnitudes of the forces and the moment arms about which they act. An increasing nose-up pitching moment from the sum of the thrust and wing lift with decreasing wing incidence is typical of tilt-wing configurations for normal center-of-gravity locations (Reference 18). The contribution of the propeller pitching moment due to the induced velocity distribution over the propeller disc is small. The flap characteristics have a significant influence on the moment required. To obtain an accurate prediction of the pitching moment required to trim, precise information on the pitching moments produced by flap deflection in a slipstream is necessary.

In conclusion, it may be noted that the magnitudes of the propeller thrust and wing lift are primarily determined by wing incidence angle. The trim velocity corresponding to this incidence angle depends strongly on the assumed relationship between the wing lift and the flight variables. Computations of both trim velocity and pitching moment are sensitive to flap characteristics. To obtain a good prediction of the wing incidence/trim velocity relationship, it is necessary to have good estimates of the wing lift curve slope and flap effectiveness of a wing immersed in a high velocity slipstream.

STABILITY DERIVATIVES

The stability derivatives of the example airplane, with respect to a stability axis system for various level flight equilibrium conditions, were calculated using the theoretical models discussed in the first section. This section presents a detailed discussion of the trends of the derivatives and the contributions of the airplane components to each of the derivatives. Detailed derivations of various formulae discussed are given in Appendix B.

Force Derivatives With Respect to Horizontal Velocity (X_u , Z_u)

The force derivatives arise primarily from propeller thrust and wing lift variations. Recall that wing lift and drag are taken perpendicular and parallel to the direction of slipstream velocity. Generally, it was found that the contributions arising from the propeller inplane force and the wing drag were small. Therefore, only the rate of change of thrust and wing lift with horizontal velocity $\left(\frac{\partial T}{\partial u} , \frac{\partial L_s}{\partial u} \right)$ will be discussed in relation to the airplane derivatives.

It is necessary first to consider the rate of change of effective wing

angle of attack and slipstream velocity with horizontal velocity $\left(\frac{\partial \alpha_e}{\partial u} , \frac{\partial V_R}{\partial u} \right)$ as well as the changes in propeller induced velocity.

Analytically, it is more convenient to consider the propeller induced velocity derivatives with respect to the nondimensional velocities υ and μ, perpendicular and parallel, respectively, to the propeller plane. In fact, it was noted during the course of this analysis that the aerodynamic force and moment expressions became considerably simplified when treated in terms of the variables υ and μ with an axis system aligned with the propeller shaft. This approach has the disadvantage that the inertia and gravity terms will appear in an unconventional form in the equations of motion, so it was decided to proceed in a more conventional manner and accept the resulting complication in the aerodynamic terms.

First, the rate of change of propeller induced velocity with a change in velocity parallel to the propeller plane $\frac{\partial \lambda_i}{\partial \mu}$ is considered. The expression as given in Appendix B is

$$\frac{\partial \lambda_i}{\partial \mu} = \frac{\frac{1}{3}\left[\frac{a\sigma}{4}\theta_{0.75R}\mu - \lambda_i \frac{\mu}{\xi}\right]}{1 + \frac{1}{\xi}\left[\frac{a\sigma}{8} + \lambda_i\left(\frac{\lambda_i + \upsilon}{\xi}\right)\right]} \qquad (21)$$

where

$$\xi = \sqrt{(\lambda_i + \upsilon)^2 + \mu^2}$$

The first term in the numerator of Equation (21) arises from the thrust variation due to the average increase in the free-stream velocity component over the disc, and the second term accounts for the variation in induced velocity resulting from the change in mass flow. The second term generally dominates this expression and is roughly proportional to $\lambda_i \mu$, since ξ is almost constant through transition as shown in Figure 8. Since μ is equal to $\frac{V_R}{\Omega R} \sin \alpha_e$, μ varies approximately as α_e. At high wing incidences, μ increases more rapidly than the induced velocity, λ_i decreases (with a change in flight velocity), and therefore the derivative $\frac{\partial \lambda_i}{\partial \mu}$ increases in value. At low wing incidences, both λ_i and μ decrease with increasing flight velocity, and so this derivative decreases. The variation of this derivative with wing incidence will be similar to

the variation of α_e . Although there is some influence on the derivative $\frac{\partial \lambda_i}{\partial \mu}$ from the denominator, the major variation arises from the numerator. The trends of the derivative $\frac{\partial \lambda_i}{\partial \mu}$ are shown in Figure 7. Physically, the magnitude of this derivative indicates that for the velocity-propeller angle of attack relationship encountered during a transition, the propeller induced velocity is rather insensitive to velocity perturbations parallel to the plane of the propeller.

The other induced velocity derivative, $\frac{\partial \lambda_i}{\partial \nu}$, may be expressed as

$$\frac{\partial \lambda_i}{\partial \nu} = \frac{-\frac{1}{\xi}\left[\frac{a\sigma}{8} + \lambda_i\left(\frac{\lambda_i + \nu}{\xi}\right)\right]}{1 + \frac{1}{\xi}\left[\frac{a\sigma}{8} + \lambda_i\left(\frac{\lambda_i + \nu}{\xi}\right)\right]} \tag{22}$$

Again, since ξ is roughly constant through transition, the variation of this quantity is dominated by the change in induced velocity, λ_i , through the transition, since $\frac{\lambda_i + \nu}{\xi} \cong 1.0$ (Figure 8). Also because the resultant velocity at the propeller plane, ξ , is approximately constant throughout most of the transition (Figure 8), the induced velocity varies as the thrust [see Equation (1)]. This derivative is shown as a function of wing incidence angle in Figure 7. Physically, the magnitude of this term indicates that variation in propeller induced velocity acts to reduce greatly the effect of a velocity perturbation normal to the propeller plane on the slipstream velocity.

The variation in the slipstream velocity (see Appendix B) is given by

$$\frac{1}{\Omega R}\frac{\partial V_R}{\partial u} = \frac{2\lambda_i + \nu}{V_R}\left(1 + 2\frac{\partial \lambda_i}{\partial \nu}\right)\cos(i_w + \alpha) + \frac{2(2\lambda_i + \nu)\frac{\partial \lambda_i}{\partial \mu} + \mu}{V_R}\sin(i_w + \alpha) \tag{23}$$

The first term represents the effect of the component of horizontal velocity normal to the propeller plane, and the second term is due to the component of horizontal velocity parallel to the propeller plane.

Since the direction of the resultant slipstream velocity is always closely aligned to the propeller shaft direction (the effective angle of attack is small), a change in the free-stream velocity component perpendicular to the

propeller plane has only a small influence on the magnitude of the resultant velocity. As discussed earlier, the induced velocity change arising from this component of free-stream velocity is small. The first term in Equation (23), arising from the change in the free-stream velocity component along the propeller shaft, will dominate this expression. However, this term will also be small due to the compensating effect of propeller induced velocity variation with ν discussed above. In hovering, $\left(1 + 2\frac{\partial\lambda_i}{\partial\nu}\right)$ is a small negative quantity. As the flight velocity increases, $\left|\frac{\partial\lambda_i}{\partial\nu}\right|$ decreases and $\left(1 + 2\frac{\partial\lambda_i}{\partial\nu}\right)$ becomes zero and then a small positive quantity with further increase in trim velocity. Therefore, $\frac{\partial V_R}{\partial u}$ varies as shown in Figure 10, and is a small quantity $\left(\left|\frac{\partial V_R}{\partial u}\right| < 0.2\right)$.

The result that this term is small will usually be the case as seen from the following. In hovering, $\xi = \lambda_i$, and therefore, from Equation (22)

$$\frac{\partial\lambda_i}{\partial\nu} = -\frac{\left(\frac{a\sigma}{8} + \lambda_i\right)}{\left(\frac{a\sigma}{8} + 2\lambda_i\right)} \qquad (22a)$$

Thus, in hovering, $-0.5 < \frac{\partial\lambda_i}{\partial\nu} < -1.0$. As the velocity component normal to the propeller plane increases, the induced velocity, λ_i, will decrease, and also its rate of change with ν will decrease.

The magnitude of the term $\left(1 + 2\frac{\partial\lambda_i}{\partial\nu}\right)$ is very sensitive to the assumption that the slipstream velocity is computed on the basis of the fully developed induced velocity. It is possible that a factor less than two should appear in front of $\frac{\partial\lambda_i}{\partial\nu}$ to account for the actual variation in induced velocity across the wing chord.

As the trim velocity corresponding to a given wing incidence becomes smaller, the larger the minimum value of $\frac{\partial V_R}{\partial u}$ will be. Figure 9 shows lines of constant $\frac{\partial V_R}{\partial u}$ as a function of trim speed and wing incidence angle. The upper boundary, for which $\frac{\partial V_R}{\partial u}$ equal to 0.2, occurs at too large a velocity to be shown on this graph. It therefore appears that in

the typical situation, the slipstream velocity will be relatively insensitive to changes in horizontal velocity if the assumption regarding the full development of the slipstream is valid.

The fourth quantity of interest here, the rate of change of wing effective angle of attack with horizontal velocity (see Appendix B) may be expressed as

$$\frac{\partial \alpha_e}{\partial u} = \frac{\sin(i_w + \alpha)}{V_R} \left(1 - \frac{V}{V_R} \frac{\partial V_R}{\partial u}\right) \tag{24}$$

Since, in this example, the trim velocity always lies well within the boundary $\left(\left|\frac{\partial V_R}{\partial u}\right| < 0.2\right)$ and $\frac{V}{V_R}$ is small when the trim velocity is within this boundary, a good approximation to Equation (24) is obtained by neglecting the second term

$$\frac{\partial \alpha_e}{\partial u} \cong \frac{\sin(i_w + \alpha)}{V_R} \tag{25}$$

For the example configuration where α is equal to zero, the agreement between Equations (24) and (25) is shown in Figure 11. Physically, this approximation implies that the primary change in effective wing angle of attack due to a horizontal velocity perturbation arises from the change in the component of the horizontal velocity parallel to the propeller plane, and the effects of component normal to the propeller plane and the variation in induced velocity are small. As the wing incidence is reduced, the increasing effect of the component parallel to the shaft is compensated by the induced velocity change.

The rate of change of propeller thrust with horizontal velocity may be expressed as

$$\frac{\partial T}{\partial u} = \rho \pi R^2 (\Omega R) \frac{a\sigma}{2} \left[-\frac{1}{2}\left(1 + \frac{\partial \lambda_i}{\partial \nu}\right) \cos(i_w + \alpha) + \left(\frac{2}{3} \theta_{0.75R} \mu - \frac{1}{2} \frac{\partial \lambda_i}{\partial \mu}\right) \sin(i_w + \alpha) \right] \tag{26}$$

This derivative is shown as a function of incidence angle in Figure 12. The first term dominates and causes the value to increase (approximately) as $\cos(i_w + \alpha)$.

The rate of change of wing lift with horizontal velocity may be expressed as

$$\frac{\partial L_s}{\partial u} = \frac{1}{2} \rho S C_{L,S_{\alpha_e}} V_R^2 \frac{\partial \alpha_e}{\partial u} + \rho S C_{L,S_{\alpha_e}} V_R (\alpha_o + \alpha_e) \frac{\partial V_R}{\partial u} + \frac{1}{2} \rho S V_R^2 (\alpha_o + \alpha_e) \frac{\partial C_{L,S_{\alpha_e}}}{\partial u} \tag{27}$$

Thus, variations in wing lift with horizontal velocity may be considered as arising from three sources: first, the change in effective angle of attack; second, the change in slipstream velocity; and third, the change in wing lift curve slope. The variation in this derivative with incidence angle and the contribution of each of the above terms are shown in Figure 13. The first term dominates at high incidence angles, and the last term becomes quite important at low incidence angles. The last term must be considered questionable due to lack of knowledge of the exact functional relationship for the lift curve slope. This particular effect was not taken into account in either Reference 3 or its equivalent form in Reference 2. The middle term seems unimportant; however, it would be larger if the slipstream velocity were computed on the basis of other than the fully developed induced velocity. As a result of these various contributions, this derivative remains roughly constant throughout the transition.

The total value (summation of all contributions) of these two stability derivatives and the manner in which they vary are discussed next. First, consider the rate of change of horizontal force with horizontal velocity:

$$\frac{\partial X}{\partial u} = \left(\frac{\partial X}{\partial u} \right)_{\text{propeller}} + \left(\frac{\partial X}{\partial u} \right)_{\text{wing}} + \left(\frac{\partial X}{\partial u} \right)_{\text{fuselage}}$$

or

$$\frac{\partial X}{\partial u} \cong \left(\frac{\partial T}{\partial u} \right) \cos i_w - \left(\frac{\partial L_s}{\partial u} \right) \sin(i_w - \alpha_e) + \left(\frac{\partial X}{\partial u} \right)_{\text{fuselage}}$$

The wing and propeller contributions to this derivative are shown in Figure 14. The wing contribution dominates at high incidence and propeller contribution dominates at low incidence. At high incidence angles,

$\frac{\partial L_s}{\partial u}$ arises primarily from $\frac{\partial \alpha_e}{\partial u} \cong \left[\frac{\sin(i_w + \alpha)}{V_R}\right]$ as shown in Figure 13.

The rate of change of vertical force with horizontal velocity may be expressed as

$$\frac{\partial Z}{\partial u} = \left(\frac{\partial Z}{\partial u}\right)_{rotor} + \left(\frac{\partial Z}{\partial u}\right)_{wing}$$

or

$$\frac{\partial Z}{\partial u} \cong -\left(\frac{\partial T}{\partial u}\right) \sin i_w - \frac{\partial L_s}{\partial u} \cos(i_w - \alpha_e) - L_s \sin(i_w - \alpha_e) \frac{\partial \alpha_e}{\partial u} \tag{29}$$

The behavior of this derivative with wing incidence is shown in Figure 15. The derivative is dominated by the wing lift contribution $\frac{\partial L_s}{\partial u} \cos(i_w - \alpha_e)$ throughout the transition regime.

Force Derivatives With Respect to Vertical Velocity (X_w , Z_w)

First, the variations in effective wing angle of attack, slipstream velocity, propeller thrust, and wing lift with vertical velocity are discussed, and then the complete vehicle derivatives.

First, the slipstream velocity derivative may be expressed as

$$\frac{1}{\Omega R}\frac{\partial V_R}{\partial w} = \left(\frac{2\lambda_i + v}{V_R}\right)\left(1 + 2\frac{\partial \lambda_i}{\partial v}\right)\left(-\sin(i_w + \alpha)\right) + \frac{2(2\lambda_i + v)\frac{\partial \lambda_i}{\partial \mu} + \mu}{V_R} \cos(i_w + \alpha) \tag{30}$$

The variation of this quantity is shown in Figure 16. At high incidence angles the first term dominates. Since both $\sin(i_w + \alpha)$ and $(1 + 2\frac{\partial \lambda_i}{\partial v})$ decrease with decreasing wing incidence, the first term decreases and at wing incidence angles below 30° the second term becomes important. The rate of change of effective wing angle of attack with vertical velocity is

$$\frac{\partial \alpha_e}{\partial w} = \frac{\cos(i_w + \alpha)}{V_R}\left(1 - \frac{\alpha_e \frac{\partial V_R}{\partial w}}{\cos(i_w + \alpha)}\right) \tag{31}$$

For the example configuration, where the fuselage angle of attack is equal to zero, Figure 17 indicates that the quantity $\frac{\partial \alpha_e}{\partial w}$ is dominated by the first term and, similarly to $\frac{\partial \alpha_e}{\partial u}$, arises primarily from the change in velocity component normal to the wing; it is not significantly influenced by the second term. The rotor induced velocity variation is compensated for by the velocity component variation parallel to the shaft. Again the magnitude of this compensating effect depends upon the assumption of a fully developed induced velocity.

The second term of Equation (31) is a rather strong function of the trim velocity due to the appearance of the effective wing angle of attack. In Figure 9, showing trim velocity plotted versus wing incidence angle, the boundaries where the second term is 10 percent and 20 percent of the first term are shown. As can be seen, it is possible that at high incidence angles, the second term may become significant.

The rate of change of thrust with vertical velocity can be expressed as

$$\frac{\partial T}{\partial w} = \rho \pi R^2 (\Omega R) \frac{a\sigma}{2}\left[\left(1 + \frac{\partial \lambda_i}{\partial \nu}\right)\sin(i_w + \alpha) + \left(-\theta_{0.75R}\,\mu - \frac{\partial \lambda_i}{\partial u}\right)\cos(i_w + \alpha)\right] \tag{32}$$

This quantity, shown in Figure 18, again at high incidence angle is dominated by the first term. The second term increases with decreasing incidence, becoming important at low tilt angles. As a result, this derivative remains roughly constant about equal to its hovering value. In hovering,

$$\frac{1}{m}\frac{\partial T}{\partial w} = \frac{N(\rho \pi R^2 (\Omega R) \frac{a\sigma}{2})}{m}\frac{1}{2}\left(1 + \frac{\partial \lambda_i}{\partial \nu}\right) \tag{33}$$

From Equation (22), with $\xi = \lambda_i$ and $\nu = 0$,

$$\frac{\partial \lambda_i}{\partial \nu} = - \frac{\left(\frac{a\sigma}{8} + \lambda_i \right)}{\left(\frac{a\sigma}{8} + 2\lambda_i \right)} \tag{22a}$$

and from Equation (1), with $\nu = \mu = 0$,

$$\lambda_i = \sqrt{\frac{C_T}{2}} \tag{1a}$$

so

$$\frac{1}{m} \frac{\partial T}{\partial w} = \frac{g\sqrt{2\sigma}}{\Omega R} \sqrt{\frac{\sigma}{C_T}} \left[\frac{1}{1 + \frac{8\sqrt{2}}{a\sqrt{\sigma}} \sqrt{\frac{C_T}{\sigma}}} \right] \tag{34}$$

Thus, since $\frac{C_T}{\sigma}$ will be relatively independent of the configuration of the vehicle (Reference 10, page 64), this derivative will primarily vary with tip speed, increasing as the tip speed decreases at constant $\frac{C_T}{\sigma}$.

The wing lift variation with vertical velocity is given by

$$\frac{\partial L_s}{\partial w} = \frac{1}{2} \rho S C_{L,S_{\alpha_e}} V_R^2 \frac{\partial \alpha_e}{\partial w} + \rho S C_{L,S_{\alpha_e}} (\alpha_o + \alpha_e) V_R \frac{\partial V_R}{\partial w} + \frac{1}{2} \rho S V_R^2 (\alpha_o + \alpha_e) \frac{\partial C_{L,S_{\alpha_e}}}{\partial w} \tag{35}$$

Similarly, three contributions appear as discussed with respect to Equation (27). The numerical values of $\frac{\partial L_s}{\partial w}$ are plotted in Figure 19. The first term dominates throughout transition. The term $\frac{\partial \alpha_e}{\partial w}$ is nearly proportional to $\cos(i_w + \alpha)$ as noted in the discussion of Equation (31).

Physically, as the wing incidence decreases, the variation in the component of vertical velocity normal to the propeller shaft increases, causing a larger effective angle of attack change from the same change in vertical velocity. Again, the last term should be considered rather questionable due to a lack of precise knowledge of the wing lift curve slope.

The total value of the airplane derivatives (summation of all contributions) is now considered. First, the rate of change of horizontal force with vertical velocity is

$$\frac{\partial X}{\partial w} = \left(\frac{\partial X}{\partial w}\right)_{\text{propeller}} + \left(\frac{\partial X}{\partial w}\right)_{\text{wing}}$$

or

$$\frac{\partial X}{\partial w} \cong \left(\frac{\partial T}{\partial w}\right) \cos i_w - \left(\frac{\partial L_s}{\partial w}\right) \sin(i_w - \alpha_e) + L_s \cos(i_w - \alpha_e) \frac{\partial \alpha_e}{\partial w} \tag{36}$$

This derivative is shown in Figure 20. At high tilt angles, $\frac{\partial L_s}{\partial w} \sin(i_w - \alpha_e)$ and $\frac{\partial T}{\partial w} \cos i_w$ dominate. Since $\frac{\partial L_s}{\partial w} \sin(i_w - \alpha_e)$ is greater than $\frac{\partial T}{\partial w} \cos i_w$ at high tilt angles, $\frac{\partial X}{\partial w}$ is negative. As the incidence decreases, $L_s \cos(i_w - \alpha_e) \frac{\partial \alpha_e}{\partial w}$ becomes increasingly important and $\frac{\partial X}{\partial w}$ becomes positive. The term involving $\frac{\partial L_s}{\partial w}$ is due to the change in magnitude of the wing lift, and the term $L_s \cos(i_w - \alpha_e) \frac{\partial \alpha_e}{\partial w}$ is due to the tilt of the wing lift vector. At high incidence angles the change in lift is important and at low incidence angles the tilt of the lift vector becomes significant, since the magnitude of the wing lift increases as the wing incidence decreases (Figure 2).

It was noted from experimental measurements that the variation of the horizontal force with vertical velocity is quite nonlinear. The theoretical computation of the horizontal force as a function of angle of attack using the expression given in Appendix B is shown in Figure 38. The nonlinear variation in this force arises from the change in the magnitude of the lift vector as it tilts. That is, as the above term, $L_s \cos(i_w - \alpha_e) \frac{\partial \alpha_e}{\partial w}$, becomes important, the wing lift also varies

appreciably with effective wing angle of attack, resulting in this term's increasing with α_e . This is probably not a particularly important effect on the dynamics, since this derivative itself usually is not important. The nonlinearity is particularly noticeable where the linearized derivative is near zero as shown in Figure 38.

The rate of change of vertical force with vertical velocity may be expressed as

$$\frac{\partial Z}{\partial w} = \left(\frac{\partial Z}{\partial w}\right)_{\text{propeller}} + \left(\frac{\partial Z}{\partial w}\right)_{\text{wing}}$$

or

$$\frac{\partial Z}{\partial w} \cong -\left(\frac{\partial T}{\partial w}\right) \sin i_w - \left(\frac{\partial L_s}{\partial w}\right) \cos(i_w - \alpha_e) - L_s \sin(i_w - \alpha_e) \frac{\partial \alpha_e}{\partial w} \tag{37}$$

The behavior of this derivative is shown in Figure 21. At large incidence angles, $\frac{\partial T}{\partial w} \sin i_w$ dominates. As the wing incidence decreases, $\frac{\partial T}{\partial w} \sin i_w$ decreases and $\frac{\partial L_s}{\partial w} \cos(i_w - \alpha_e)$ becomes dominant. This derivative increases roughly proportional to $\cos(i_w - \alpha_e)$ due to the wing lift contribution.

Pitching Moment Derivatives With Respect to Horizontal Velocity, Vertical Velocity and Pitch Rate (M_u , M_w , $M_{\dot{\theta}}$)

The pitching moment derivatives are now considered. First, examine the variation of the pitching moment with horizontal velocity, which may be broken down into the following contributions:

$$\frac{\partial M}{\partial u} = \left(\frac{\partial M}{\partial u}\right)_{\text{propeller}} + \left(\frac{\partial M}{\partial u}\right)_{\text{wing}} + \left(\frac{\partial M}{\partial u}\right)_{\substack{\text{horizontal} \\ \text{tail}}} + \left(\frac{\partial M}{\partial u}\right)_{\substack{\text{tail} \\ \text{rotor}}} + \left(\frac{\partial M}{\partial u}\right)_{PD} \tag{38}$$

As may be seen from Figure 22, the primary contributions to $\frac{\partial M}{\partial u}$ arise from the propeller and the wing. The major contribution from the wing arises

from the term $\frac{\ell_W}{I}\left(\frac{\partial L_s}{\partial u}\cos\alpha_e\right)$ as shown. Since ℓ_W decreases roughly in proportion to $\sin i_w$ (Figure A-3), the wing contribution varies roughly as $\sin i_w$. The propeller contribution, arising from the variation in induced velocity across the propeller disc, Equation (2), has a noticeable contribution in hovering. As the wing incidence decreases, the propeller contribution decreases. As a result M_u decreases rapidly as wing incidence is decreased.

The contribution of the horizontal tail to this derivative will depend upon the tail incidence and downwash characteristics at the horizontal tail. The tail contribution may be evaluated from Equation (14).

$$\left(M_u\right)_{HT} = -\rho V S_T \ell_{HT} C_{L_T} - \frac{1}{2}\rho V^2 S_T C_{L_{\alpha_T}} \ell_{HT}\left(\frac{\partial\epsilon}{\partial u} + \frac{\partial\epsilon_P}{\partial u}\right) \qquad (39)$$

The first term depends upon the tail incidence and the downwash angle. To estimate the importance of this term, its magnitude for a tail lift coefficient equal to 1.0 is shown in Figure 23. While the actual tail lift coefficient would vary in some complex way, this indicates the importance of the term. Thus, as a result of the tail incidence, there may be a significant contribution to the variation of pitching moment with horizontal speed at lower wing incidence angles. An increase in tail efficiency, η_T, would, of course, increase the magnitude of this term.

The second term arises from the wing and propeller downwash variation with horizontal velocity. The downwash behind a wing immersed in a high velocity slipstream is difficult to estimate, and so only the following rough indications of the size of the second term in Equation (39) are considered. The propeller downwash contribution would be

$$\frac{\partial\epsilon_P}{\partial u} = -\frac{\partial\alpha_e}{\partial u} \qquad (40)$$

and the wing downwash would be

$$\frac{\partial\epsilon}{\partial u} = \frac{2}{\pi AR} C_{L,S_{\alpha_e}}\left(1 - M_T^2\right)\frac{V_R}{V}\frac{\partial\alpha_\epsilon}{\partial u} \qquad (41)$$

These two terms are plotted in Figure 23. Thus, assuming that the horizontal tail characteristics are proportional to free-stream dynamic pressure, rather small contributions to the derivative M_u are indicated. Further experimental data are necessary before downwash effects can be evaluated in more detail.

The rate of change of pitching moment with vertical velocity (attitude stability), shown in Figure 24a, is made up of the following contributions:

$$\frac{\partial M}{\partial w} = \left(\frac{\partial M}{\partial w}\right)_{wing} + \left(\frac{\partial M}{\partial w}\right)_{propeller} + \left(\frac{\partial M}{\partial w}\right)_{horizontal} + \left(\frac{\partial M}{\partial w}\right)_{\substack{tail \\ rotor}} + \left(\frac{\partial M}{\partial w}\right)_{PD}$$

The pitching moment derivative contribution of the fuselage, $\left(\frac{\partial M}{\partial w}\right)_{fuselage}$, was not calculated due to lack of experimental data and is not included in this summation.

At high incidence angles, the wing and propeller terms dominate. A breakdown of the various wing contributions is also shown in Figure 24b. As the wing incidence decreases and the trim velocity increases, the horizontal tail provides the dominant term, as in a conventional aircraft. At high incidence, that is, low speed, the wing and rotor combine to produce a statically unstable aircraft (M_w positive). As the flight speed is increased, the effect of the horizontal tail increases and the aircraft becomes statically stable. The wing incidence angle at which $\frac{\partial M}{\partial w}$ has a maximum positive value is strongly dependent upon the trim velocity corresponding to this incidence, due to the increasing importance of the horizontal tail. The horizontal tail contributions have been computed essentially neglecting the effects of slipstream velocity. While this may affect the precise numerical values obtained, it would be expected that the trend of M_w would not be significantly altered. This theoretical variation of angle of attack stability agrees with the general behavior of this derivative noted in Reference 9 for various VTOL aircraft.

During the course of these computations, it was also noted that there were nonlinearities in this derivative. Figure 39 shows the pitching moment variation versus airplane angle of attack for various wing incidences. The nonlinearity arises primarily from the change in direction of the wing lift with vertical velocity and is particularly noticeable near the incidence angle where the linearized derivative is zero. In the actual case, this derivative may be considerably more nonlinear than indicated, due to fuselage and downwash characteristics.

Figure 25 shows the variation of the pitch damping derivative with wing

incidence. Contributions to the pitch damping of the vehicle arises from the following sources:

$$\frac{\partial M}{\partial \dot{\theta}} = \left(\frac{\partial M}{\partial \dot{\theta}}\right)_{\text{wing}} + \left(\frac{\partial M}{\partial \dot{\theta}}\right)_{\text{propeller}} + \left(\frac{\partial M}{\partial \dot{\theta}}\right)_{\substack{\text{horizontal} \\ \text{tail}}} + \left(\frac{\partial M}{\partial \dot{\theta}}\right)_{\substack{\text{tail} \\ \text{rotor}}}$$

At high incidence, the contributions of the propeller and tail rotor dominate and are generally rather small. As the forward speed increases, the horizontal tail provides an increasing damping. The wing provides only a very small contribution, as would be expected. It should be recalled that the propeller damping arises primarily from the change in inflow distribution and may be somewhat overestimated, since the change in induced velocity has not been included. It appears, then, that any significant pitch damping arises from the horizontal tail, and that the rest of the components give generally negligible contributions.

LOCUS OF ROOTS AND SENSITIVITY TO STABILITY DERIVATIVE VARIATIONS

Using the values of the stability derivatives calculated in the previous section, the characteristic roots of the aircraft have been calculated [(using Equations (B-4), (B-5), and (B-6)] and are shown in Figure 26 as a function of wing incidence. The horizontal tail contribution to M_u has been neglected.

At hovering and slow forward speeds, the dynamics are similar to a conventional helicopter (Reference 11). The modes of motion consist of an unstable oscillation, a real convergence that is relatively fast, and a slow convergence. In hovering, the vertical degree of freedom (vertical velocity) is uncoupled and is a slow convergence. The other three roots comprise a convergence and an unstable oscillation due to the coupling of pitch attitude and horizontal velocity. As the horizontal velocity increases (wing incidence decreases), the period of unstable oscillation increases and the oscillation becomes stable, tending towards the characteristics of a conventional airplane phugoid (Reference 11). The vertical motion becomes coupled with the attitude and horizontal velocity, and the two real roots coalesce and then break away from the negative real axis to form a well damped motion, similar to the conventional aircraft short-period motion at low incidence angles.

Since numerous assumptions have been made in the foregoing analysis, it is of interest to evaluate the sensitivity of the root location to variations in the stability derivatives. In order to evaluate the variations in roots, each derivative was individually reduced to zero and doubled. Care should be taken in interpreting these loci for zero values of the important stability derivatives, since nonlinearities are present which will become more important when the linearized derivative is zero. The resulting changes in the characteristic roots of the vehicle are shown in Figures 27 through 31.

For clarity, the roots located on the negative real axis and computed for the incremental values compared to the basic values of Figure 26 are shown on two additional "displaced" real axes so that they are not confusingly superposed, thereby making it impossible to discern their value and location. Of course, they are located on the abscissa of the original axis system at the appropriate values shown on the displaced axes. Also, in order to distinguish between the two oscillatory modes that occur, one mode of motion is referred to as the unstable mode, even though it becomes stable at higher trim velocities, and the other is referred to as the stable mode.

Variation in X_u (Figure 27)

X_u is most noticeable in influencing the damping of the unstable mode. An increase in $|X_u|$ increases the damping. It also has some effect on the comparatively rapid convergence. It has only a small effect on the stable mode that appears at lower tilt angles.

Variation in Z_w (Figure 28)

Increasing the magnitude of lift curve slope of the airplane Z_w increases the damping of the stable mode and has little effect on the unstable mode. A rather radical alteration in the general appearance of the locus occurs at low incidence angles when Z_w is set equal to zero. The association of the unstable mode with the classical phugoid is less clear, since as wing incidence decreases, this mode tends towards what would probably be considered the short-period motion. Physically, the zero lift curve slope would represent a rather unusual airplane.

Variation in $M_{\dot{\theta}}$ (Figure 29)

Increasing $M_{\dot{\theta}}$ in a negative sense (stable) at high incidence angles reduces the instability of the unstable mode as well as increases the damping of the stable mode, that is, it contributes favorably to both modes of motion.

Variation in M_w (Figure 30)

At high incidence angles, an increase in the positive value (unstable) of M_w causes a loss in damping of the unstable mode. At low incidence angles, the increasing negative value (stable) results in a marked increase in the damping of the unstable mode. Increasing the stable value of M_w at low incidence angles causes a marked increase in the frequency of the stable mode, as would be expected.

Variation in M_u (Figure 31)

Decreasing M_u causes a lengthening of the period and a slight increase in damping of the unstable mode. Increasing M_u causes a decrease in the period of the unstable mode. The term M_u was not reduced to zero since it causes a radical reorientation of the locus. With M_u equal to zero in hovering, the attitude and horizontal velocity are essentially uncoupled. A positive value of this derivative is typical of all of these vehicles near hovering.

Variation in Z_u and X_w

The variations in Z_u and X_w over the range considered were found to produce only small changes in the loci.

GENERAL TRENDS OF LOCI OF ROOTS

In order to understand more clearly the general tendencies of these loci, some sketches are given below considering only the effects of M_w and M_u, at fixed values of the other derivatives. The variations of these two derivatives dominate the general shapes of the loci presented.

In the case where $M_w = 0$ and M_u is varied, the characteristic equation is approximately

$$1 + \frac{g\, M_u\, (s - Z_w)}{s(s - X_u)(s - M_{\dot{\theta}})(s - Z_w)} \cong 0 \qquad (42)$$

and the root locus for varying M_u (indicated by the square symbols and solid line) is as shown in the sketch below:

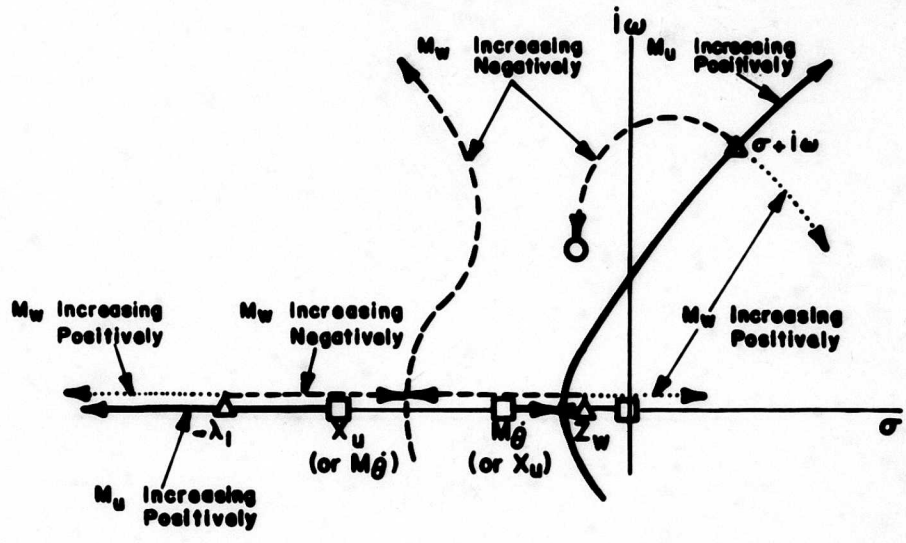

For some value of M_u, there are four roots $(-\lambda_1 , \sigma \pm i\omega)$ and the uncoupled root Z_w, which are shown in the sketch by the triangle symbols. Also, in the sketch, is a pair of zeroes, which are shown by the circle symbol. When M_w is not zero the characteristic equation is approximately

$$1 + \frac{V_o M_w \left(s^2 - X_u s + \frac{Z_u g}{V_o}\right)}{(s - Z_w)(s + \lambda_1)\left[s^2 - 2\sigma s + (\sigma^2 + \omega^2)\right]} = 0 \qquad (43)$$

and the root locus for varying M_w is as shown by the dotted line $(M_w > 0)$ and by the dashed line $(M_w < 0)$.

When the wing incidence varies, a family of loci results as shown below:

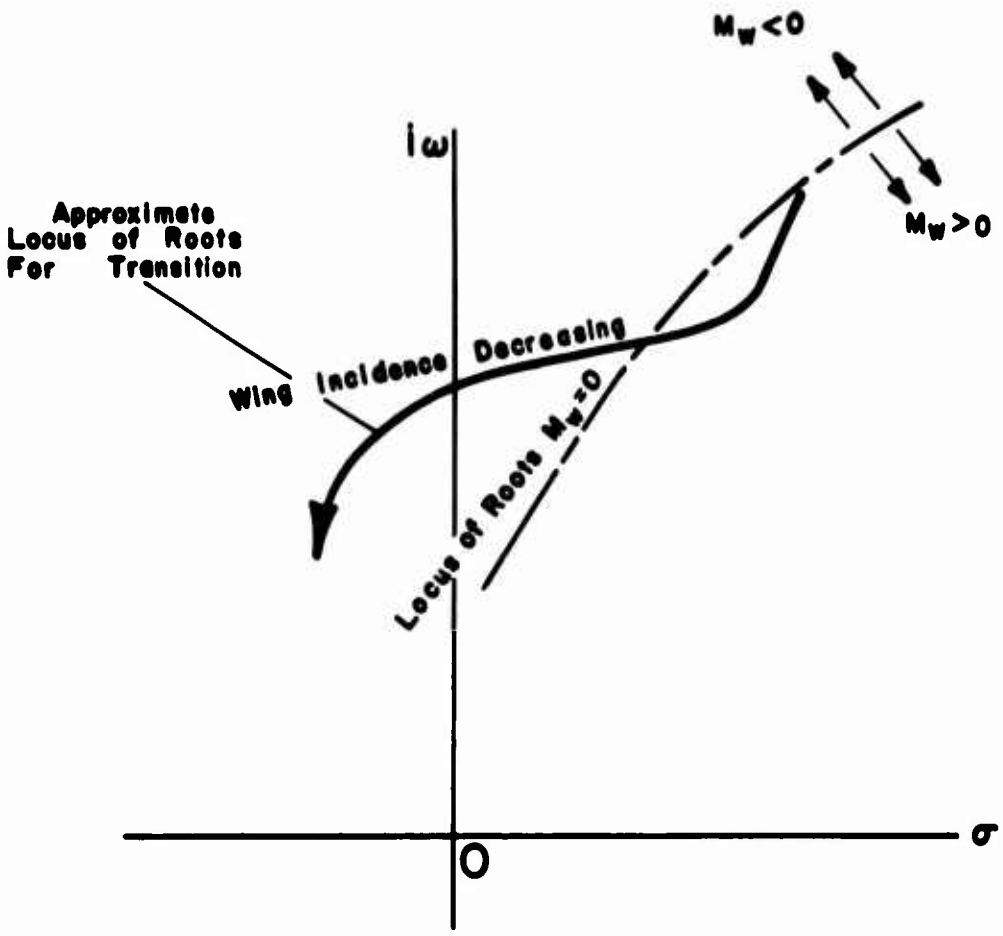

The locus of roots of the unstable mode which result for the case when M_w equals zero during a transition is shown by a double dashed line. At high incidence angles, the actual locus indicates a somewhat larger instability than the M_w equals zero case due to the small positive value of M_w. When the wing incidence is less than roughly 40°, the unstable mode becomes markedly more stable because of the rapid increase of M_w with incidence in a statically stable sense (negative), as shown in Figure 24.

From this brief discussion, it can be seen that the transition from "helicopter-like" motions to "airplane-like" motions is strongly influenced by the sign and magnitude of M_w. For example, at i_w equal to 35 degrees, if M_w is doubled, the dynamics will be very similar to those of a normal airplane; and if at i_w equal to 20 degrees, M_w is set equal to zero, the characteristic modes will be very similar to a conventional helicopter (Figure 30).

The horizontal center-of-gravity location will influence the term M_w as the forward speed increases and the variation of wing lift with vertical velocity becomes significant. In the design stage, then, some control over this derivative is available at higher trim speeds. Various programmed tail incidence settings have been suggested for these aircraft, and it should be realized that if the tail is programmed in such a way that it inadvertently stalls at some forward speed condition, then a marked unfavorable change in M_w can result because of the loss of the horizontal tail contribution (Figure 24). It may be difficult to estimate when stalling may occur due to lack of detailed knowledge of downwash angles at the tail. The possible changes in this derivative due to stalling of the horizontal tail are of considerably more significance than any effects that tail incidence may have on M_u because M_w has a stronger effect on the initial stages of the response.

Figure 26 indicates a trend of the characteristic modes that would be physically expected in changing from hovering to forward flight. That is, the unstable oscillation in hovering becomes the conventional phugoid mode in forward flight, and the two convergences present in hovering form the short-period mode in forward flight. A somewhat more peculiar transition of the modes occurs if the lift curve slope Z_w or the pitch damping M_θ of the vehicle remains very small, as may be seen from Figures 28 and 29. In these cases, the unstable oscillation becomes the short-period mode in forward flight and the two real roots become the phugoid. This is probably an unusual tendency since for any reasonable vehicle configuration the lift curve slope would increase with forward speed. If the lift curve slope remains zero, the airplane would certainly have peculiar handling qualities from other considerations. Also, if the angular damping is small, the dynamics would be poor.

To summarize the results of this section, the following additional comments are made.

With respect to the unstable mode that becomes the conventional phugoid mode as the trim speed increases, the stability derivative M_u is very important in determining the motion characteristics, until flight conditions are encountered where M_w becomes large. The large values of M_w (in this case $i_w \leq 20^\circ$) tend to wash out the effects of M_u. The damping of this mode is primarily determined by X_u and M_q. The angular damping M_q becomes less important as the period becomes longer.

At low speeds, the other modes consist of two convergences; the large root is determined by X_u and M_q and the small root by Z_w. It is a peculiarity of these aircraft at low speeds that $|X_u| > |M_q|$, which is opposite from the usual case of a helicopter (Reference 12). These two real roots combine to become an oscillatory motion as M_w increases with trim speed. This oscillatory mode is primarily determined by M_w, $M_{\dot{\theta}}$ and Z_w, as would be expected on the basis of the conventional short-period approximation (Reference 11).

COMPARISON OF THEORY AND EXPERIMENT

Comparisons of the theory presented here and experimental data measured on a 0.10 scale model using the Princeton Dynamic Model Track are shown in Figures 32 through 36. A detailed discussion of the experimental results appears in Reference 20. In particular, various nonlinearities appeared in the experimental results that are not considered here.

The comparison of trim velocity and wing incidence is shown in Figure 32. The model exhibited higher trim velocities than calculated by the theory. Inspection of Equation (20b), which is an approximation to the trim velocity/wing incidence relationship, indicates either that the flap effectiveness used in the calculations was higher than actually present on the model or that the wing lift curve slope in the slipstream is smaller than the theoretical value.

However, as noted in the previous section, the horizontal velocity derivatives are not particularly sensitive to the calculation of trim velocity. If the horizontal velocity derivatives are reasonably linear, then it is implied that they are not strongly dependent upon trim velocity. Therefore, no attempt was made to improve this trim calculation before proceeding with the derivative comparisons. It is felt that considerably more detailed aerodynamic information would be desirable before proceeding into further specific investigations of this nature; that is, to decide exactly which terms are in error.

For the derivative comparisons, only the force and moment variations with horizontal velocity are considered here since these were all reasonably linear. The comparisons are shown in Figures 33, 34 and 35. While the general trend of the derivatives is predicted, the agreement is not particularly good. The term M_u is predicted reasonably well in hovering,

but experimentally decreases considerably faster than the theoretical value. The term X_u is underestimated in hover and agrees reasonably well at lower incidence angles. The term Z_u is predicted reasonably well at incidence angles above 60°. The general indications are that at high incidence angles, $\frac{\partial L_s}{\partial u}$ is predicted reasonably well, but that the prediction becomes poorer as the trim speed is increased. This is probably due to the term arising from the lift curve slope variation which becomes quite large at low incidence as well as increased areas of separation on the wing, arising from the increase in average effective wing angle of attack (Figure 5). Thus, it appears that $\frac{\partial L_s}{\partial u}$ is overestimated. It is also possible that the contributions of the horizontal tail to the derivative M_u are considerably different than indicated by Figure 23. That is, the slipstream may produce dynamic pressures at the tail that are considerably greater than free stream, causing larger effects than shown in Figure 23. The experimental values of M_u presented differ somewhat from those obtained in a preliminary analysis of the data made by LTV. Detailed analysis of the static and dynamic data (Reference 20) by Princeton indicates that M_u is negative in the vicinity of 60° wing incidence as shown.

The experimental and theoretical comparison of the pitch damping is shown in Figure 36. The theoretical and experimental comparison was made without tail rotor. The agreement with the general trend of this derivative is good. While at very low speeds, the percentage error is large, the actual derivative is so small that it is probably unreasonable to expect better agreement, and the correct order of magnitude is obtained.

No comparison is made of the derivatives due to vertical velocity because of the nonlinearities appearing in this data. The majority of this theoretical work was completed prior to a detailed investigation of the experimental data (Reference 20). Further remarks on the comparison of this theory with experiment will be found in Reference 20.

CONCLUSIONS

For the example configuration studied, a tilt-wing VTOL aircraft of the XC-142A class with double slotted flaps, and the assumptions made, the following general conclusions are stated:

1. In order to predict accurately the trim velocity/wing incidence relationship and the pitching moment required to trim during transitions of tilt-wing VTOL type vehicles, it is necessary to have precise knowledge of:

    a. The aerodynamic characteristics of the wing/flap combination with the authentic slipstream/relative wind flow field representation.

    b. The aerodynamic characteristics of the horizontal tail, with attention to the downwash behavior and dynamic pressure variations.

2. Correlation with experimental data may be poor because of the assumed values of the wing lift curve slope and the flap effectiveness. It appears on the basis of the predicted "wing incidence/forward speed" relationship and the importance of the wing contributions to the stability derivatives X_u and M_u that the assumed wing lift curve slope is too high in the wing incidence range between 70° and 40°.

    Data available after this report was written indicate that the assumed flap effectiveness did not correspond well with the experimental value.

3. On the basis of the analysis, the propeller inplane force and wing drag appear to have relatively small contributions to the stability derivatives.

4. The slipstream/wing lift variations dominate the changes in the vehicle stability derivatives at slow speeds. The propeller thrust force variations do give appreciable contributions, but they appear to be relatively less significant when compared to the gross changes in the derivatives caused by the slipstream/wing lift variations. This particular relative proportion of changes is due to some extent to the layout design or geometry of the vehicle studied, but the example configuration geometry is generally typical of tilt-wing-type aircraft.

5. On the basis of a limited comparison with experimental results from a scale model of the XC-142A, the important stability derivatives were predicted quite well in hovering, and the general trend with decreasing incidence was predicted; however, the magnitudes predicted are considerably in error for wing incidences representing the region of

flight midway through transition (around 45 degrees). The assumed configuration is somewhat dissimilar from the scale model.

6. Favorable effects on the attitude stability (M_w) and pitch damping (M_q) arise from the increasing dynamic pressure at the tail as wing incidence is reduced.

7. The change in stability characteristics from "helicopter-like" dynamics at high incidence to "airplane-like" dynamics at low incidence is largely determined by the magnitude and sign of the attitude stability (M_w) of the vehicle.

RECOMMENDATIONS

1. Further comparison of this theory with experiment is desirable. It would be valuable to pursue comparison of the expressions developed with various experimental data on isolated components available before proceeding with further comparisons of complete configurations.

2. Due to the increasing importance of the horizontal tail in providing favorable effects as the incidence decreases, experimental information on downwash characteristics in the vicinity of the horizontal tail of tilt-wing configurations is desirable.

3. Consideration should be given to the importance of nonlinearities in regions where the linearized theory predicts derivatives near zero, as for example in the region where the attitude stability (M_w) changes sign.

4. Since there is at present considerable experimental information on the aerodynamic characteristics of wing-propeller combinations, these data should be organized in such a fashion as to verify the semi-empirical approach used to predict wing lift curve slope, or to suggest modification to the form used here.

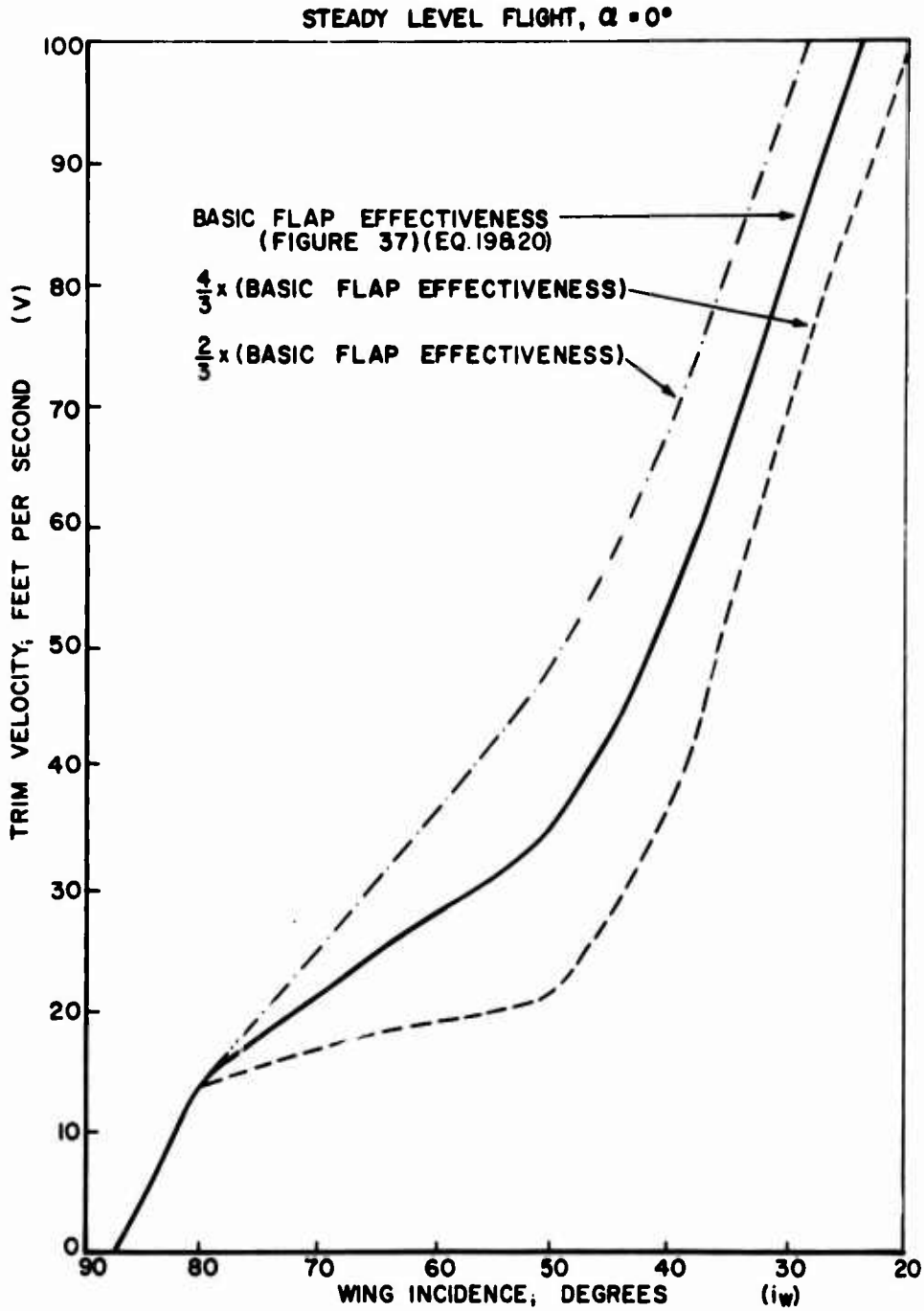

FIGURE 1. TRIM VELOCITY VS. WING INCIDENCE ANGLE FOR VARIOUS VALUES OF FLAP EFFECTIVENESS.

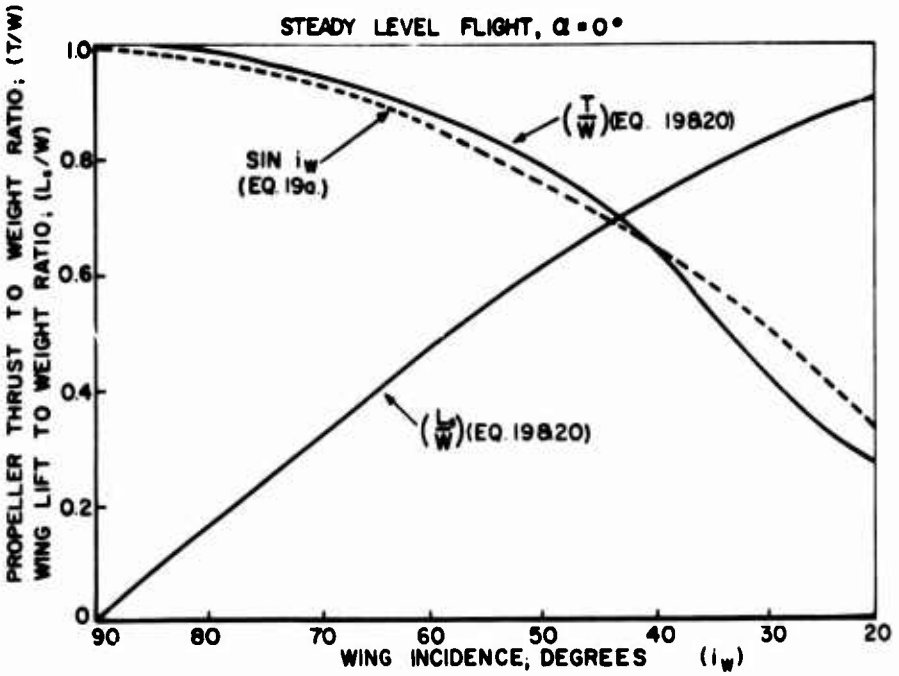

FIGURE 2. PROPELLER THRUST AND WING LIFT VS. WING INCIDENCE.

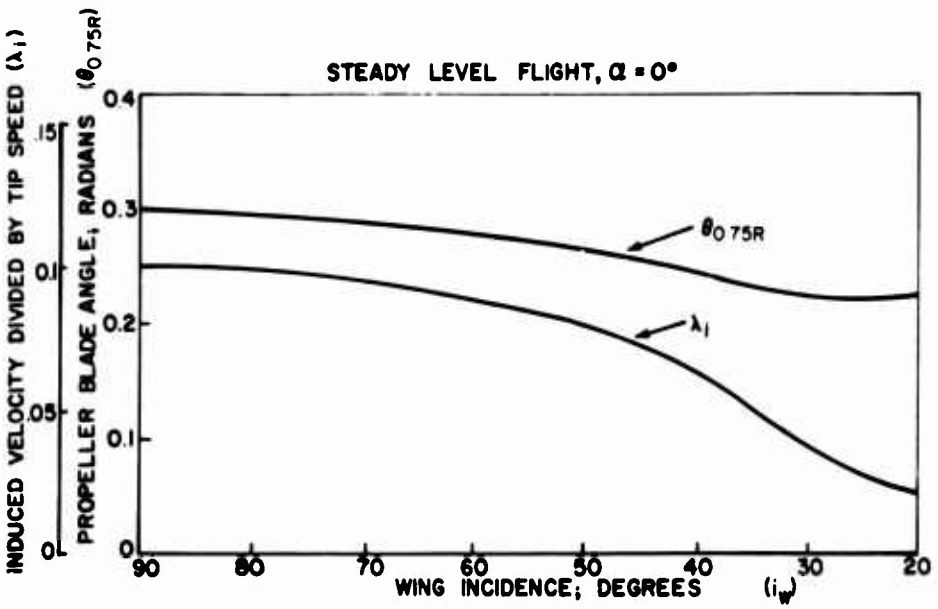

FIGURE 3. PROPELLER BLADE ANGLE AND NONDIMENSIONAL INDUCED VELOCITY VS. WING INCIDENCE.

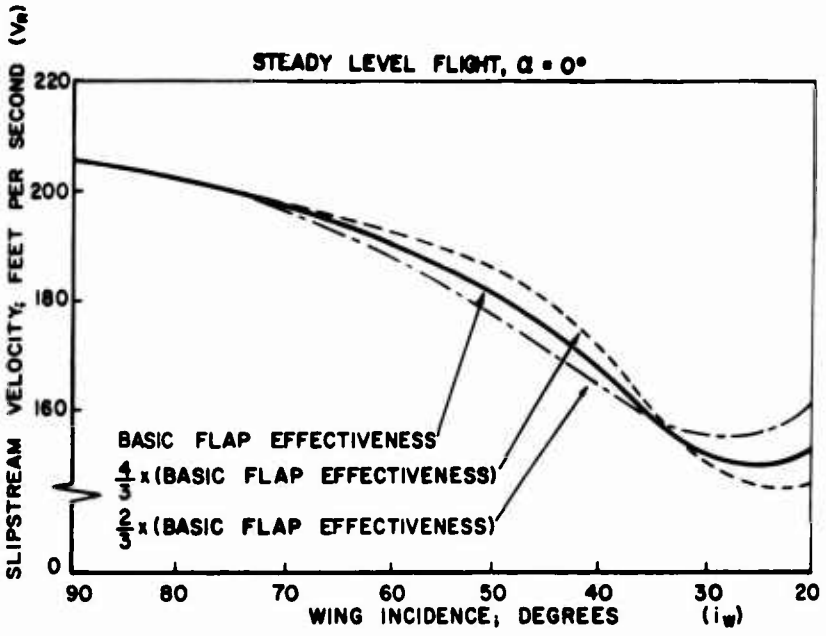

FIGURE 4. SLIPSTREAM VELOCITY VS. WING INCIDENCE FOR VARIOUS VALUES OF FLAP EFFECTIVENESS.

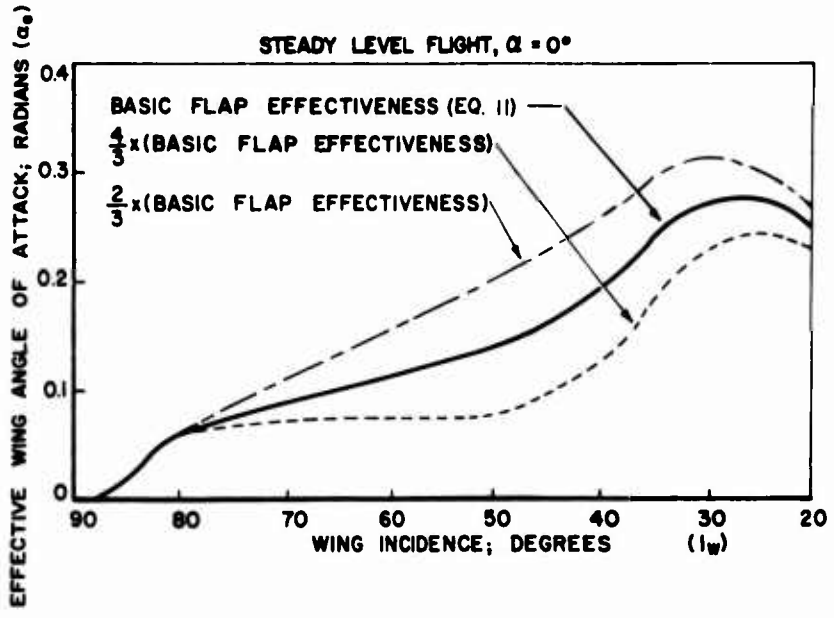

FIGURE 5. EFFECTIVE WING ANGLE OF ATTACK VS. WING INCIDENCE.

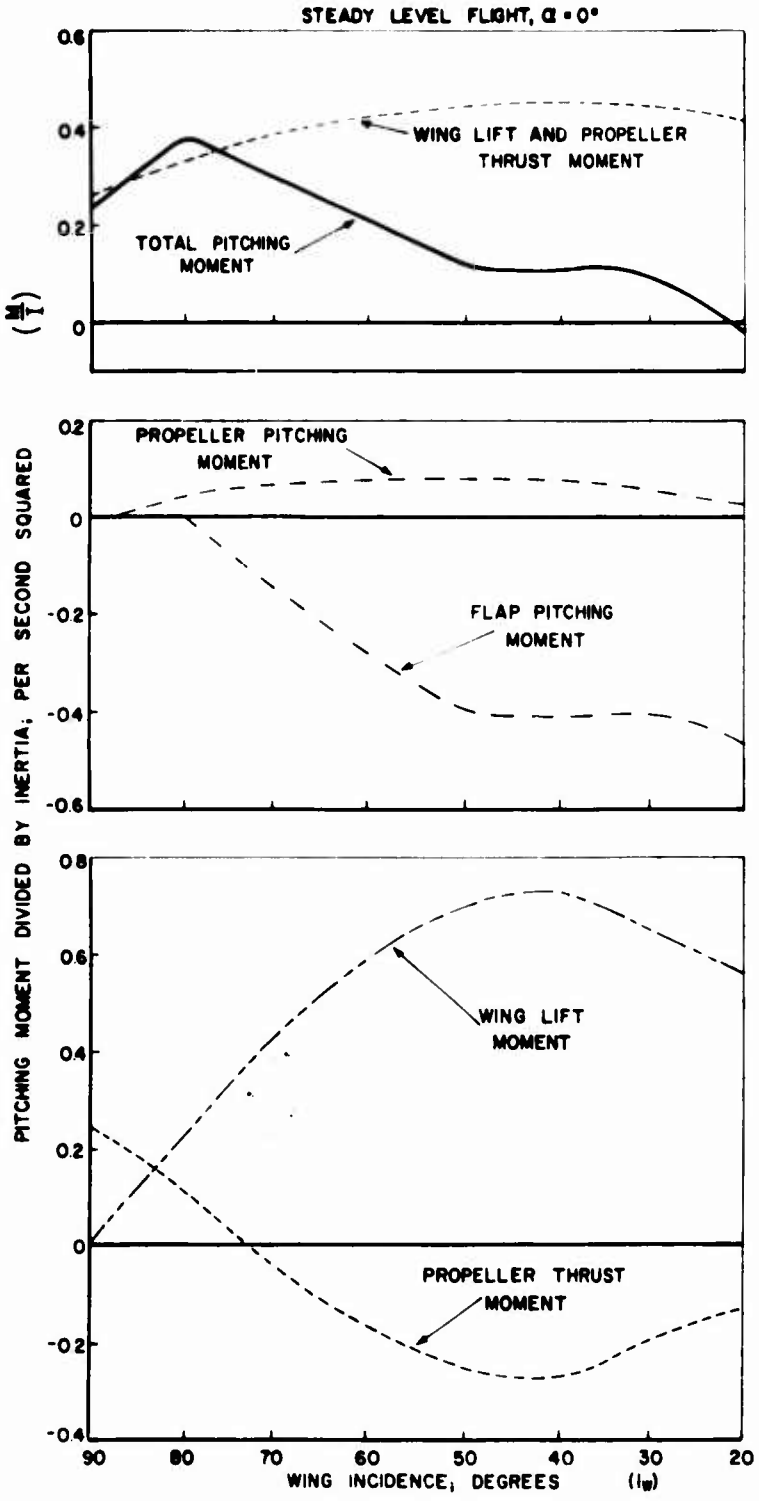

FIGURE 6. PITCHING MOMENT REQUIRED TO TRIM VS. WING INCIDENCE.

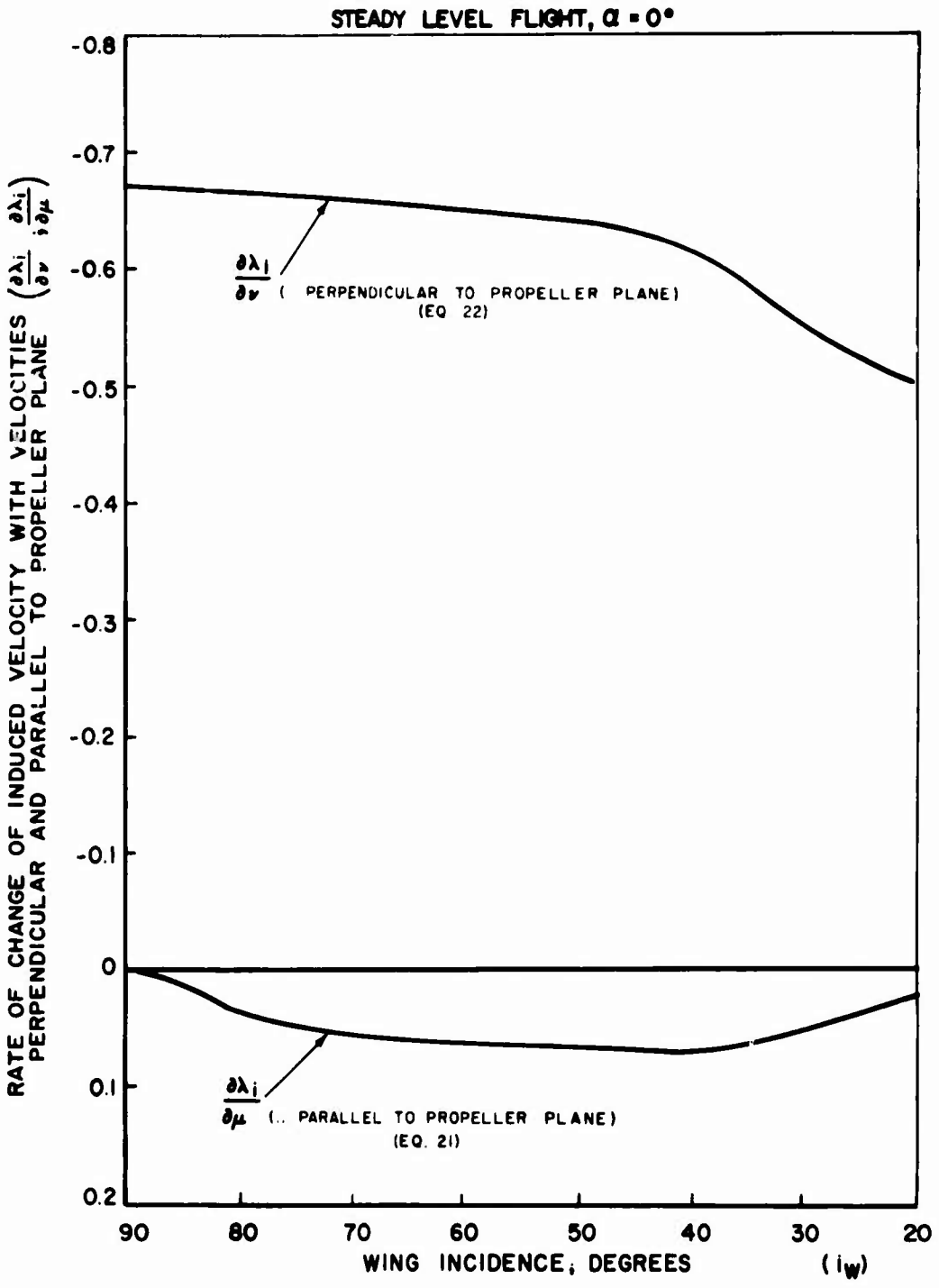

FIGURE 7. INDUCED VELOCITY DERIVATIVES VS. WING INCIDENCE.

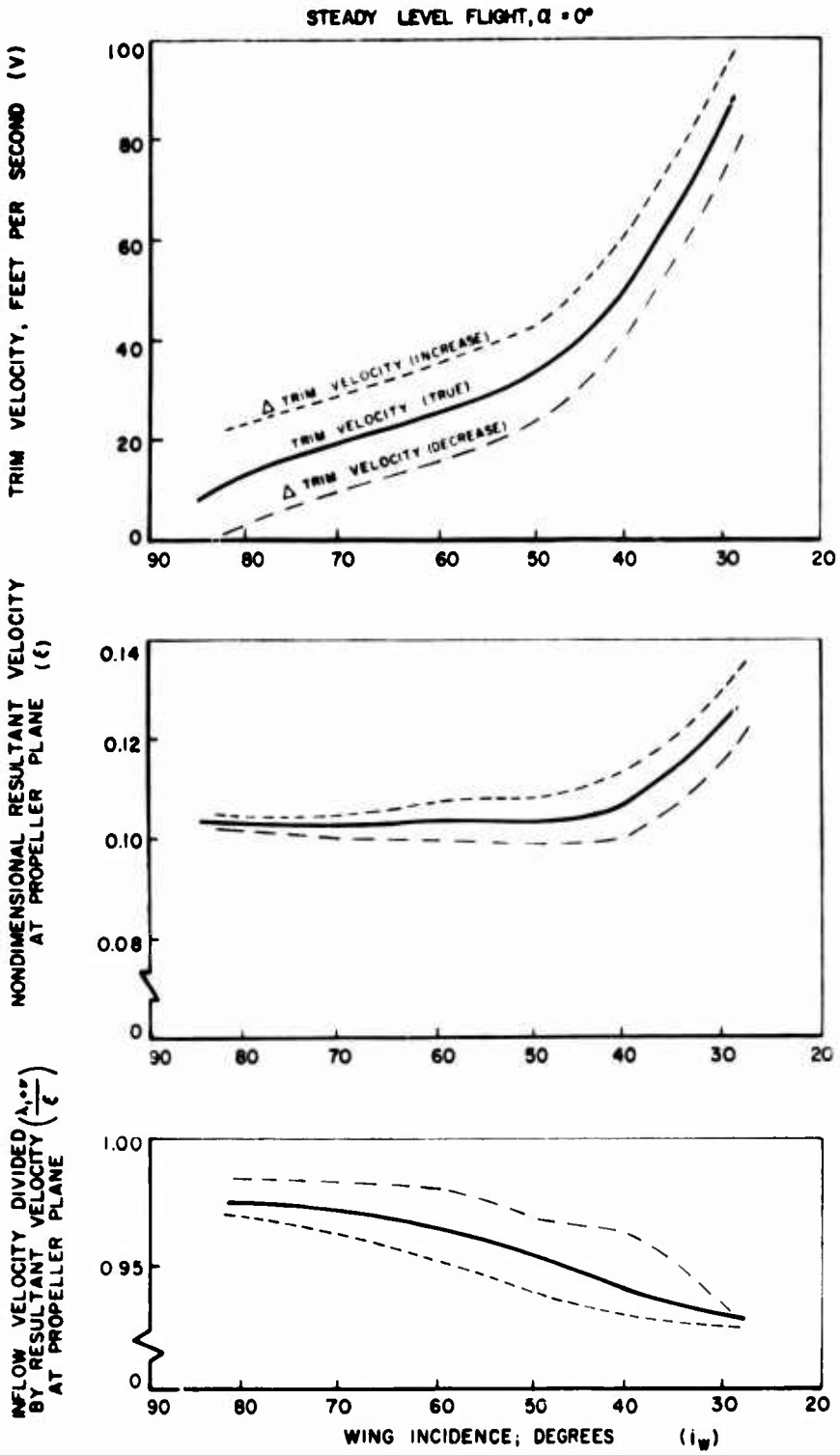

FIGURE 8. VELOCITIES AT PROPELLER PLANE VS. WING INCIDENCE AS A FUNCTION OF TRIM VELOCITY.

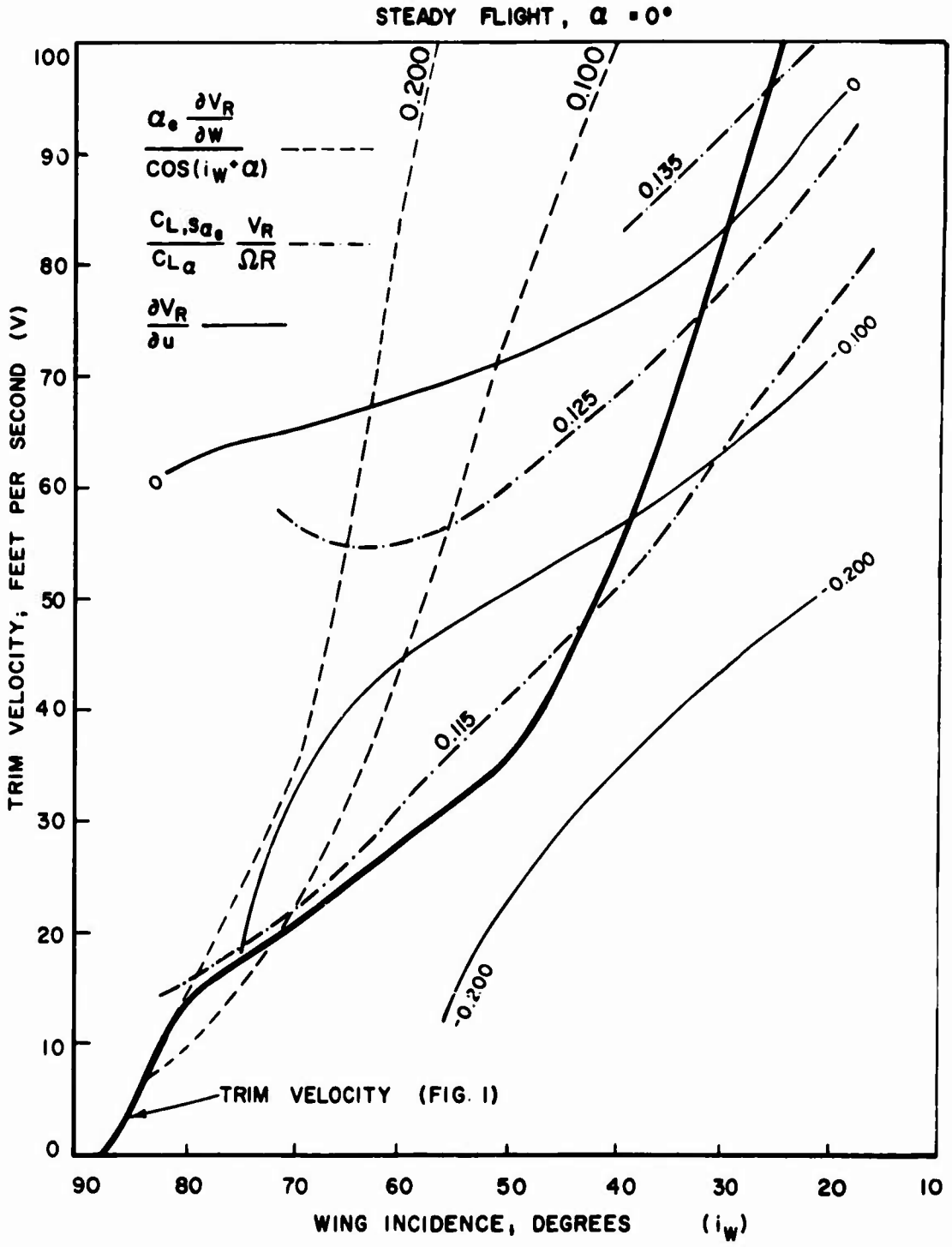

FIGURE 9. DEPENDANCE OF VARIOUS SLIPSTREAM PARAMETERS ON WING INCIDENCE / TRIM VELOCITY RELATIONSHIP.

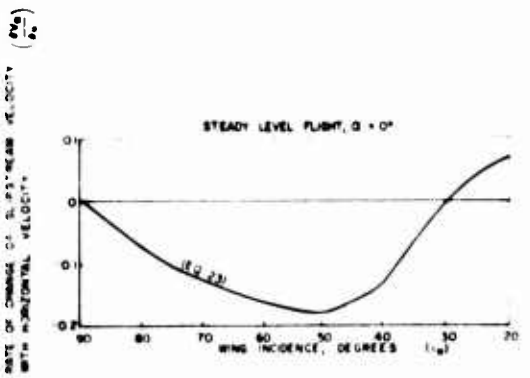

FIGURE 10 RATE OF CHANGE OF SLIPSTREAM VELOCITY WITH HORIZONTAL VELOCITY VS WING INCIDENCE

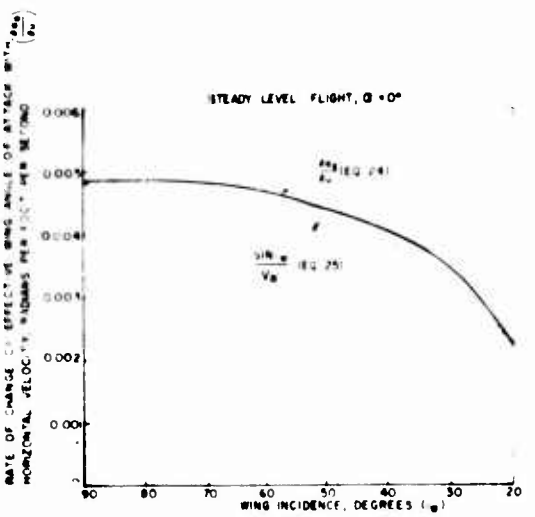

FIGURE 11 RATE OF CHANGE OF EFFECTIVE WING ANGLE OF ATTACK WITH HORIZONTAL VELOCITY VS WING INCIDENCE

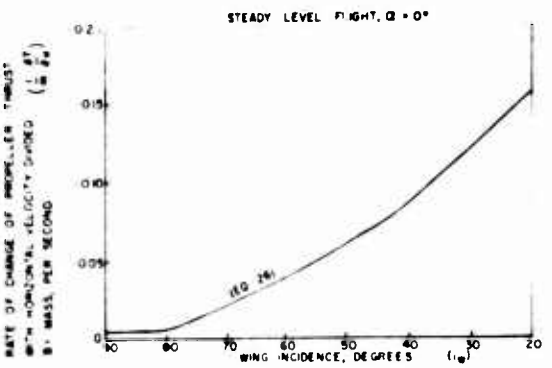

FIGURE 12 RATE OF CHANGE OF THRUST WITH HORIZONTAL VELOCITY VS WING INCIDENCE

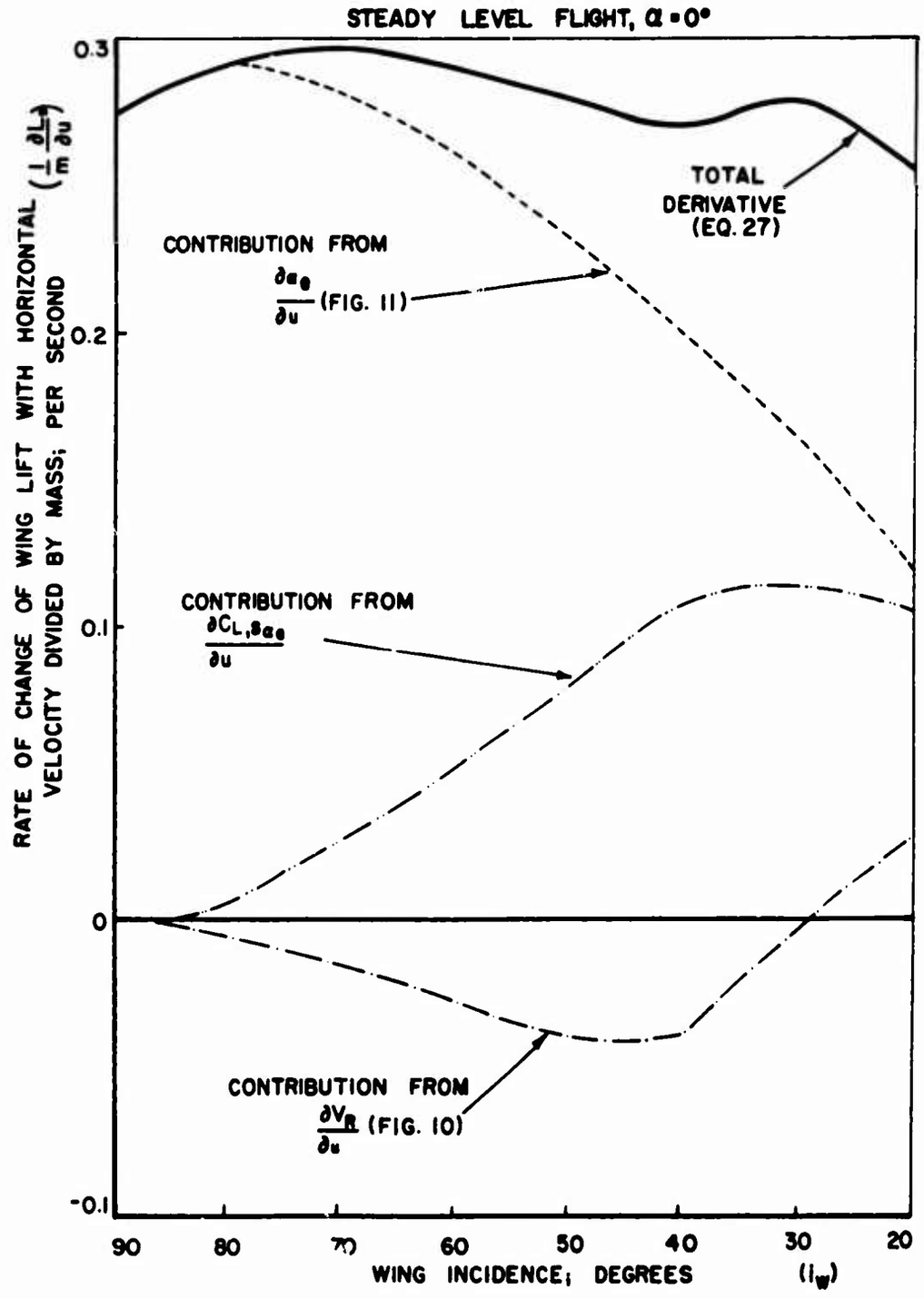

FIGURE 13. RATE OF CHANGE OF WING LIFT WITH HORIZONTAL VELOCITY VS. WING INCIDENCE.

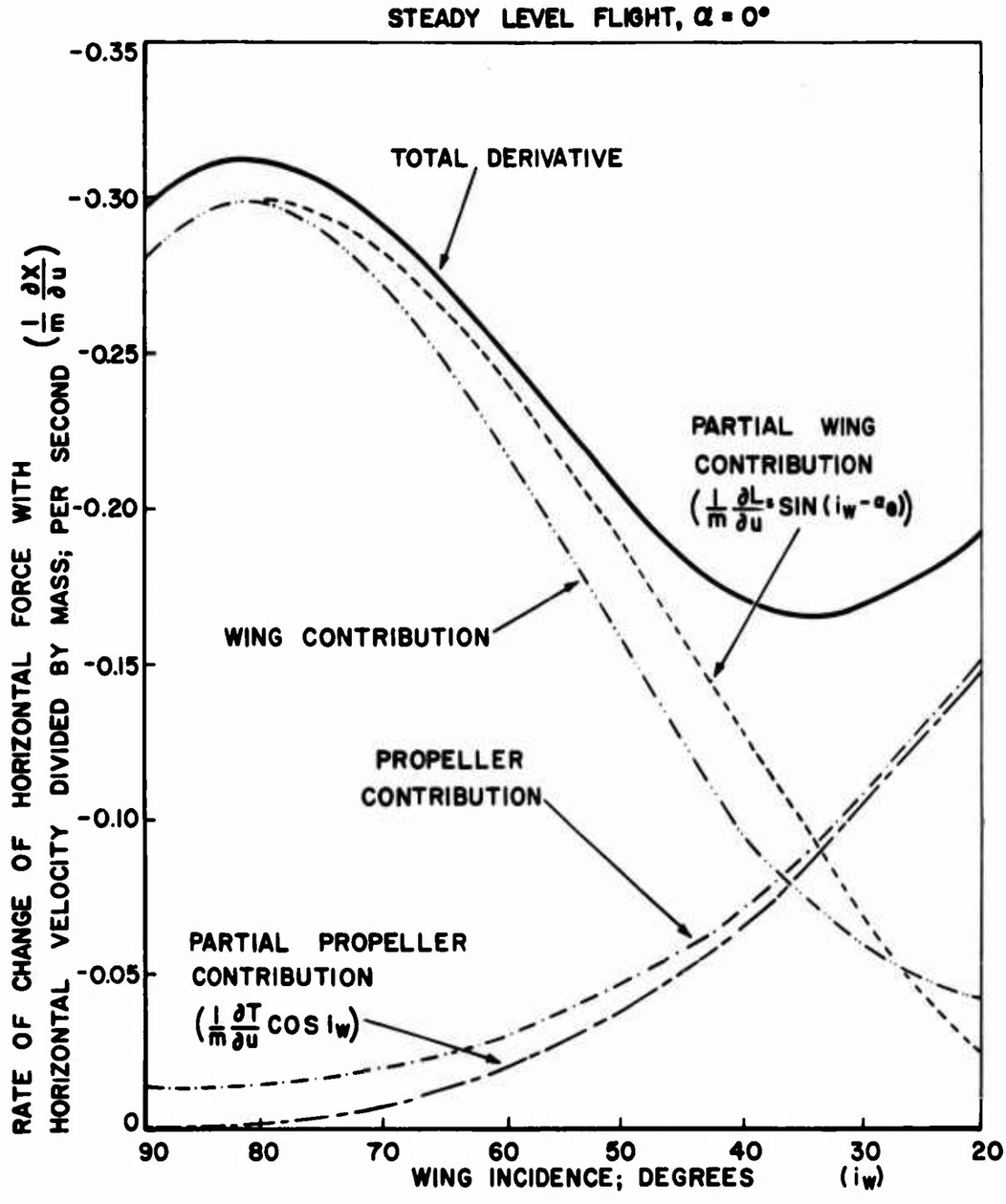

FIGURE 14. STABILITY DERIVATIVES - RATE OF CHANGE OF HORIZONTAL FORCE WITH HORIZONTAL VELOCITY VS. WING INCIDENCE.

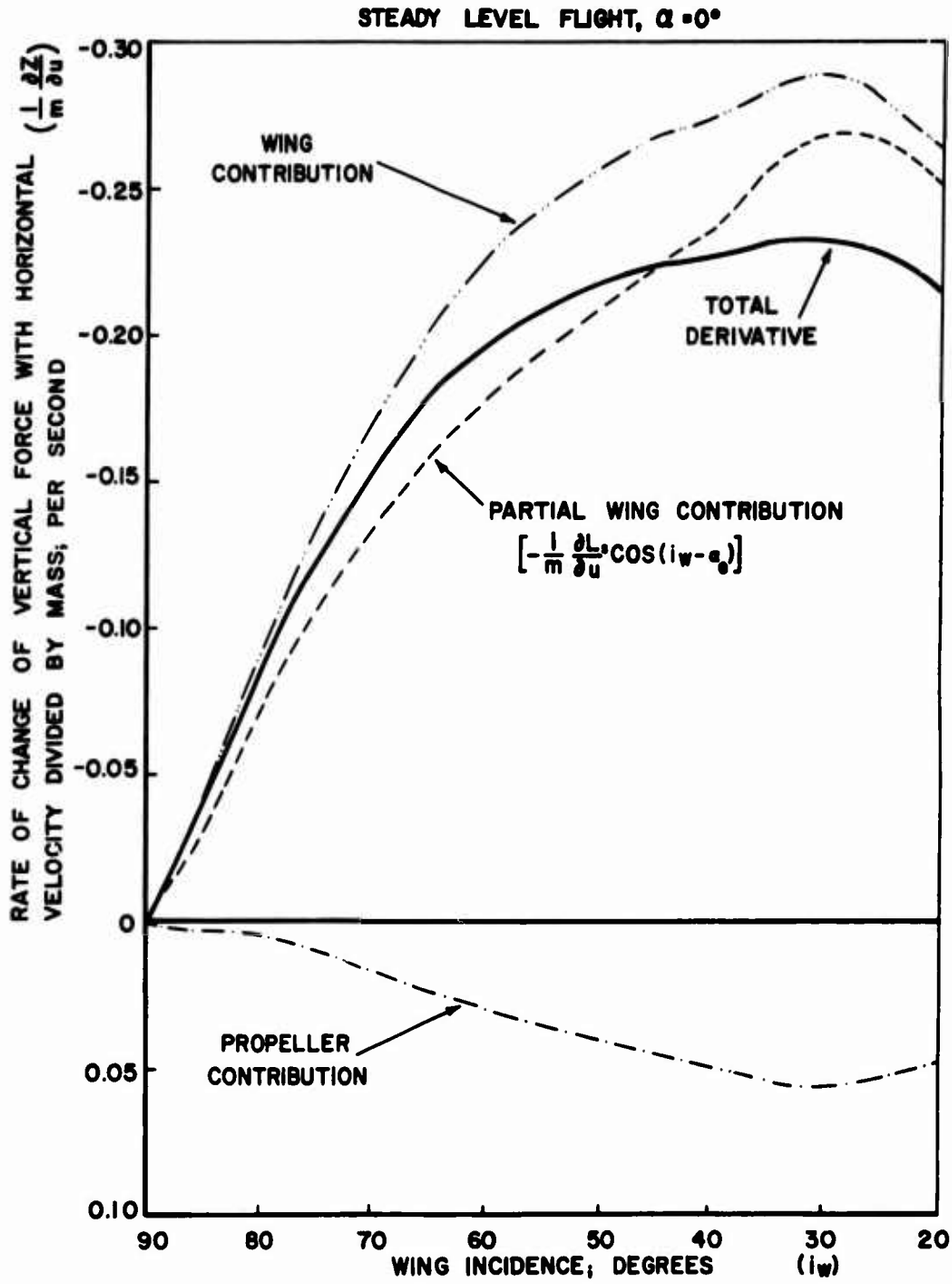

FIGURE 15. STABILITY DERIVATIVES - RATE OF CHANGE OF VERTICAL FORCE WITH HORIZONTAL VELOCITY VS. WING INCIDENCE.

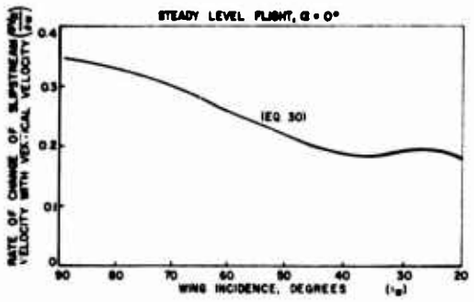

FIGURE 16 RATE OF CHANGE OF SLIPSTREAM VELOCITY WITH VERTICAL VELOCITY VS WING INCIDENCE

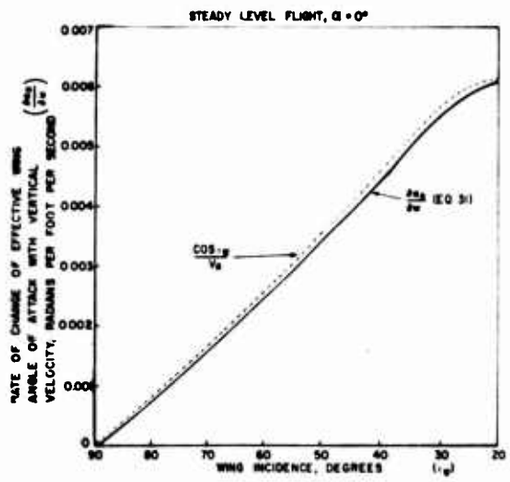

FIGURE 17 RATE OF CHANGE OF EFFECTIVE WING ANGLE OF ATTACK WITH VERTICAL VELOCITY VS WING INCIDENCE

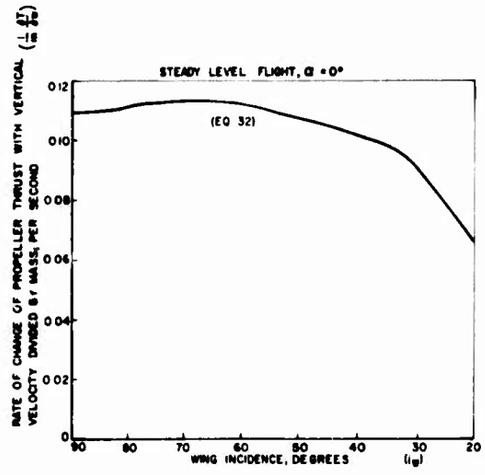

FIGURE 18 RATE OF CHANGE OF PROPELLER THRUST WITH VERTICAL VELOCITY VS WING INCIDENCE

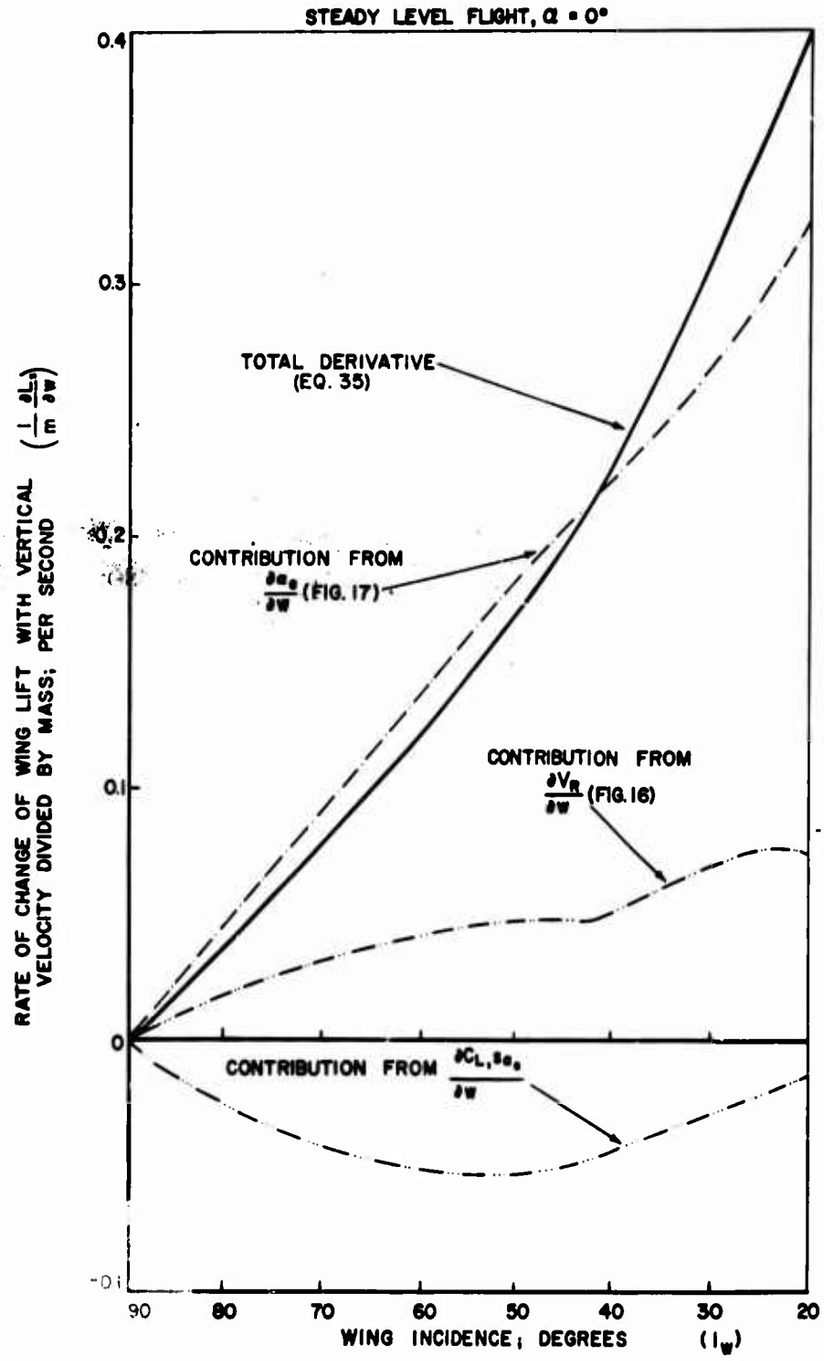

FIGURE 19. RATE OF CHANGE OF WING LIFT WITH VERTICAL VELOCITY VS. WING INCIDENCE.

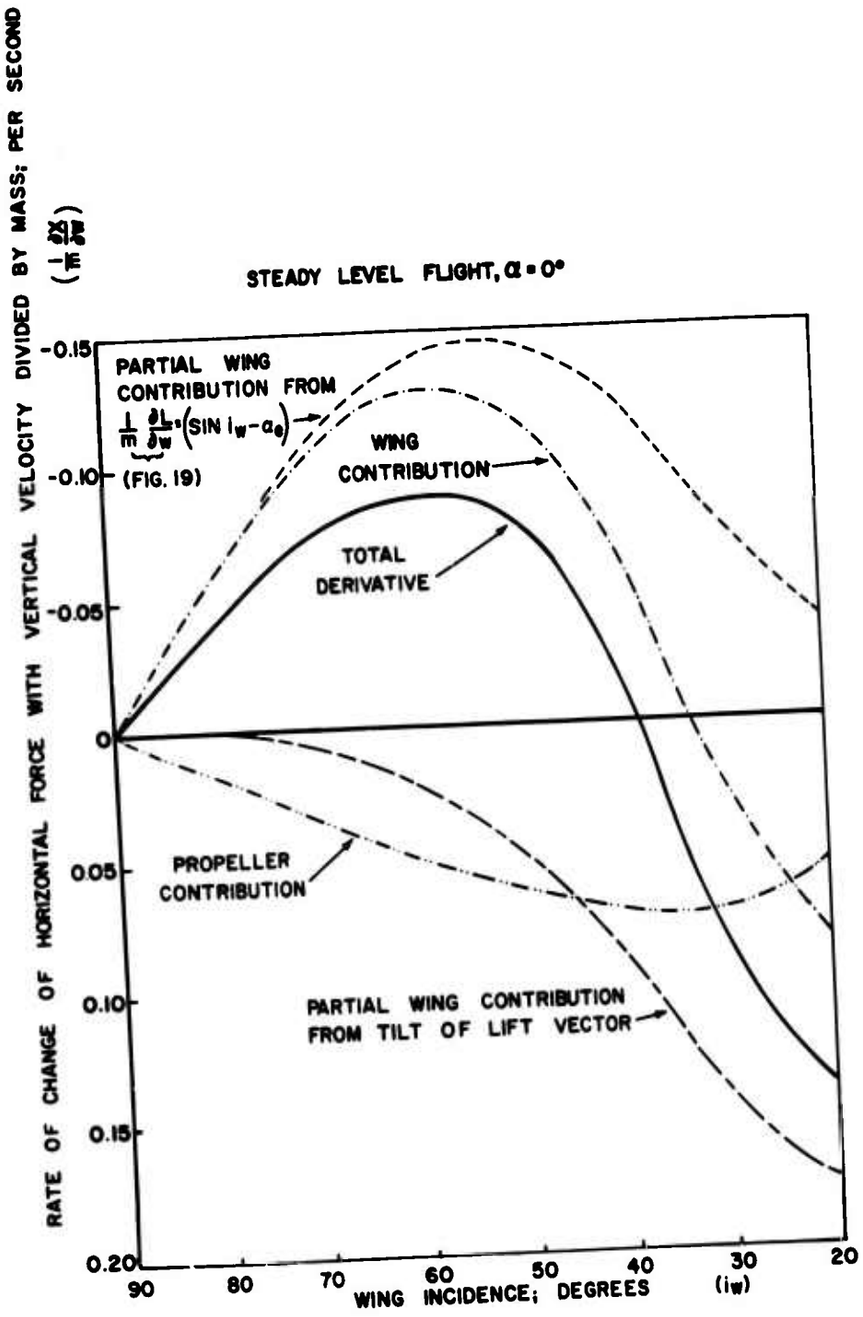

FIGURE 20. STABILITY DERIVATIVES - RATE OF CHANGE OF HORIZONTAL FORCE WITH VERTICAL VELOCITY VS. WING INCIDENCE.

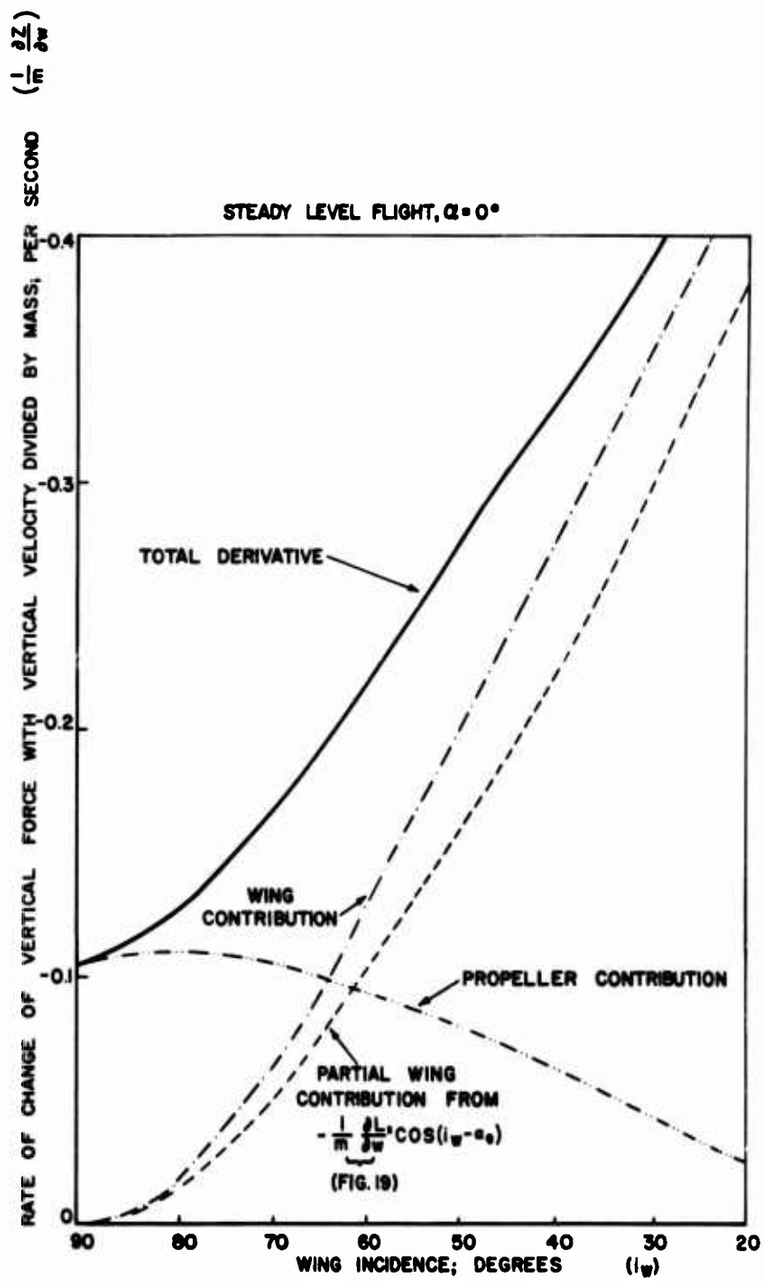

FIGURE 21. STABILITY DERIVATIVES - RATE OF CHANGE OF VERTICAL FORCE WITH VERTICAL VELOCITY VS. WING INCIDENCE.

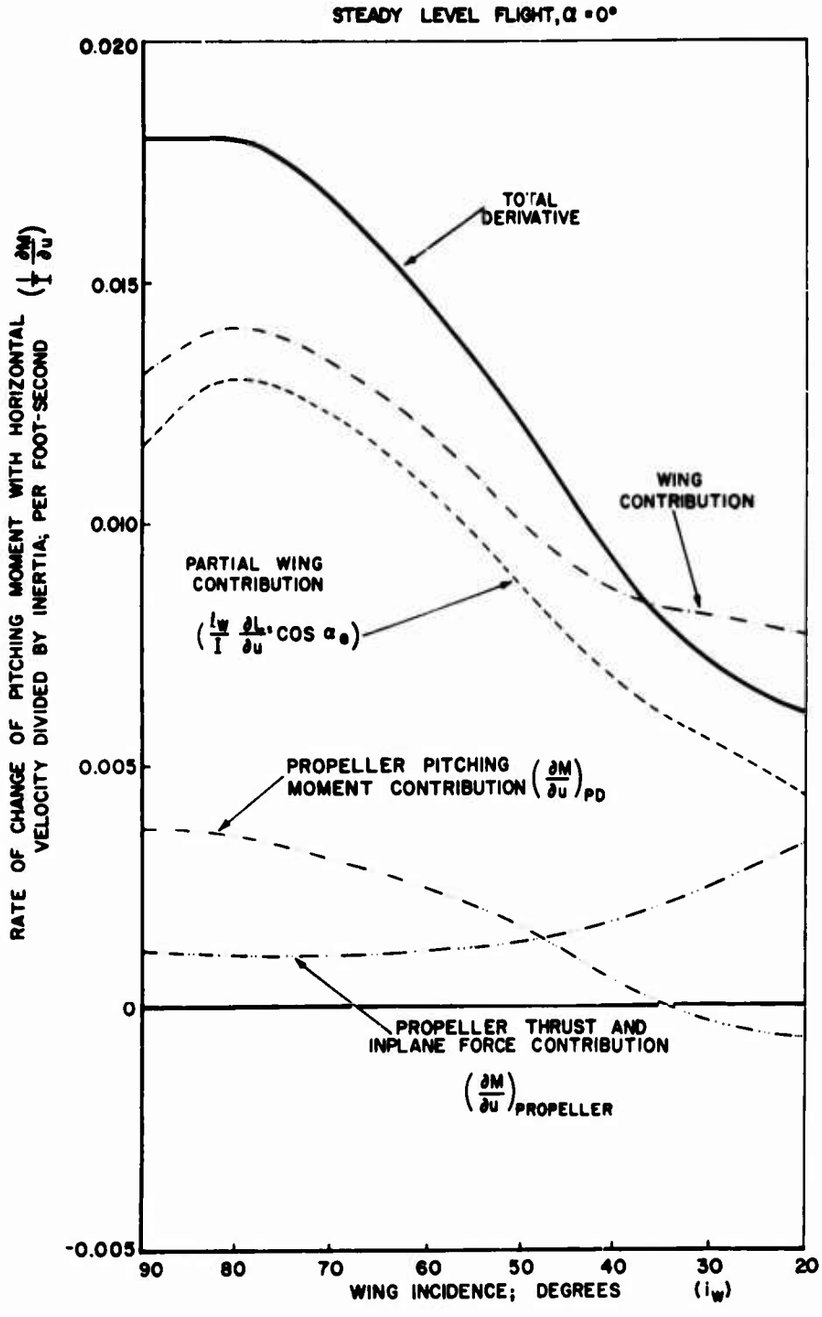

FIGURE 22. STABILITY DERIVATIVES - RATE OF CHANGE OF PITCHING MOMENT WITH HORIZONTAL VELOCITY VS. WING INCIDENCE. (NO HORIZONTAL TAIL)

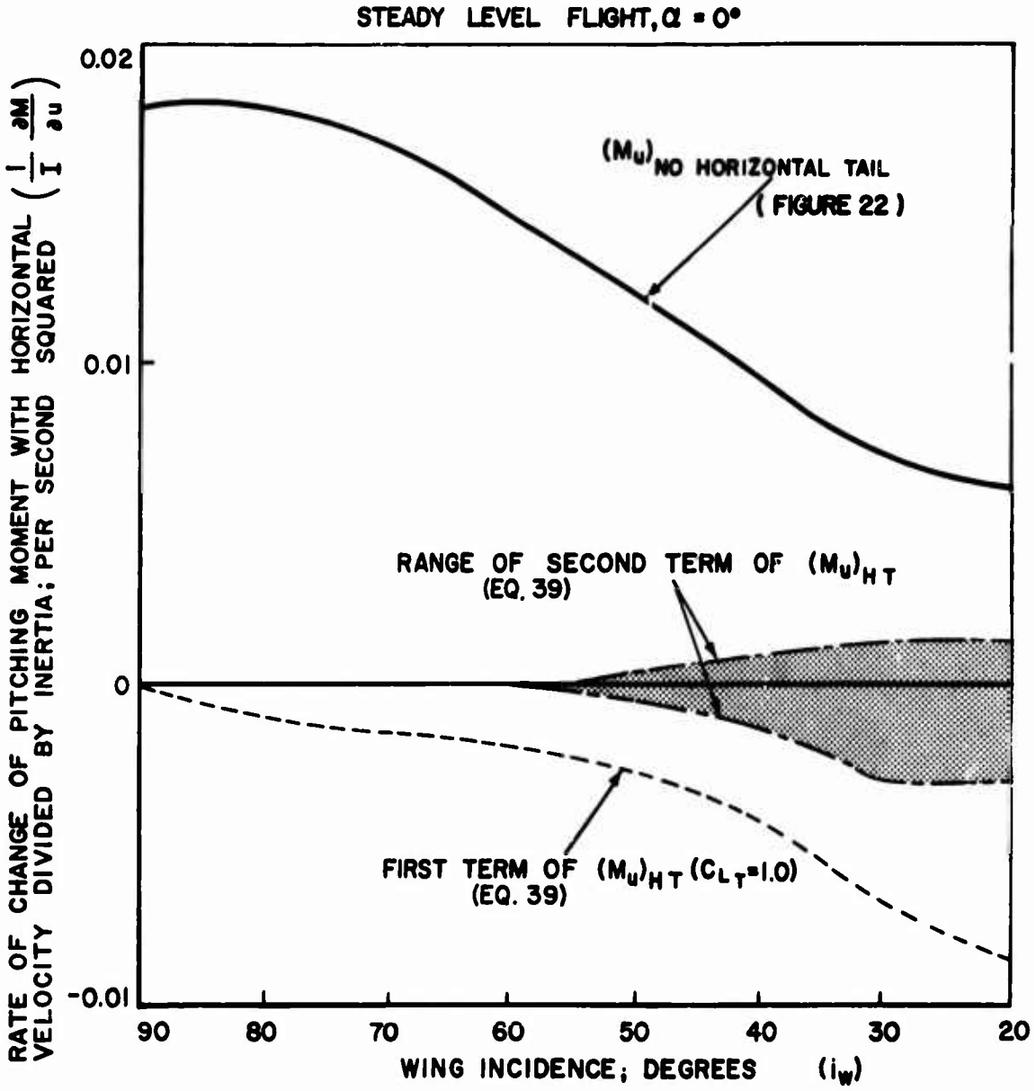

$$(M_u)_{HT} = -\rho V S_T \ell_{HT} C_{L_T} - \frac{1}{2}\rho V^2 S_T C_{L_{\alpha_T}} \ell_{HT}\left(\frac{\partial \epsilon}{\partial u} + \frac{\partial \epsilon_R}{\partial u}\right)$$

(EQ. 39, p. 23)

FIGURE 23. HORIZONTAL TAIL CONTRIBUTIONS TO PITCHING MOMENT CHANGE WITH HORIZONTAL VELOCITY.

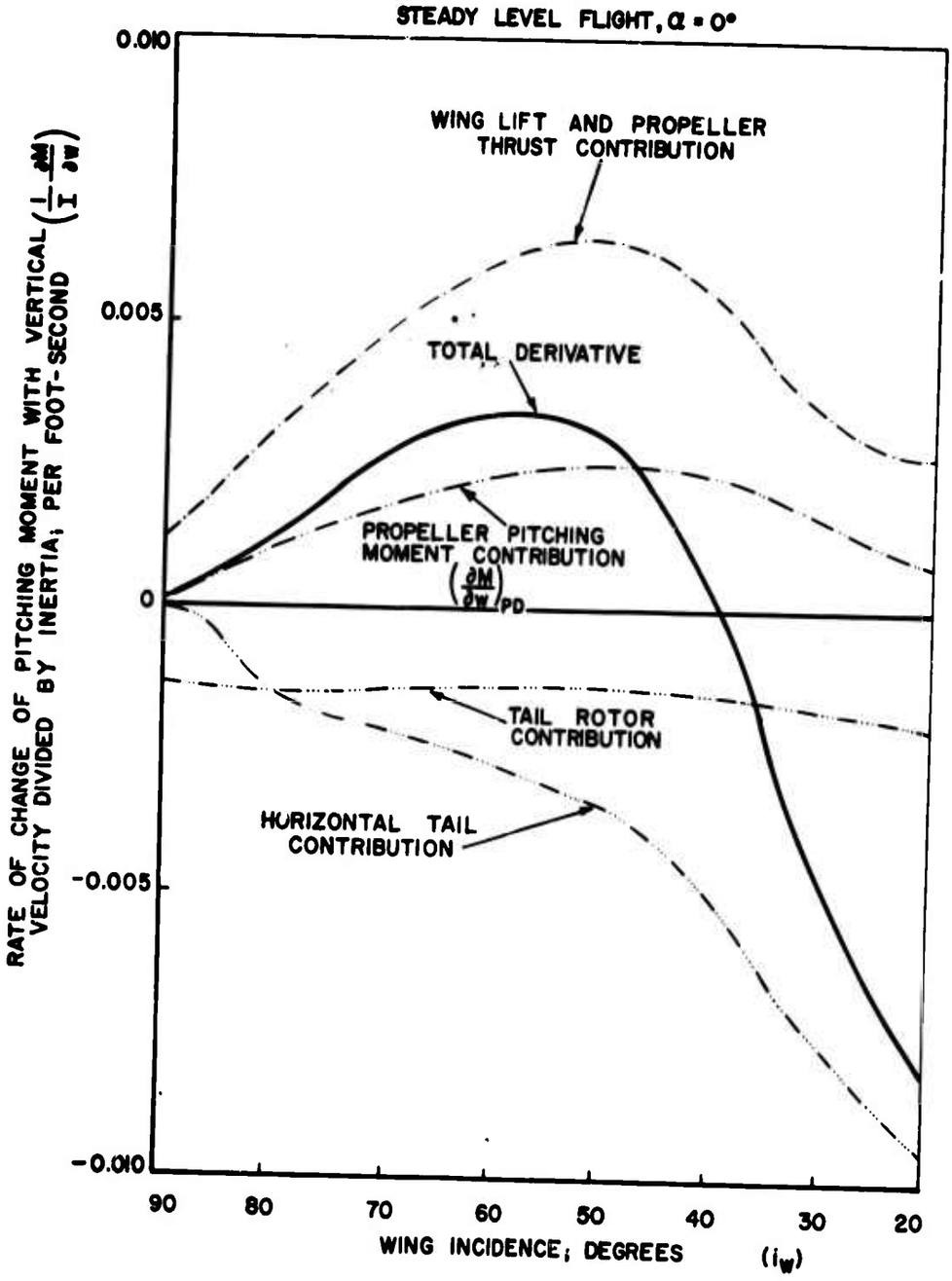

FIGURE 24a. STABILITY DERIVATIVES - RATE OF CHANGE OF PITCHING MOMENT WITH VERTICAL VELOCITY VS. WING INCIDENCE.

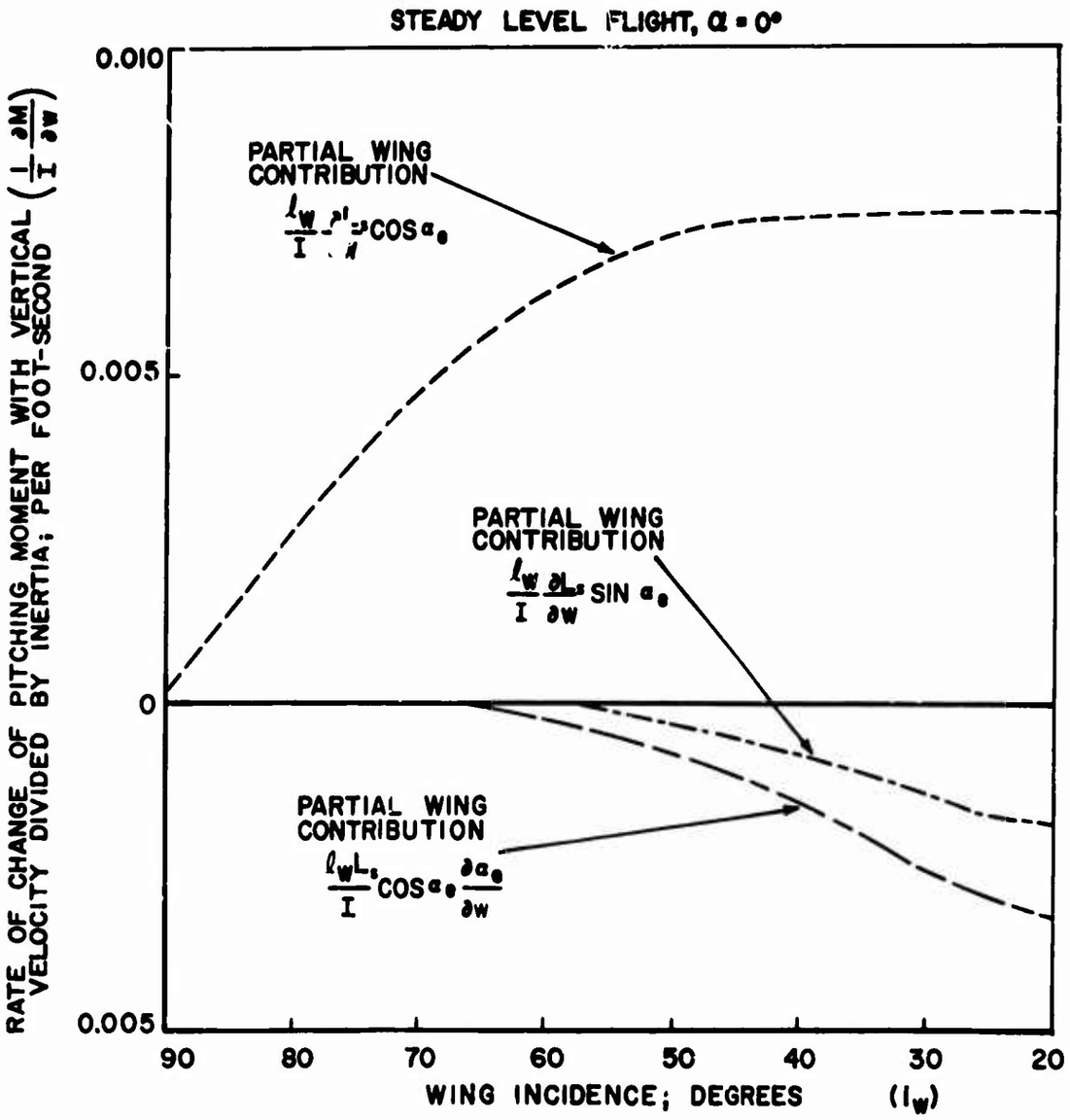

FIGURE 24b. WING CONTRIBUTIONS TO RATE OF CHANGE OF PITCHING MOMENT WITH VERTICAL VELOCITY VS. WING INCIDENCE.

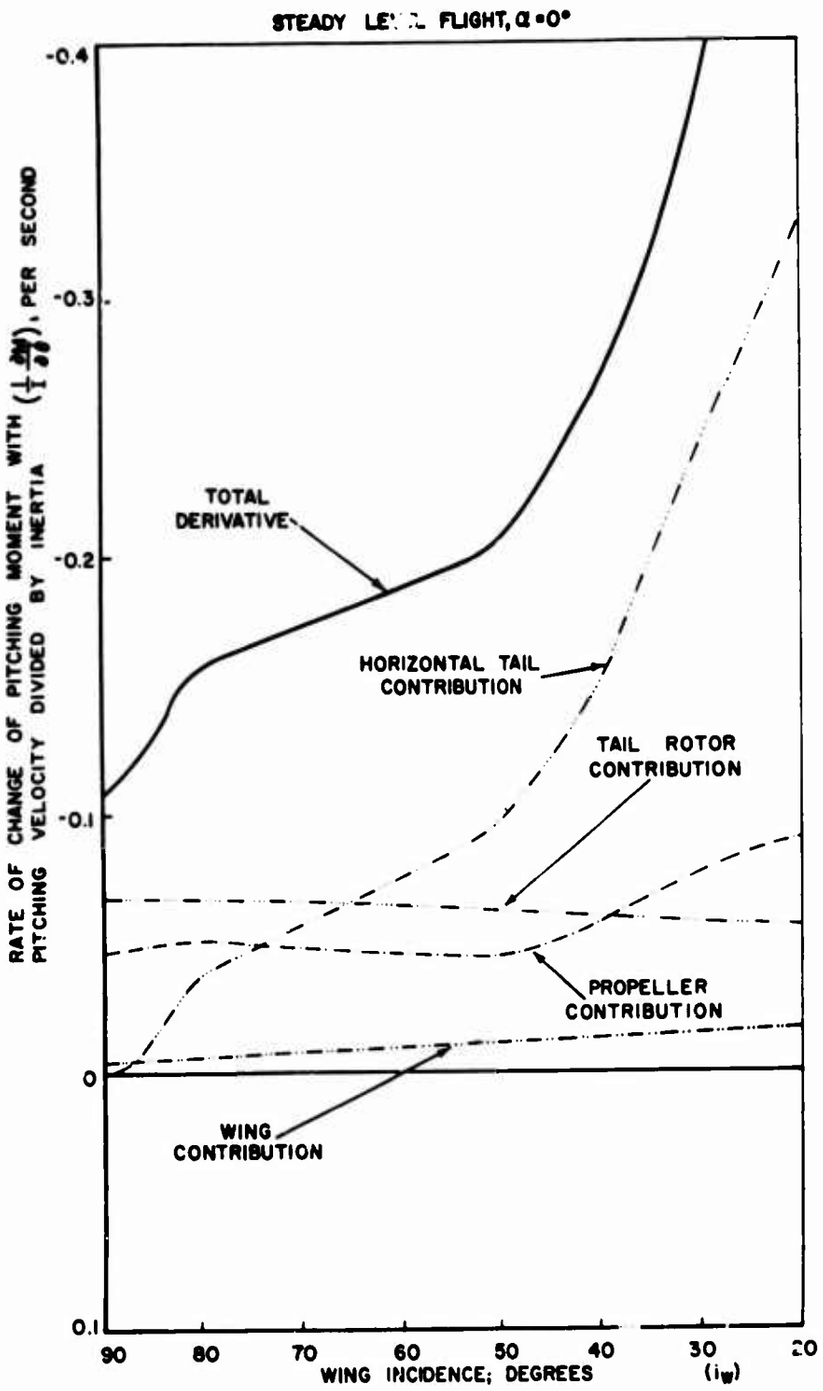

FIGURE 25. RATE OF CHANGE OF PITCHING MOMENT WITH PITCHING VELOCITY VS. WING INCIDENCE.

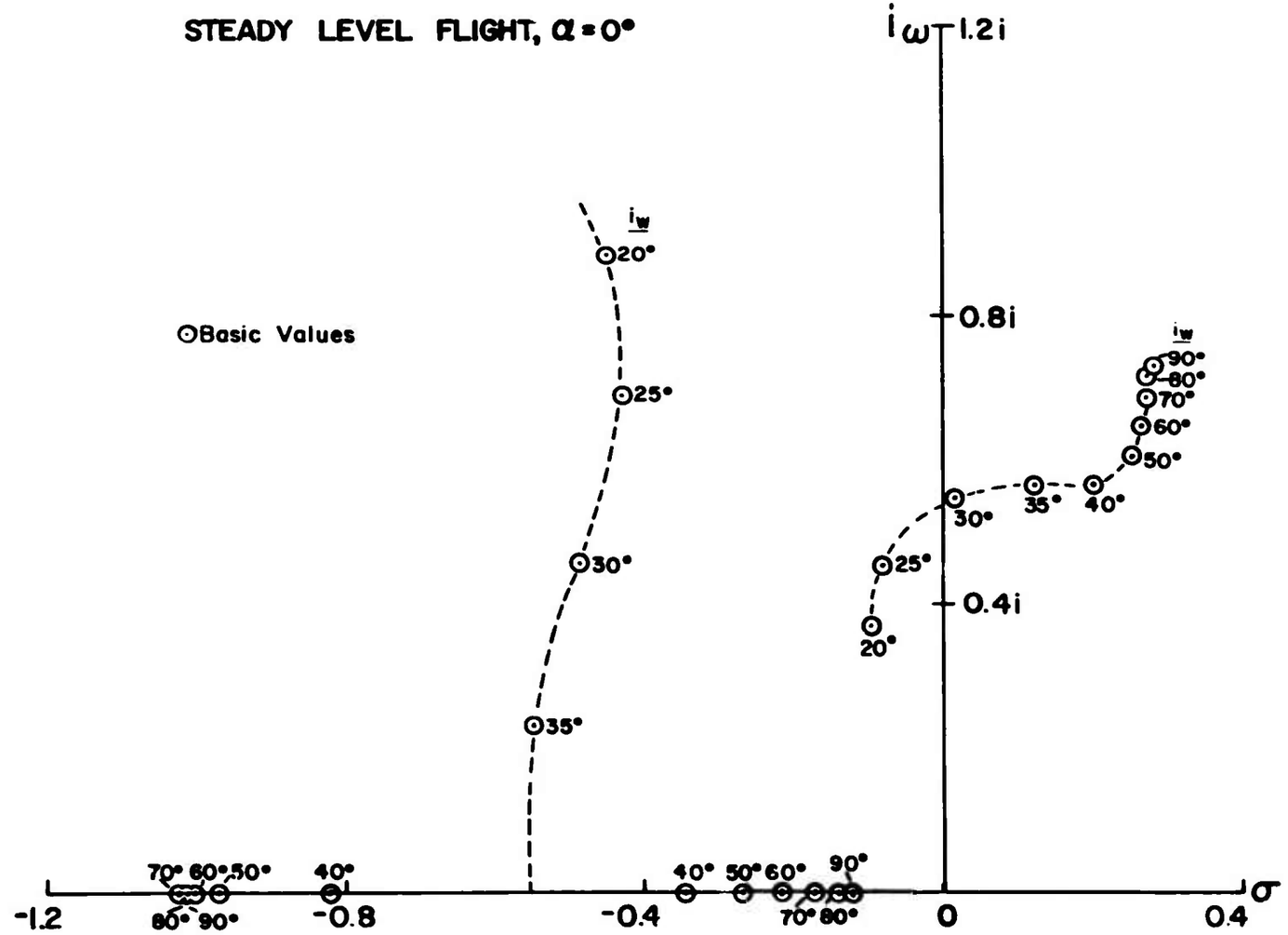

FIGURE 26. LOCUS OF ROOTS AS A FUNCTION OF WING INCIDENCE.

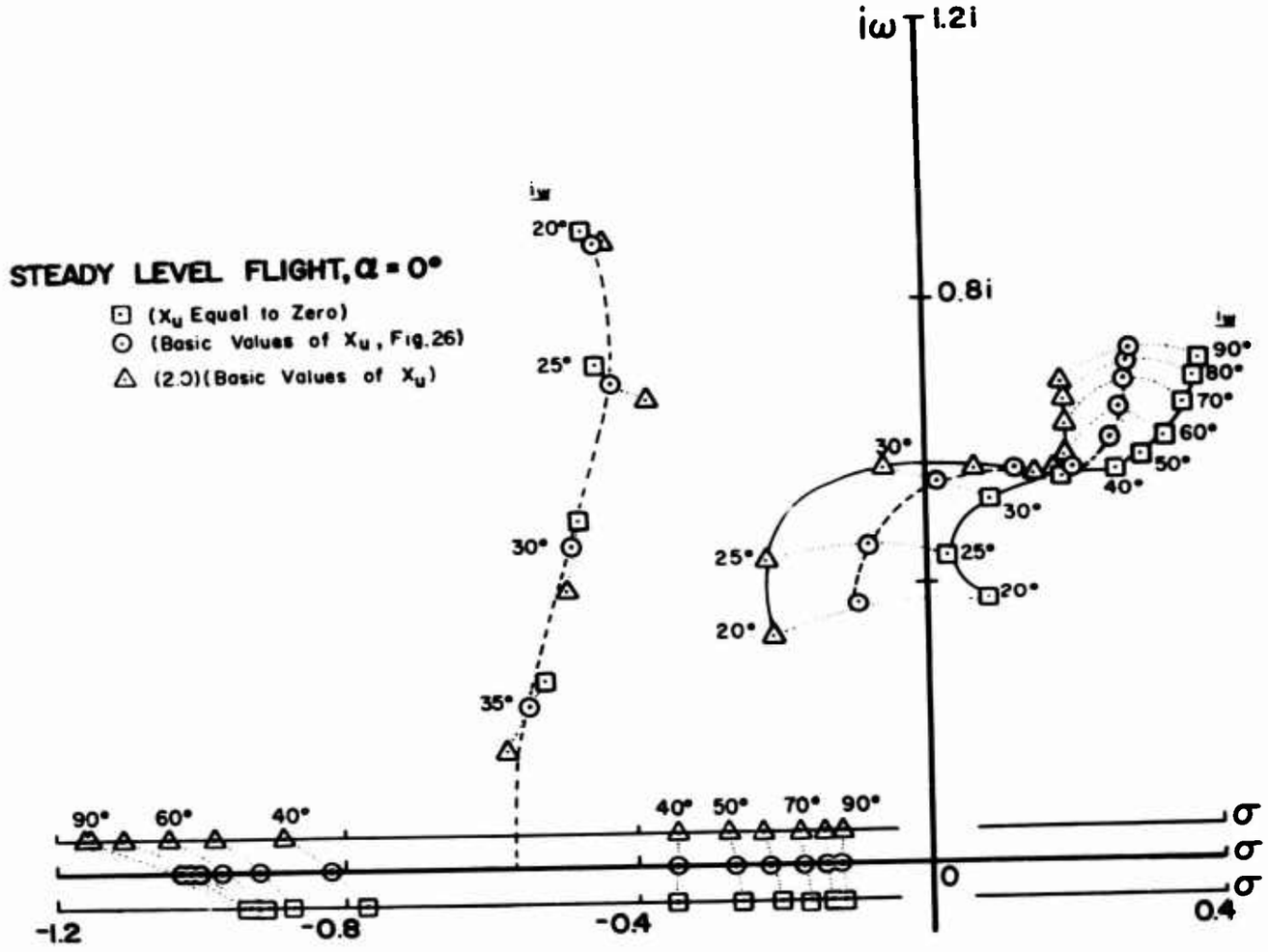

FIGURE 27. LOCUS OF ROOTS AS A FUNCTION OF WING INCIDENCE - SENSITIVITY TO X_u.

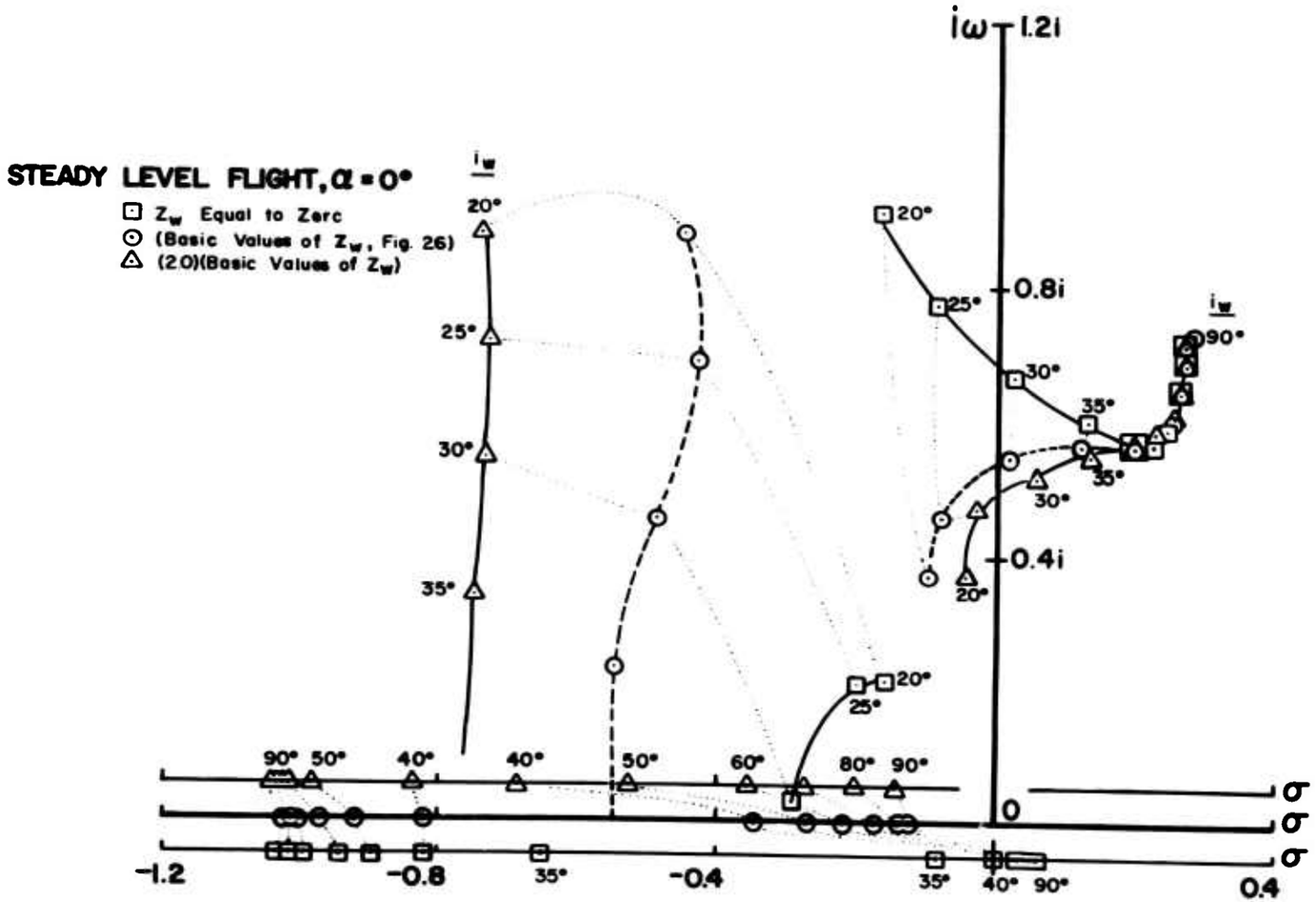

FIGURE 28. LOCUS OF ROOTS AS A FUNCTION OF WING INCIDENCE - SENSITIVITY TO Z_w.

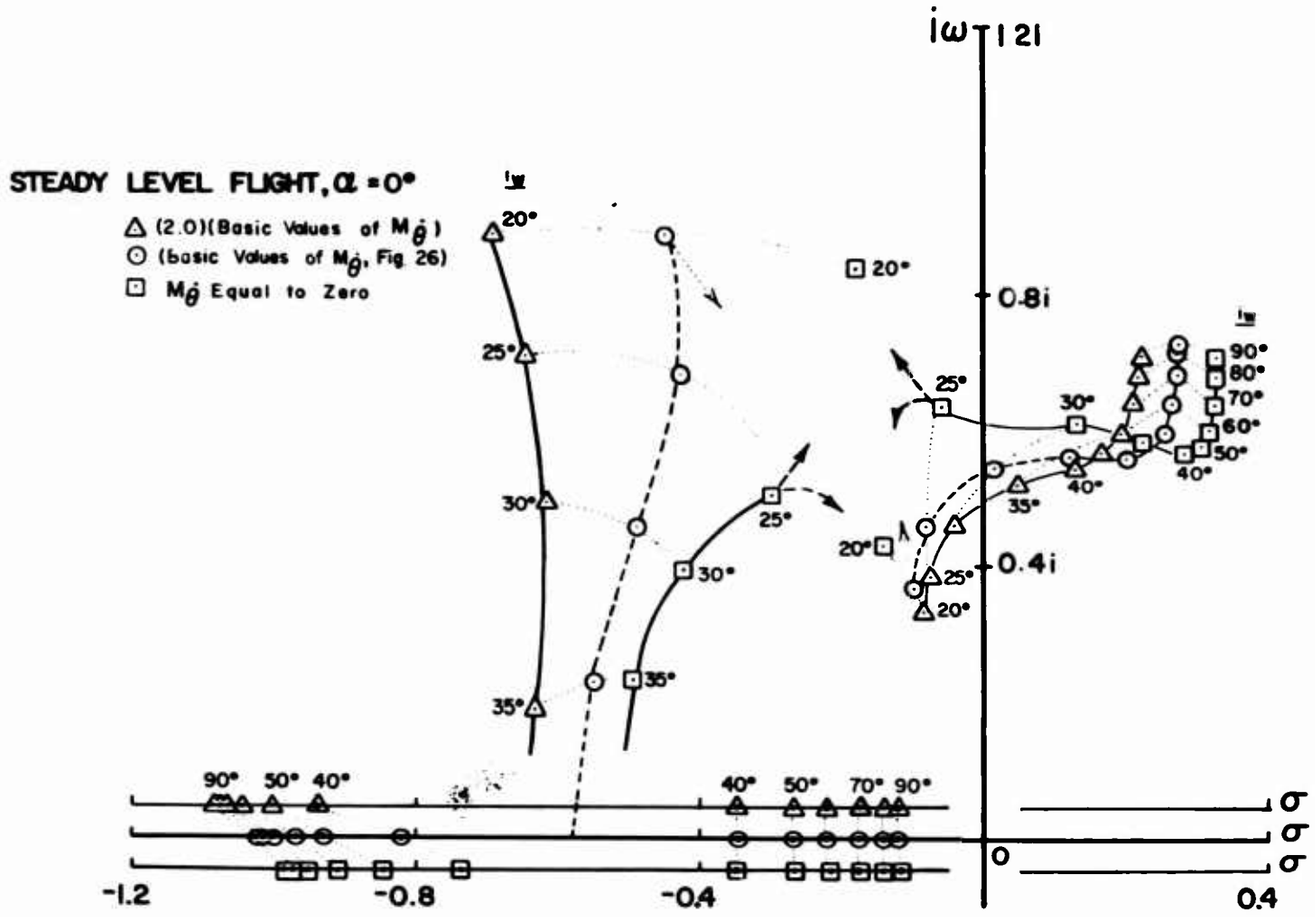

FIGURE 29. LOCUS OF ROOTS AS A FUNCTION OF WING INCIDENCE - SENSITIVITY TO $M_{\dot{\theta}}$.

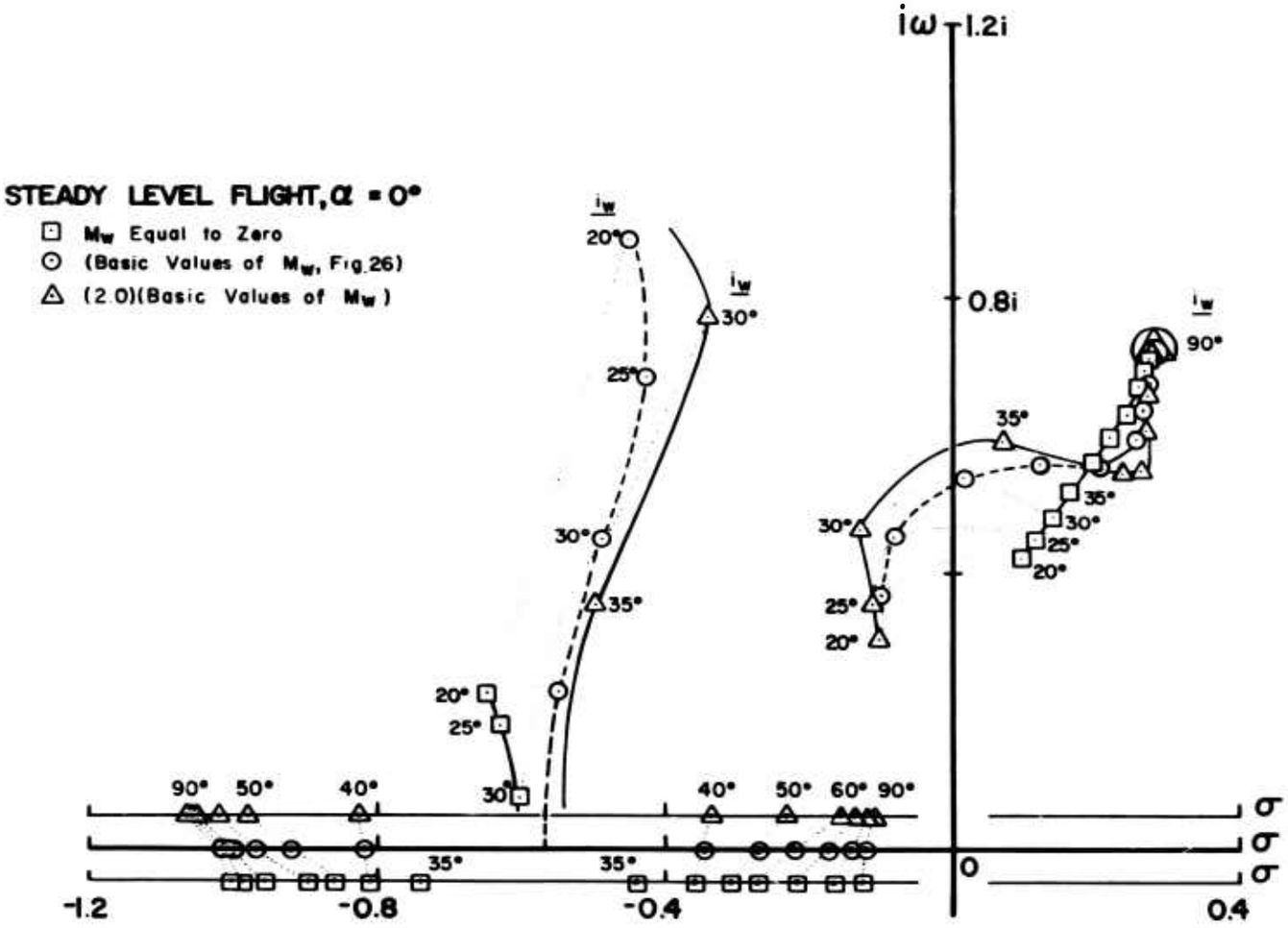

FIGURE 30. LOCUS OF ROOTS AS A FUNCTION OF WING INCIDENCE - SENSITIVITY TO M_w.

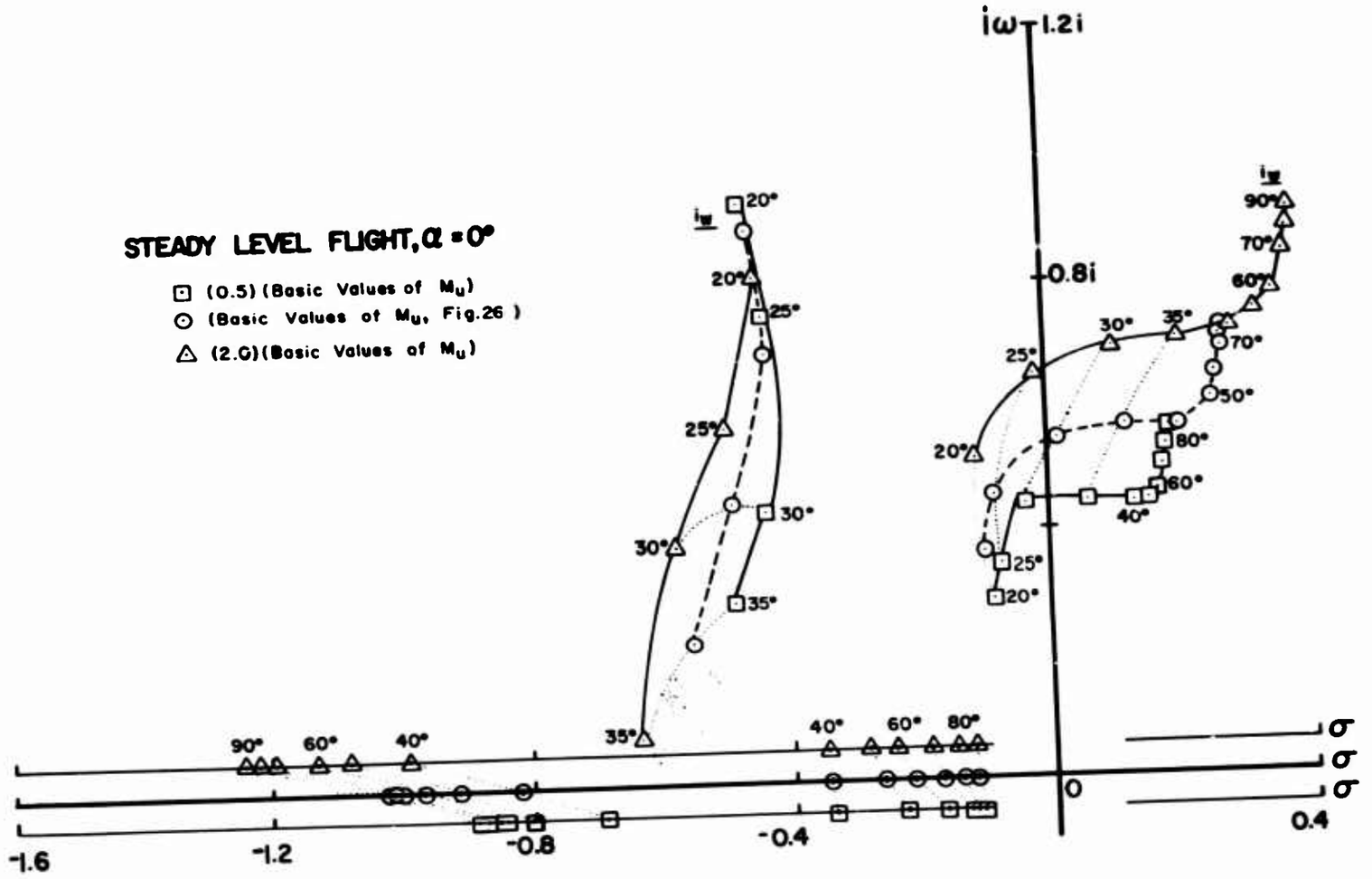

FIGURE 31. LOCUS OF ROOTS AS A FUNCTION OF WING INCIDENCE - SENSITIVITY TO M_u.

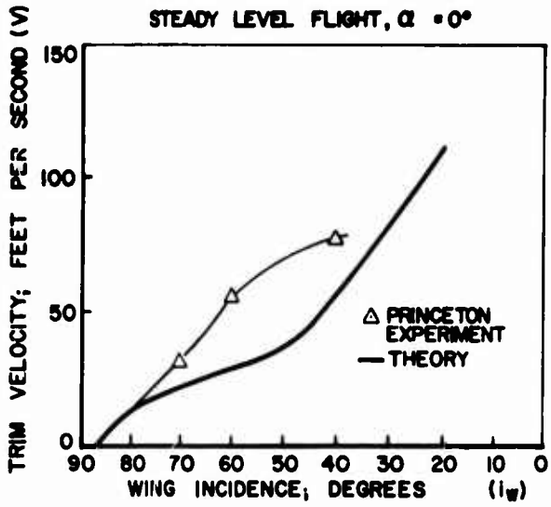

FIGURE 32. COMPARISON OF THEORY AND EXPERIMENT - TRIM VELOCITY VS. WING INCIDENCE.

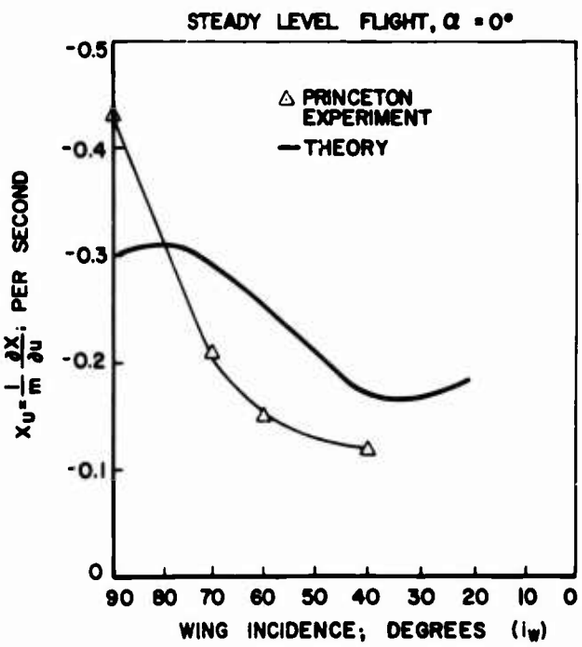

FIGURE 33. COMPARISON OF THEORY AND EXPERIMENT - X_u VS. WING INCIDENCE.

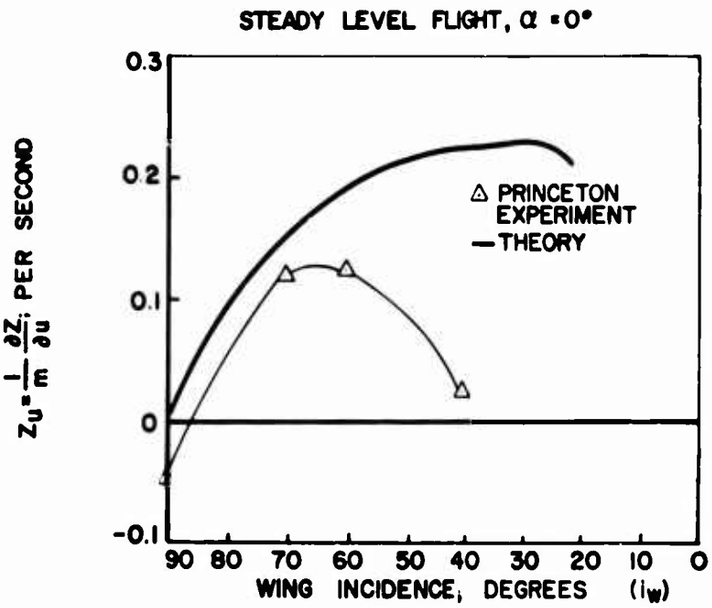

FIGURE 34. COMPARISON OF THEORY AND EXPERIMENT - Z_u VS. WING INCIDENCE.

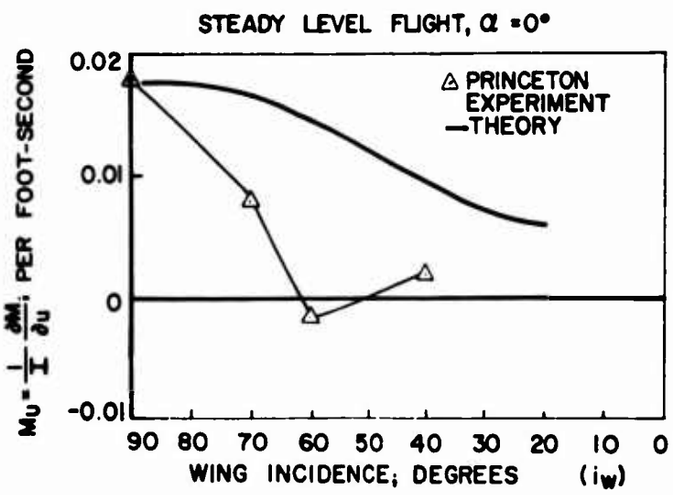

FIGURE 35. COMPARISON OF THEORY AND EXPERIMENT - M_u VS. WING INCIDENCE.

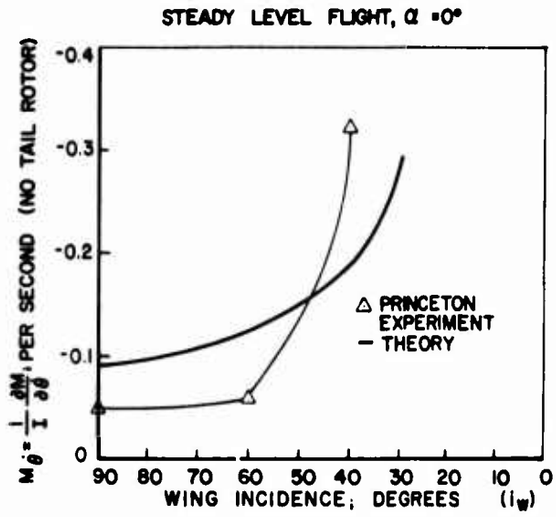

FIGURE 36. COMPARISON OF THEORY AND EXPERIMENT - M_θ VS. WING INCIDENCE.

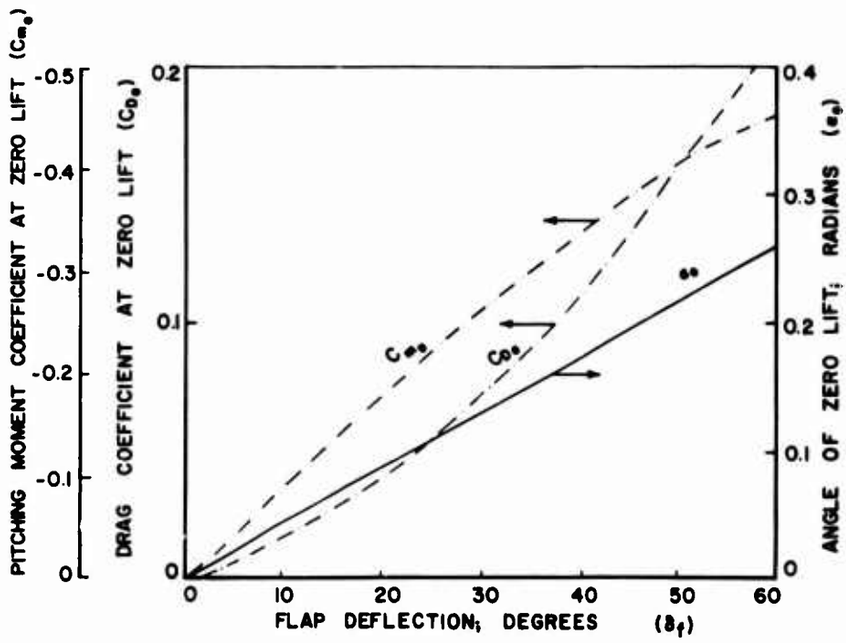

FIGURE 37. ASSUMED FLAP CHARACTERISTICS.

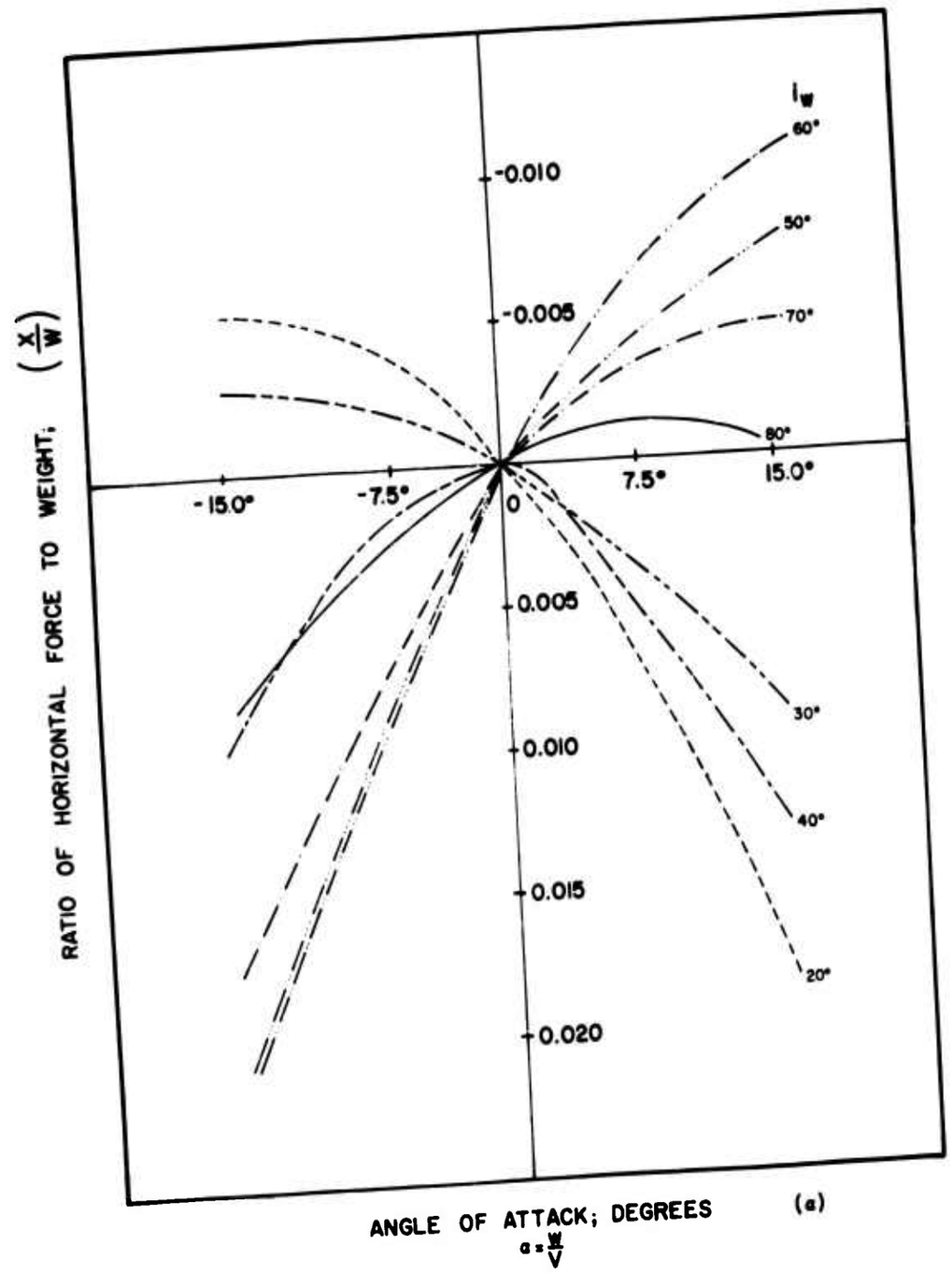

FIGURE 38. HORIZONTAL FORCE VS. ANGLE OF ATTACK FOR VARIOUS WING INCIDENCES.

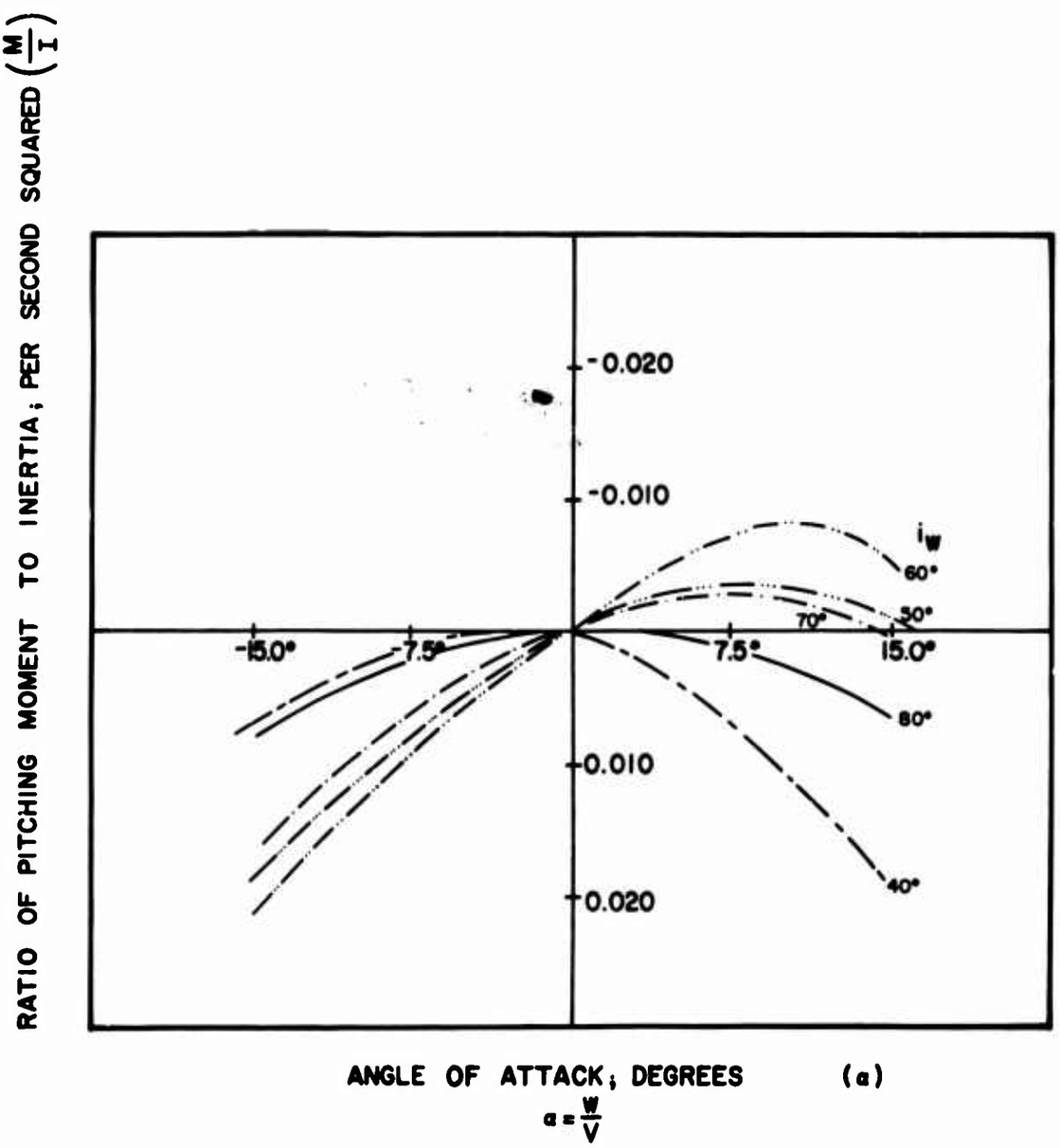

FIGURE 39. PITCHING MOMENT VS. ANGLE OF ATTACK FOR VARIOUS WING INCIDENCES.

REFERENCES

1. Putman, W. F., "Results of Experiments on a Tilt-Wing VTOL Aircraft Using the Princeton University Forward Flight Facility," Report No. 542, Department of Aeronautical Engineering, Princeton University, Princeton, New Jersey, May 1961.

2. Cromwell, C. H., and Payne, H. E., "A Stability Analysis of Tilt-Wing Aircraft," Report No. 477, Department of Aeronautical Engineering, Princeton University, Princeton, New Jersey, May 1960.

3. Hargraves, C. R., "An Analytical Study of the Longitudinal Dynamics of a Tilt-Wing VTOL," Report No. 561, Department of Aeronautical Engineering, Princeton University, Princeton, New Jersey, February 1962.

4. Koning, C., "Influence of the Propeller on Other Parts of the Airplane Structure," Aerodynamic Theory, Edited by W. F. Durand, Volume IV, Dover Publications, Inc., New York, 1963.

5. Smelt, R., and Davies, H., "Estimation of Increase in Lift due to Slipstream," ARC R & M No. 1788, February 1957.

6. Castles, Walter, Jr., and DeLeeuw, Jacob Henri, "The Normal Component of the Induced Velocity in the Vicinity of a Lifting Rotor and Some Examples of its Application," NACA Report No. 1184, 1954.

7. Draper, J. W., and Kuhn, R. E., "Investigation of the Aerodynamic Characteristics of a Model Wing-Propeller Combination and of the Wing and Propeller Separately at Angles of Attack up to 90°," NACA TN 3304, 1954.

8. Coleman, R. P., "Evaluation of the Induced Velocity Field of an Idealized Helicopter Rotor," NACA ARR. L5E1, 1945.

9. NASA Conference on V/STOL Aircraft, "A Compilation of the Papers Presented," Langley Research Center, Langley Field, Virginia, November 1960.

10. Gessow, A., and Myers, G. C., Jr., "Aerodynamics of the Helicopter," Macmillan Company, New York, 1952.

11. Seckel, Edward, "Stability and Control of Airplanes and Helicopters," Academic Press, New York, 1964.

12. Curtiss, H. C., Jr., "Some Basic Considerations Regarding the Longitudinal Dynamics of Aircraft and Helicopters," Report No. 562, Department of Aeronautical Engineering, Princeton University, Princeton, New Jersey, July 1961.

13. Seckel, Edward, and Curtiss, H. C., Jr., "Aerodynamic Characteristics of Helicopter Rotors, Rotor Contribution to Helicopter Stability Parameters," Report No. 659, Department of Aeronautical Engineering, Princeton University, Princeton, New Jersey, December 1963.

14. Rethorst, S., Royce, W., and Wu, T., "Lift Characteristics of Wings Extending Through Propeller Slipstreams," Report No. 1, Vehicle Research Corporation, 1958.

15. Th. von Kármán and J. M. Burgers, "General Aerodynamic Theory—Perfect Fluids," Aerodynamic Theory, Edited by W. F. Durand, Volume II, Dover Publications, 1963.

16. Goland, L., Miller, N., Butler, L., "Effects of Propeller Slipstream on V/STOL Aircraft Performance and Stability," TRECOM Technical Report 64-47, U. S. Army Transportation Research Command*, Fort Eustis, Virginia, August 1964.

17. Sweet, George E., "Static-Stability Measurements of a Stand-On Type Helicopter With Rigid Blades, Including a Comparison With Theory," NASA TN D-189, February 1960, 50 p. diagrams, photos.

18. Taylor, Robert T., "Wind-Tunnel Investigation of Effect of Ratio of Wing-Chord to Propeller Diameter With Addition of Slats on the Aerodynamic Characteristics of Tilt-Wing VTOL Configurations in the Transition Speed Range," NASA TN D-17, September 1959.

19. Brotherhood, P., "An Investigation in Flight of the Induced Velocity Distribution Under a Helicopter Rotor When Hovering," ARC R & M No. 2521, 1951.

20. "An Experimental Investigation of the Longitudinal Stability Characteristics of a Four Propeller Tilt-Wing VTOL Aircraft at Low Speeds," Department of Aerospace and Mechanical Sciences, Princeton University, Princeton, New Jersey, to be published as USAAVLABS Report.

21. Hoerner, S. F., Fluid-Dynamic Drag, Published by the Author, 1958.

22. Curtiss, H. C., Putman, W. F., and Traybar, J. J., "The Princeton Dynamic Model Track," Presented at the AIAA Aerodynamic Testing Conference, Washington, D. C., March 9-10, 1964.

*Now U. S. Army Aviation Materiel Laboratories

DISTRIBUTION

US Army Materiel Command	5
US Army Mobility Command	3
US Army Aviation Materiel Command	5
US Army Aviation Materiel Laboratories	12
US Army R&D Group (Europe)	2
US Army Limited War Laboratory	1
US Army Human Engineering Laboratories	1
US Army Research Office-Durham	1
US Army Test and Evaluation Command	1
US Army Medical R&D Command	1
US Army Engineer Waterways Experiment Station	1
US Army Combat Developments Command, Fort Belvoir	2
US Army Combat Developments Command Experimentation Command	3
US Army Command and General Staff College	1
US Army Aviation School	1
US Army Infantry Center	2
US Army Tank-Automotive Center	2
US Army Aviation Maintenance Center	2
US Army Electronics Command	2
US Army Aviation Test Activity, Edwards AFB	2
Air Force Flight Test Center, Edwards AFB	2
US Army Field Office, AFSC, Andrews AFB	1
Air Force Flight Dynamics Laboratory, Wright-Patterson AFB	1
Systems Engineering Group (RTD), Wright-Patterson AFB	3
Naval Air Systems Command	2
Bureau of Ships, DN	1
Bureau of Naval Weapons, DN	3
Chief of Naval Research	4
David Taylor Model Basin	1
Ames Research Center, NASA	1
Lewis Research Center, NASA	1
Manned Spacecraft Center, NASA	1
NASA Representative, Scientific and Technical Information Facility	2
NAFEC Library (FAA)	2
US Army Aviation Human Research Unit	2
US Army Board for Aviation Accident Research	1
Bureau of Safety, Civil Aeronautics Board	2
US Naval Aviation Safety Center, Norfolk	1
Federal Aviation Agency, Washington, D. C.	1
The Surgeon General	1
Defense Documentation Center	20

APPENDIX A

PHYSICAL PARAMETERS OF ASSUMED AIRCRAFT AND DESCRIPTION OF APPARATUS AND EXPERIMENTS

ASSUMED AIRCRAFT

W = 37,350 pounds

I_y = 100,000 slug-feet squared

Propellers

$N = 4$

R = 7.75 feet

Ω = 129 radians per second

$\sigma = 0.153$

$b = 4$

a = 5.73 per radian

Wing

S = 534 square feet

b_w = 67.5 feet

c = 8.07 feet

$AR = 8.53$

$K = 0.5$

C_{l_α} = 5.0 per radian

$C_{D_o} = 0.0130$

α_o = 0.027 radian

$\frac{S_{\delta_f}}{S} = 0.333$ (double-slotted flap)

Horizontal Tail

S_T = 140 square feet

$AR_T = 5.08$

$C_{l_{\alpha_T}} = 3.0$ radian

ℓ_{HT} = 24.3 feet

ℓ_H = 6.16 feet

Tail Rotor

R_T = 4 feet

Ω_T = 363.4 radians per second

$\sigma_T = 0.124$

ℓ_{TR} = 31.4 feet

$b = 3$

a_T = 5.73 per radian

The flap effectiveness is shown in Figure 37. The angle of zero lift of the wing (α_o), the zero lift drag coefficient (C_{D_o}), and the pitching moment about the aerodynamic center (C_{M_o}) are assumed to vary as shown with flap deflection. The flap deflection is programmed as a function of wing incidence (Figure A-2).

Various geometric distances of the aircraft, ℓ_{OW} , ℓ_W , ℓ_{OP} , ℓ_P , which are measured from the center of gravity of the airplane, as shown in Figure A-1b, are expressed analytically (in feet) as follows:

$$\ell_{OW} = 0.158 + (0.19) \sin i_w + (2.64) \cos i_w$$

$$\ell_W = 1.105 + (2.64) \sin i_w + (0.19) \cos i_w$$

$$\ell_{OP} = -1.06 + \ell_{OW}$$

$$\ell_P = 3.75 + \ell_W$$

These quantities are shown graphically in Figure A-3.

DESCRIPTION OF APPARATUS AND EXPERIMENTS

The experimental results presented were obtained from a 0.10 scale dynamic model of the XC-142A tested on the Princeton Dynamic Model Track.

Test Facility

The Princeton University Dynamic Model Track is a unique facility, designed expressly for the study of the dynamic motions of helicopter and VTOL models at equivalent flight speeds of up to 60 knots (for a one-tenth scale model). Basic components of the facility include a servo-driven carriage riding on a track 750 feet long, located in a building of cross section 30 x 30 feet; the carriage has an acceleration potential of 0.6g and a maximum speed of 40 feet per second. A detailed description of the facility and the testing techniques employed may be found in Reference 22.

A model may be attached to the carriage by one of several booms. One mount permits relative displacements of the model with respect to the carriage in horizontal and vertical directions, as well as allowing it to rotate in the plane determined by these two directions. Horizontal relative motion of the model with respect to the carriage is sensed and used to command the carriage to follow the model in a closed loop fashion. Similarly, vertical displacement of the model with respect to the carriage commands the boom to move vertically. This servo operation of the carriage allows the model to fly "free" with no restraints on the dynamic motions being investigated.

This method of testing may be considered similar to dynamic flight testing, with considerably more control over the experiment possible.

In addition to the dynamic testing as described above, static testing is conducted by programming carriage movement in accordance with pre-selected velocity profiles at constant angle of attack. Programmed angle-of-attack changes at constant velocity are also possible. The model is rigidly mounted on the carriage and forces and moments acting on the model are measured with strain gauges. Although these static experiments are similar to wind tunnel tests, this facility offers the advantages of a 30 x 30 foot test section with a uniform air velocity, free from turbulence. Precise speed control over a range of speeds from backward flight through hover to forward flight is available.

Model

A three-view drawing of the 0.10 scale dynamic model of the XC-142A is shown in Figure A-4.

The fuselage is constructed of an inner and outer Fiberglas skin, vacuum molded and bonded to a styrofoam core. An aluminum box spar is the main structural member of the wing. Mahogany ribs and a vacuum molded Fiberglas wing surface form the external airfoil shape. The double-slotted flaps were constructed of low density styrofoam with a Fiberglas covering.

The model drive motor is a 200-volt, 400-cycle, three-phase electric motor, rated at five horsepower, mounted on a bulkhead in the fuselage. Power for the four propellers was transmitted to a central transmission and from thence to right-angle gear boxes located in the wing by flexible shafting. A separate power take-off is used to drive the tail rotor. Propeller gear boxes and housings were mounted directly on the wing spar. The propeller blades were constructed of Fiberglas by the Hamilton Standard Division of the United Aircraft Corporation.

Model control positions are set from a control console on the carriage. The model incorporated electrically controllable blade angles on each of the four propellers. The blade angle of the tail rotor is also variable to provide pitching moment trim. Wing incidence, flaps, ailerons, and the horizontal tail are also power operated so that transition runs may be made with selected programming of all required controls. All of these systems are closed loop position controls. The response characteristics of each of these loops is sufficiently fast to permit study of automatic stabilization systems.

Static Data

Measurements of vertical force (perpendicular to the free stream), horizontal force (parallel to the free stream), and pitching moment acting on the model near trim conditions ($\dot{X} = 0$) were made to determine the static stability derivatives of this vehicle at various wing incidences. The flap deflection is given as a function of wing incidence in Figure A-2.

Fuselage angle of attack, propeller blade angle, and propeller RPM were held constant, and the carriage was programmed for a very small acceleration ($\cong$ 0.01g's) such that the velocity of the model was varied about a trim condition (X = 0). This velocity program was conducted at three fuselage angles of attack ($\alpha = 0$, $\alpha \cong + 15°$, $\alpha \cong - 15°$), one propeller rotational speed (4000 RPM), and one blade angle (17.5°) setting. At a wing incidence of 40°, some data were taken at two other blade angle settings.

Previous experience with this technique of quasi-static testing has shown that the derivatives are identical to those obtained from point by point measurements at velocity increments about a trim condition. A considerable reduction in testing time is realized provided that the carriage accelerations involved are kept very small.

The values of the stability derivatives determined from these experiments are given in Figures 32 through 36. Detailed consideration of these data may be found in Reference 20.

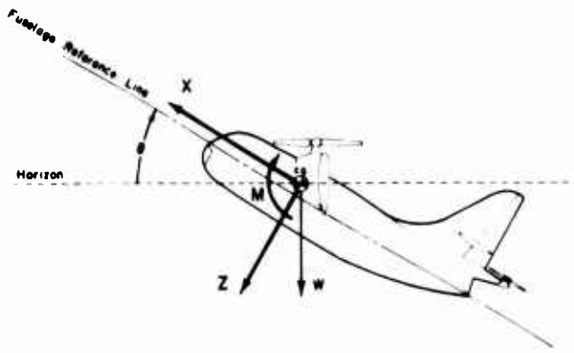

a. AXIS SYSTEM.

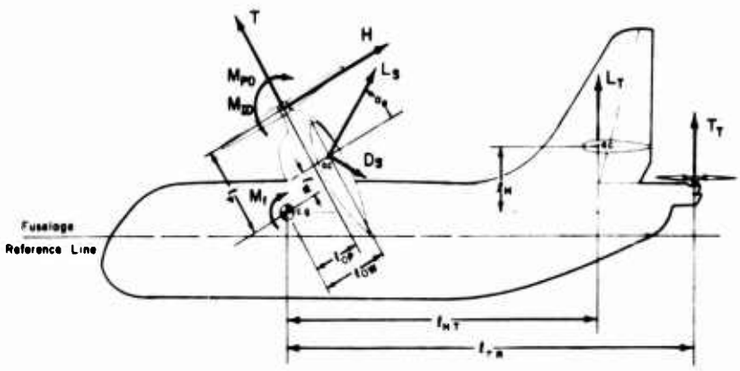

b. GEOMETRIC DISTANCES FROM CENTER OF GRAVITY.

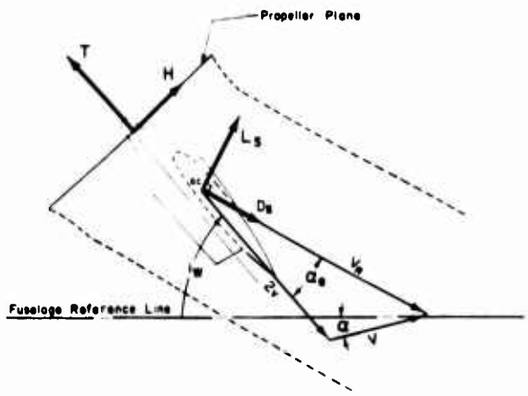

c. PROPELLER AND WING FORCES AND VELOCITIES IN SLIPSTREAM

FIGURE A-1. AXIS SYSTEM AND NOTATION.

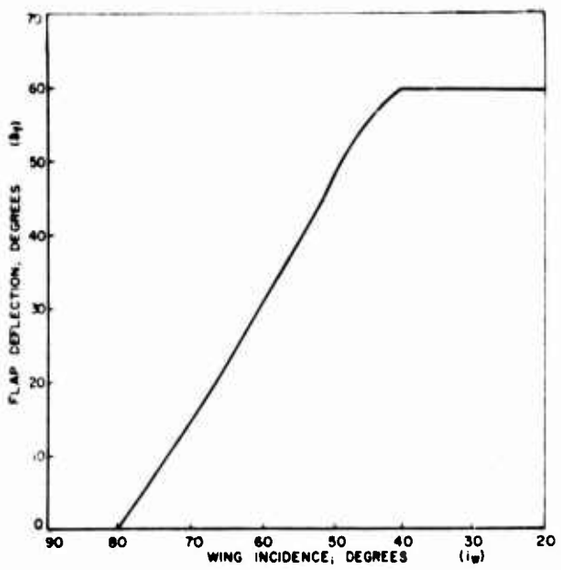

FIGURE A-2 FLAP PROGRAM VS WING INCIDENCE

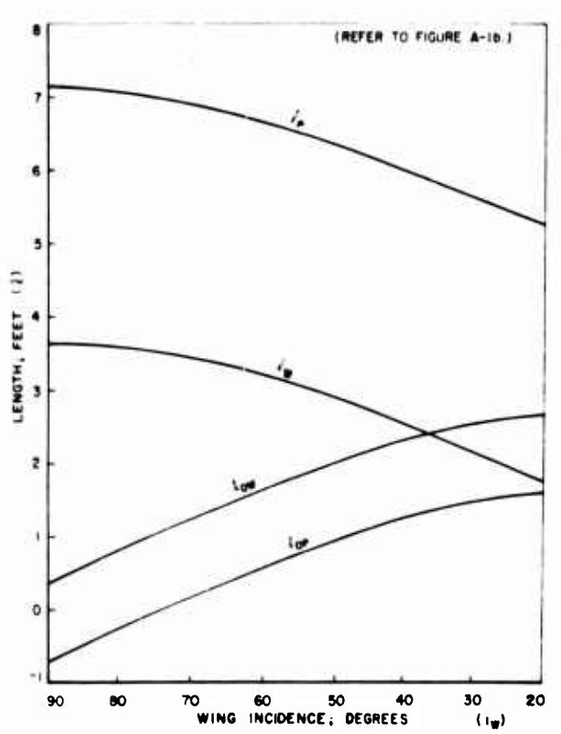

FIGURE A-3 AIRCRAFT GEOMETRIC CHARACTERISTICS

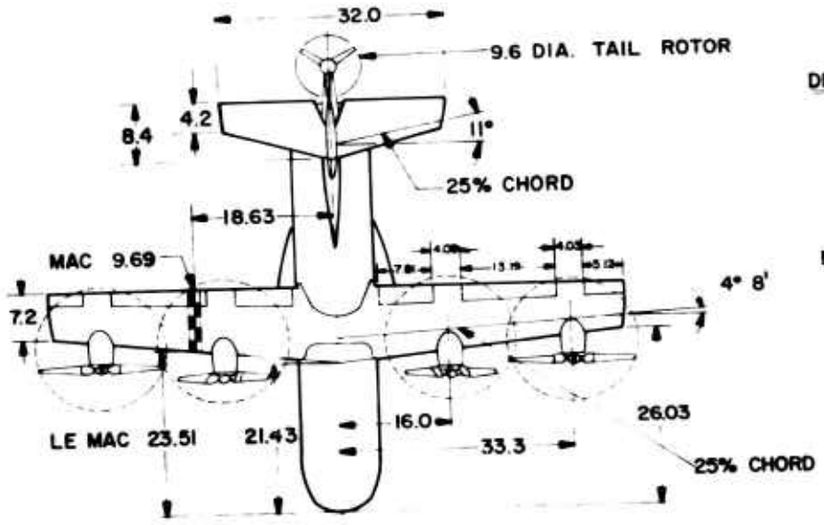

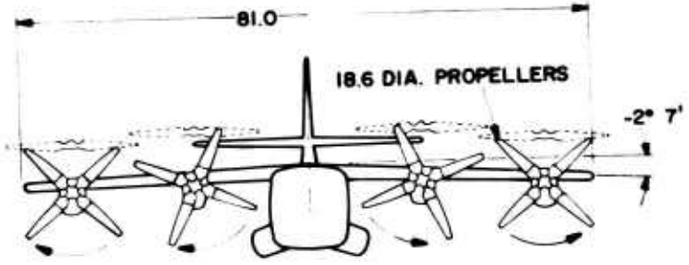

DESIGNATION OF AIRFOIL SECTIONS:

WING	ROOT @ BL 0.0	NACA	63-318
	TIP	NACA	63-318
UNIT HORIZONTAL TAIL	ROOT	NACA	0015
	TIP	NACA	0012
VERTICAL TAIL	ROOT	NACA	0018
	WL 215	NACA	0012
	TIP	NACA	0012

NOTE: ALL DIMENSIONS GIVEN IN MODEL SCALE (IN INCHES)

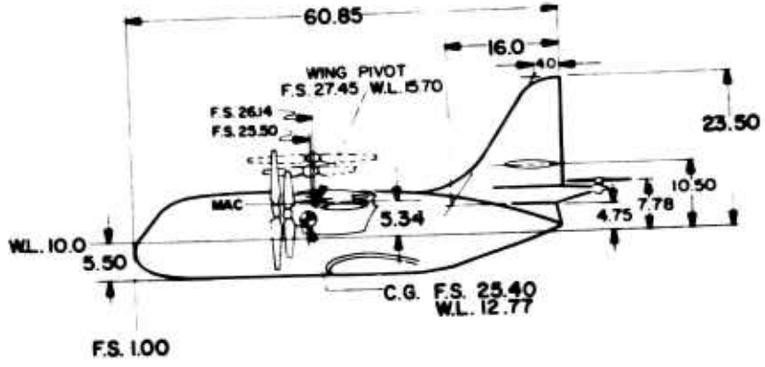

FIGURE A-4. GENERAL ARRANGEMENT 1/10 SCALE XC-142 MODEL.

APPENDIX B

ANALYTICAL EXPRESSIONS FOR STABILITY DERIVATIVES

EQUATIONS OF MOTION

The equations of motion with respect to stability axes for motions in the plane of symmetry of an aircraft (Reference 11) may be written as follows:

$$m(\dot{u} + w\,\dot{\theta}) = X(u,w) - W \sin\theta \tag{B-1}$$

$$m(\dot{w} - u\,\dot{\theta}) = Z(u,w) - W \cos\theta \tag{B-2}$$

$$I\,\ddot{\theta} = M(u,w,\dot{\theta}) \tag{B-3}$$

Expanding the aerodynamic forces X, Z, and M in a Taylor series about level, unaccelerated flight, retaining only first-order terms, and linearizing the inertia and gravity terms about $\theta_o = 0$, $u_o = V_o$, $w_o = 0$, result in the following:

$$\dot{u} = \left(\frac{1}{m}\frac{\partial X}{\partial u}\right) u + \left(\frac{1}{m}\frac{\partial X}{\partial w}\right) w - g\,\theta \tag{B-4}$$

$$\dot{w} = V_o\,\dot{\theta} + \left(\frac{1}{m}\frac{\partial Z}{\partial u}\right) u + \left(\frac{1}{m}\frac{\partial Z}{\partial w}\right) w \tag{B-5}$$

$$\ddot{\theta} = \left(\frac{1}{I}\frac{\partial M}{\partial u}\right) u + \left(\frac{1}{I}\frac{\partial M}{\partial w}\right) w + \left(\frac{1}{I}\frac{\partial M}{\partial \dot{\theta}}\right) \dot{\theta} \tag{B-6}$$

The stability derivatives have been calculated using the following expressions, based on the assumptions discussed in the text.

STABILITY DERIVATIVES

Resolving the propeller and wing forces in the horizontal direction as shown in Figure A-1, the X-force may be written as

$$X(u,w) = T \cos i_w - H \sin i_w - L_s \sin(i_w - \alpha_e) - D_s \cos(i_w - \alpha_e) + (X)_f \tag{B-7}$$

Taking derivatives of the above expression, the horizontal force derivatives are

$$\frac{\partial X}{\partial u} = \frac{\partial T}{\partial u} \cos i_w - \frac{\partial H}{\partial u} \sin i_w - \frac{\partial L_s}{\partial u} \sin(i_w - \alpha_e) - \frac{\partial D_s}{\partial u} \cos(i_w - \alpha_e) + L_s \cos(i_w - \alpha_e) \frac{\partial \alpha_e}{\partial u} - D_s \sin(i_w - \alpha_e) \frac{\partial \alpha_e}{\partial u} - \rho V f \qquad (B\text{-}8)$$

$$\frac{\partial X}{\partial w} = \frac{\partial T}{\partial w} \cos i_w - \frac{\partial H}{\partial w} \sin i_w - \frac{\partial L_s}{\partial w} \sin(i_w - \alpha_e) - \frac{\partial D_s}{\partial w} \cos(i_w - \alpha_e) + L_s \cos(i_w - \alpha_e) \frac{\partial \alpha_e}{\partial w} - D_s \sin(i_w - \alpha_e) \frac{\partial \alpha_e}{\partial w} \qquad (B\text{-}9)$$

Resolving forces in the vertical direction, the Z-force is

$$Z(u,w) = - T \sin i_w - H \cos i_w - L_s \cos(i_w - \alpha_e) + D_s \sin(i_w - \alpha_e) \qquad (B\text{-}10)$$

and the Z-force derivatives are

$$\frac{\partial Z}{\partial u} = - \frac{\partial T}{\partial u} \sin i_w - \frac{\partial H}{\partial u} \cos i_w - \frac{\partial L_s}{\partial u} \cos(i_w - \alpha_e) + \frac{\partial D_s}{\partial u} \sin(i_w - \alpha_e) - L_s \sin(i_w - \alpha_e) \frac{\partial \alpha_e}{\partial u} - D_s \cos(i_w - \alpha_e) \frac{\partial \alpha_e}{\partial u} \qquad (B\text{-}11)$$

$$\frac{\partial Z}{\partial w} = -\frac{\partial T}{\partial w}\sin i_w - \frac{\partial H}{\partial w}\cos i_w - \frac{\partial L_s}{\partial w}\cos(i_w - \alpha_e) +$$

$$\frac{\partial D_s}{\partial w}\sin(i_w - \alpha_e) - L_s \sin(i_w - \alpha_e)\frac{\partial \alpha_e}{\partial w} - D_s \cos(i_w - \alpha_e)\frac{\partial \alpha_e}{\partial w} \qquad \text{(B-12)}$$

The pitching moment acting on the airplane may be expressed as

$$M = -T\,\ell_{OP} + H\,\ell_P + L_s \cos\alpha_e\,\ell_W - L_s \sin\alpha_e\,\ell_{OW} + D_s \cos\alpha_e\,\ell_{OW} -$$
$$D_s \sin\alpha_e\,\ell_W - T_T\,\ell_{TR} - L_T\,\ell_{HT} + (M)_{PD} + (M_{\dot\theta}\dot\theta)_{ID} + (M)_f \qquad \text{(B-13)}$$

The pitching moment derivatives are obtained by taking derivatives of this expression:

$$\frac{\partial M}{\partial u} = -\frac{\partial T}{\partial u}\ell_{OP} + \frac{\partial H}{\partial u}\ell_P + \frac{\partial L_s}{\partial u}\cos\alpha_e\,\ell_W - \frac{\partial L_s}{\partial u}\sin\alpha_e\,\ell_{OW} +$$

$$\frac{\partial D_s}{\partial u}\cos\alpha_e\,\ell_{OW} - \frac{\partial D_s}{\partial u}\sin\alpha_e\,\ell_W - L_s\sin\alpha_e\,\ell_W\frac{\partial \alpha_e}{\partial u} -$$

$$L_s\cos\alpha_e\,\ell_{OW}\frac{\partial \alpha_e}{\partial u} - D_s\sin\alpha_e\,\ell_{OW}\frac{\partial \alpha_e}{\partial u} - D_s\cos\alpha_e\,\ell_W\frac{\partial \alpha_e}{\partial u} -$$

$$\frac{\partial T_T}{\partial u}\ell_{TR} - \frac{\partial L_T}{\partial u}\ell_{HT} + \frac{\partial}{\partial u}(M)_{PD} \qquad \text{(B-14)}$$

$$\frac{\partial M}{\partial w} = -\frac{\partial T}{\partial w}\ell_{OP} + \frac{\partial H}{\partial w}\ell_P + \frac{\partial L_s}{\partial w}\cos\alpha_e\,\ell_W - \frac{\partial L_s}{\partial w}\sin\alpha_e\,\ell_{OW} +$$

$$\frac{\partial D_s}{\partial w}\cos\alpha_e\,\ell_{OW} - \frac{\partial D_s}{\partial w}\sin\alpha_e\,\ell_W - L_s\sin\alpha_e\,\ell_W\frac{\partial \alpha_e}{\partial w} -$$

$$L_s\cos\alpha_e\,\ell_{OW}\frac{\partial \alpha_e}{\partial w} - D_s\sin\alpha_e\,\ell_{OW}\frac{\partial \alpha_e}{\partial w} - D_s\cos\alpha_e\,\ell_W\frac{\partial \alpha_e}{\partial w} +$$

Eq. (B-15) cont.

$$+ \frac{\partial T_T}{\partial w} \ell_{TR} - \frac{\partial L_T}{\partial w} \ell_{HT} + \frac{\partial}{\partial w} (M)_{PD} + \frac{\partial}{\partial w} (M)_f$$

(B-15)

$$\frac{\partial M}{\partial \dot{\theta}} = - \frac{\partial T}{\partial \dot{\theta}} \ell_{OP} + \frac{\partial H}{\partial \dot{\theta}} \ell_P + \frac{\partial L_s}{\partial \dot{\theta}} \cos \alpha_e \ell_W - \frac{\partial L_s}{\partial \dot{\theta}} \sin \alpha_e \ell_{OW} +$$

$$\frac{\partial D_s}{\partial \dot{\theta}} \cos \alpha_e \ell_{OW} - \frac{\partial D_s}{\partial \dot{\theta}} \sin \alpha_e \ell_W - L_s \sin \alpha_e \ell_W \frac{\partial \alpha_e}{\partial \dot{\theta}} -$$

$$L_s \cos \alpha_e \ell_{OW} \frac{\partial \alpha_e}{\partial \dot{\theta}} - D_s \sin \alpha_e \ell_{OW} \frac{\partial \alpha_e}{\partial \dot{\theta}} - D_s \cos \alpha_e \ell_W \frac{\partial \alpha_e}{\partial \dot{\theta}} -$$

$$\frac{\partial T_T}{\partial \dot{\theta}} \ell_{TR} - \frac{\partial L_T}{\partial \dot{\theta}} \ell_{HT} + (M_{\dot{\theta}})_{ID}$$

(B-16)

PROPELLER EQUATIONS

Induced Velocity

The average value of the propeller induced velocity may be expressed in terms of the propeller blade angle and the velocities at the propeller plane by eliminating the thrust coefficient from the momentum equation using the blade element equation for thrust coefficient.

$$\lambda_i = \frac{\frac{a\sigma}{4}\left[\frac{\theta_{0.75R}}{3}\left(1 + \frac{3}{2}\mu^2\right) - \frac{\lambda_i + v}{2}\right]}{\sqrt{(\lambda_i + v)^2 + \mu^2}} = \frac{\frac{a\sigma}{4}\left[\frac{\theta_{0.75R}}{3}\left(1 + \frac{3}{2}\mu^2\right) - \frac{\lambda_i + v}{2}\right]}{\sqrt{\quad}}$$

(B-17)

This equation may be rearranged to give a fourth order equation for λ_i

$$\lambda_i^4 + 2v\lambda_i^3 + \left[v^2 + \mu^2 - \left(\frac{a\sigma}{8}\right)^2\right]\lambda_i^2 + \left(\frac{a\sigma}{4}\right)^2\left[\frac{\theta_{0.75R}}{3}\left(1 + \frac{3}{2}\mu^2\right) - \frac{v}{2}\right]\lambda_i -$$

$$\left(\frac{a\sigma}{4}\right)^2\left[\frac{\theta_{0.75R}}{3}\left(1 + \frac{3}{2}\mu^2\right) - \frac{v}{2}\right]^2 = 0$$

(B-18)

The derivatives of the induced velocity are obtained from Equation (B-18) as

$$\frac{\partial \lambda_i}{\partial \mu} = \frac{\frac{1}{\xi}\left[\frac{a\sigma}{4}\theta_{0.75R}\mu - \lambda_i \frac{\mu}{\xi}\right]}{1 + \frac{1}{\xi}\left[\frac{a\sigma}{8} + \lambda_i \frac{\lambda_i + \upsilon}{\xi}\right]} \tag{B-19}$$

$$\frac{\partial \lambda_i}{\partial \upsilon} = \frac{-\frac{1}{\xi}\left[\frac{a\sigma}{8} + (\lambda_i)\left(\frac{\lambda_i + \upsilon}{\xi}\right)\right]}{1 + \frac{1}{\xi}\left[\frac{a\sigma}{8} + (\lambda_i)\left(\frac{\lambda_i + \upsilon}{\xi}\right)\right]} \tag{B-20}$$

Thrust Equations

The blade element expression for the thrust (Reference 10, page 190) is

$$T = \rho \pi R^2 (\Omega R)^2 \frac{a\sigma}{2}\left[\frac{\theta_{0.75R}}{3}\left(1 + \frac{3\mu^2}{2}\right) - \frac{\lambda_i + \upsilon}{2}\right] \tag{B-21}$$

This expression is written in terms of nondimensional velocities perpendicular and parallel to the propeller plane (υ,μ). To convert to the velocities u and w used in the stability analysis, the following relationships are used:

$$\mu = \frac{V \sin(i_w + \alpha)}{\Omega R} \quad , \quad \text{and} \quad \upsilon = \frac{V \cos(i_w + \alpha)}{\Omega R} \tag{B-22}$$

$$\text{and} \qquad w = V \sin\alpha \quad , \qquad u = V \cos\alpha \tag{B-23}$$

Therefore, the relationships between derivatives are

$$\frac{\partial}{\partial u} = \frac{\partial}{\partial \mu}\frac{\partial \mu}{\partial u} + \frac{\partial}{\partial \upsilon}\frac{\partial \upsilon}{\partial u} = \frac{\partial}{\partial \mu}\frac{\sin(i_w + \alpha)}{\Omega R} + \frac{\partial}{\partial \upsilon}\frac{\cos(i_w + \alpha)}{\Omega R} \tag{B-24}$$

$$\frac{\partial}{\partial w} = \frac{\partial}{\partial \mu}\frac{\partial \mu}{\partial w} + \frac{\partial}{\partial \nu}\frac{\partial \nu}{\partial w} = \frac{\partial}{\partial \mu}\frac{\cos(i_w + \alpha)}{\Omega R} - \frac{\partial}{\partial \nu}\frac{\sin(i_w + \alpha)}{\Omega R} \qquad \text{(B-24a)}$$

Then the thrust derivatives are

$$\frac{\partial T}{\partial u} = \rho \pi \Omega R^3 \frac{a\sigma}{2}\left[\left(\frac{2}{3}\theta_{0.75R}\,\mu - \frac{1}{2}\frac{\partial \lambda_i}{\partial \mu}\right)\sin(i_w + \alpha) - \frac{1}{2}\left(1 + \frac{\partial \lambda_i}{\partial \nu}\right)\cos(i_w + \alpha)\right] \qquad \text{(B-25)}$$

$$\frac{\partial T}{\partial w} = \rho \pi \Omega R^3 \frac{a\sigma}{2}\left[\left(\frac{2}{3}\theta_{0.75R}\,\mu - \frac{1}{2}\frac{\partial \lambda_i}{\partial \mu}\right)\cos(i_w + \alpha) + \frac{1}{2}\left(1 + \frac{\partial \lambda_i}{\partial \nu}\right)\sin(i_w + \alpha)\right]. \qquad \text{(B-26)}$$

The variation of propeller thrust with pitching velocity arises from the fact that the propellers are not located at the center of gravity of the vehicle. This derivative may be expressed as

$$\frac{\partial T}{\partial \dot{\theta}} = \frac{\partial T}{\partial \mu}\frac{\partial \mu}{\partial \dot{\theta}} + \frac{\partial T}{\partial \nu}\frac{\partial \nu}{\partial \dot{\theta}} =$$

$$\rho \pi R^2 (\Omega R)^2 \frac{a\sigma}{2}\left[\left(\frac{2}{3}\theta_{0.75R}\,\mu - \frac{1}{2}\frac{\partial \lambda_i}{\partial \mu}\right)(-\ell_p) - \frac{1}{2}\left(1 + \frac{\partial \lambda_i}{\partial \nu}\right)(-\ell_{OP})\right] \qquad \text{(B-27)}$$

Inplane Force

The expression for inplane force also is taken from Reference 10, page 198, with flapping terms set equal to zero:

$$H = \rho \pi R^2 (\Omega R)^2 \frac{a\sigma}{2}\left[\frac{\delta}{2a} + \frac{\lambda_i + \nu}{2}\theta_{0.75R}\right]\mu \qquad \text{(B-28)}$$

The derivatives are, using transformation Equations (B-24) and (B-24a),

$$\frac{\partial H}{\partial u} = \rho \pi R^2 (\Omega R)^2 \frac{ac}{2} \left[\left\{ \left(\frac{\delta}{2a} + \frac{\lambda_i + \nu}{2} \theta_{0.75R} \right) + \frac{\theta_{0.75R}\, \mu}{2} \frac{\partial \lambda_i}{\partial \mu} \right\} \frac{\sin(i_w + \alpha)}{\Omega R} + \frac{\theta_{0.75R}\, \mu}{2} \left(1 + \frac{\partial \lambda_i}{\partial \nu} \right) \frac{\cos(i_w + \alpha)}{\Omega R} \right] \tag{B-29}$$

$$\frac{\partial H}{\partial w} = \rho \pi R^2 (\Omega R)^2 \frac{ac}{2} \left[\left\{ \left(\frac{\delta}{2a} + \frac{\nu + \lambda_i}{2} \theta_{0.75R} \right) + \frac{\theta_{0.75R}\, \mu}{2} \frac{\partial \lambda_i}{\partial \mu} \right\} \frac{\cos(i_w + \alpha)}{\Omega R} - \frac{\theta_{0.75R}\, \mu}{2} \left(1 + \frac{\partial \lambda_i}{\partial \nu} \right) \frac{\sin(i_w + \alpha)}{\Omega R} \right] \tag{B-30}$$

Pitching Moment Equations

The propeller pitching moment, arising from the variation in induced velocity across the disc, is

$$M_{PD} = \frac{b}{16} \rho \Omega c a R^3 v_1 \tag{B-31}$$

where, from Reference 8,

$$v_1 = v_o \left(\frac{V \sin(i_w + \alpha)}{v_o + V \cos(i_w + \alpha)} \right) \tag{B-32}$$

and the pitching moment variations are

$$\frac{\partial M_{PD}}{\partial u} = \frac{b}{16} \rho \Omega c a R^3 \frac{\partial v_1}{\partial u} \tag{B-33}$$

$$\frac{\partial M_{PD}}{\partial w} = \frac{b}{16} \rho \Omega c a R^3 \frac{\partial v_1}{\partial w} \tag{B-34}$$

where, from Equation (B-32),

$$\frac{\partial v_1}{\partial u} = \frac{\partial v_o}{\partial u} \frac{V \sin(i_w + \alpha)}{v_o + V \cos(i_w + \alpha)} + \frac{\sin(i_w + \alpha)\left[v_o - V \frac{\partial v_o}{\partial V}\right]}{\left[v_o + V \cos(i_w + \alpha)\right]^2} \tag{B-35}$$

$$\frac{\partial v_1}{\partial w} = \frac{\partial v_o}{\partial w} \frac{V \sin(i_w + \alpha)}{v_o + V \cos(i_w + \alpha)} + \frac{V + v_o \cos(i_w + \alpha) - V \frac{\partial v_o}{\partial w} \sin(i_w + \alpha)}{\left[v_o + V \cos(i_w + \alpha)\right]^2} \tag{B-36}$$

and from Equations (B-24) and (B-24a), and using the definition of λ_i,

$$\frac{\partial v_o}{\partial u} = \frac{\partial v_o}{\partial \mu} \frac{\sin(i_w + \alpha)}{\Omega R} + \frac{\partial v_o}{\partial v} \frac{\cos(i_w + \alpha)}{\Omega R} =$$

$$\frac{\partial \lambda_i}{\partial \mu} \sin(i_w + \alpha) + \frac{\partial \lambda_i}{\partial v} \cos(i_w + \alpha) \tag{B-37}$$

$$\frac{\partial v_o}{\partial w} = \frac{\partial \lambda_i}{\partial \mu} \cos(i_w + \alpha) - \frac{\partial \lambda_i}{\partial v} \sin(i_w + \alpha) \tag{B-38}$$

The pitching moment arising from an angular velocity about the hub is

$$(M_{\dot{\theta}})_{ID} = - \rho \frac{a\sigma}{16} \pi \Omega R^5 \tag{B-39}$$

when the induced velocity has been assumed constant, as discussed in the text.

WING EQUATIONS

The wing is assumed to be completely immersed in the slipstream, and so only those contributions are given.

Slipstream Velocity

With the assumption that the wing forces are dependent upon the fully developed induced velocity, the slipstream velocity is expressed as

$$V_R = \Omega R \sqrt{(2\lambda_i + v)^2 + \mu^2} \tag{B-40}$$

The slipstream velocity derivatives are

$$\frac{\partial V_R}{\partial u} = \frac{\left[(2\lambda_i + v)\frac{\partial \lambda_i}{\partial \mu} + \mu\right]\sin(i_w + \alpha)}{V_R/\Omega R} + \frac{(2\lambda_i + v)}{V_R/\Omega R}\left(1 + 2\frac{\partial \lambda_i}{\partial v}\right)\cos(i_w + \alpha) \tag{B-41}$$

$$\frac{\partial V_R}{\partial w} = \frac{\left[(2\lambda_i + v)\frac{\partial \lambda_i}{\partial \mu} + \mu\right]}{V_R/\Omega R}\cos(i_w + \alpha) - \frac{(2\lambda_i + v)}{V_R/\Omega R}\left(1 + 2\frac{\partial \lambda_i}{\partial v}\right)\sin(i_w + \alpha) \tag{B-42}$$

Effective Wing Angle of Attack

The effective wing angle of attack in the slipstream may be expressed as

$$\alpha_e = \sin^{-1}\left[\frac{V\sin(i_w + \alpha)}{V_R}\right] \approx \frac{V\sin(i_w + \alpha)}{V_R}$$

The effective angle of attack derivatives are

$$\frac{\partial \alpha_e}{\partial u} = \frac{\sin(i_w + \alpha)}{V_R} - \frac{V\sin(i_w + \alpha)}{V_R}\frac{1}{V_R}\frac{\partial V_R}{\partial u} \tag{B-43}$$

$$\frac{\partial \alpha_e}{\partial w} = \frac{\cos(i_w + \alpha)}{V_R} - \frac{V\sin(i_w + \alpha)}{V_R}\frac{1}{V_R}\frac{\partial V_R}{\partial w} \tag{B-44}$$

where the slipstream velocity derivatives are given by Equations (B-41) and (B-42).

Wing Lift

The wing lift in the slipstream is expressed as

$$L_s = \frac{1}{2} \rho S C_{L,S_{\alpha_e}} V_R^2 (\alpha_o + \alpha_e) \qquad (B-45)$$

where $C_{L,S_{\alpha_e}} = C_{L,S_{\alpha_e}} \left(C_{L_\alpha} , \frac{V}{V_R} , i_w , \alpha \right)$

The derivatives are

$$\frac{\partial L_s}{\partial u} = \frac{1}{2} \rho S C_{L,S_{\alpha_e}} V_R^2 \frac{\partial \alpha_e}{\partial u} + \rho S C_{L,S_{\alpha_e}} (\alpha_o + \alpha_e) V_R \frac{\partial V_R}{\partial u} - \frac{1}{2} \rho S V_R^2 (\alpha_o + \alpha_e) \frac{\partial C_{L,S_{\alpha_e}}}{\partial u} \qquad (B-46)$$

$$\frac{\partial L_s}{\partial w} = \frac{1}{2} \rho S C_{L,S_{\alpha_e}} V_R^2 \frac{\partial \alpha_e}{\partial w} + \frac{1}{2} \rho S C_{L,S_{\alpha_e}} (\alpha_o + \alpha_e) 2V_R \frac{\partial V_R}{\partial w} + \frac{1}{2} \rho S V_R^2 (\alpha_o + \alpha_e) \frac{\partial C_{L,S_{\alpha_e}}}{\partial w} \qquad (B-47)$$

where the effective angle of attack and slipstream velocity derivatives are given above. The lift curve slope derivatives are listed below.

Wing Drag

The wing drag in the slipstream is expressed as:

$$D_s = \frac{1}{2} \rho S V_R^2 \left[C_{D,S_o} + \frac{C_{L,S_{\alpha_e}}^2}{\pi AR} (\alpha_o + \alpha_e)^2 \right] \qquad \text{(B-48)}$$

The derivatives are

$$\frac{\partial D_s}{\partial u} = \rho S \left[C_{D,S_o} + \frac{C_{L,S_{\alpha_e}}^2}{\pi AR} (\alpha_o + \alpha_e)^2 \right] V_R \frac{\partial V_R}{\partial u} +$$

$$\rho S V_R^2 \frac{C_{L,S_{\alpha_e}}^2}{\pi AR} (\alpha_o + \alpha_e) \frac{\partial \alpha_e}{\partial u} + \rho S V_R^2 \frac{(\alpha_o + \alpha_e)}{\pi AR} C_{L_\alpha} \frac{\partial C_{L,S_{\alpha_e}}}{\partial u} \qquad \text{(B-49)}$$

$$\frac{\partial D_s}{\partial w} = \rho S \left[C_{D,S_o} + \frac{C_{L,S_{\alpha_e}}^2}{\pi AR} (\alpha_o + \alpha_e)^2 \right] V_R \frac{\partial V_R}{\partial w} +$$

$$\rho S V_R^2 \frac{C_{L,S_{\alpha_e}}^2}{\pi AR} (\alpha_o + \alpha_e) \frac{\partial \alpha_e}{\partial w} + \rho S V_R^2 \frac{(\alpha_o + \alpha_e)}{\pi AR} C_{L_\alpha} \frac{\partial C_{L,S_{\alpha_e}}}{\partial w} \qquad \text{(B-50)}$$

Wing Lift Curve Slope in Slipstream

As discussed in the text, it is assumed that the wing lift curve slope in the slipstream may be expressed as

$$C_{L,S_{\alpha_e}} = C_{L_\alpha} \left[(1 - K) + K \frac{V \cos(i_w + \alpha - \alpha_e)}{V_R} \right] \qquad \text{(B-51)}$$

$$\frac{\partial C_{L,S_{\alpha_e}}}{\partial u} = C_{L_\alpha} K \left[\frac{\cos(i_w + \alpha - \alpha_e)}{V_R} + \frac{V \sin(i_w + \alpha - \alpha_e)}{V_R} \frac{\partial \alpha_e}{\partial u} - \right.$$

$$\left. \frac{V \cos(i_w + \alpha - \alpha_e)}{V_R^2} \frac{\partial V_R}{\partial u} \right] \qquad \text{(B-52)}$$

$$\frac{\partial C_{L,S_{\alpha_e}}}{\partial w} = C_{L_\alpha} K \left[\frac{-\sin(i_w + \alpha - \alpha_e}{V_R} + \frac{V \sin(i_w + \alpha - \alpha_e)}{V_R} \frac{\partial \alpha_e}{\partial w} - \right.$$

$$\left. \frac{V \cos(i_w + \alpha - \alpha_e)}{V_R^2} \frac{\partial V_R}{\partial w} \right] \qquad \text{(B-53)}$$

TAIL ROTOR EQUATIONS

The calculation of the tail rotor forces is based on the same assumptions as used for the propellers.

$$T_T = \rho \pi R_T^2 (\Omega R)_T^2 \frac{a\sigma_T}{2} \left[\frac{\theta_{0.75R_T}}{3} \left(1 + \frac{3\mu_T^2}{2}\right) - \frac{\lambda_{i_T} + \nu_T}{2} \right] \qquad \text{(B-54)}$$

The nondimensional velocities perpendicular and parallel to the plane of the tail rotor (taken parallel to the fuselage reference here) are

$$\mu_T = \frac{V \cos \alpha}{(\Omega R)_T} \qquad \text{(B-55)}$$

$$\nu_T = \frac{1}{(\Omega R)_T} \left[- V \sin \alpha + \epsilon V + \epsilon_T V + \dot{\theta} \ell_{TR} \right] \qquad \text{(B-56)}$$

The downwash angle, ϵ_T, arises from the lift of the horizontal tail and is expressed as

$$\epsilon_T = \frac{2C_{L_{\alpha_T}}}{\pi AR_T} (\alpha + i_t - \epsilon)$$

The relationship between the derivatives with respect to the velocities used in the stability analysis and the derivatives taken with respect to velocities perpendicular and parallel to the plane of the tail rotor is

$$\frac{\partial T_T}{\partial u} = \frac{\partial T_T}{\partial \mu_T}\frac{\partial \mu_T}{\partial u} + \frac{\partial T_T}{\partial \nu_T}\frac{\partial \nu_T}{\partial u} \tag{B-57}$$

$$\frac{\partial T_T}{\partial w} = \frac{\partial T_T}{\partial \mu_T}\frac{\partial \mu_T}{\partial w} + \frac{\partial T_T}{\partial \nu_T}\frac{\partial \nu_T}{\partial w} \tag{B-58}$$

$$\frac{\partial T_T}{\partial \dot{\theta}} = \frac{\partial T_T}{\partial \mu_T}\frac{\partial \mu_T}{\partial \dot{\theta}} + \frac{\partial T_T}{\partial \nu_T}\frac{\partial \nu_T}{\partial \dot{\theta}} \tag{B-59}$$

where, from Equation (A-54),

$$\frac{\partial T_T}{\partial \mu_T} = \rho \pi R_T^2 (\Omega R)_T^2 \frac{a\sigma_T}{2}\left[\frac{2}{3}\theta_{0.75R_T}\mu_T - \frac{1}{2}\frac{\partial \lambda_{i_T}}{\partial \mu_T}\right] \tag{B-60}$$

$$\frac{\partial T_T}{\partial \nu_T} = \rho \pi R_T^2 (\Omega R)_T^2 \frac{a\sigma_T}{2}\left[-\frac{1}{2}\left(1 + \frac{\partial \lambda_{i_T}}{\partial \nu_T}\right)\right] \tag{B-61}$$

where $\frac{\partial \lambda_{i_T}}{\partial \mu_T}$ and $\frac{\partial \lambda_{i_T}}{\partial \nu_T}$ can be calculated by the same method as that of the propellers.

The transformation equations are

$$\frac{\partial \mu_T}{\partial u} = \frac{1}{(\Omega R)_T} \quad , \quad \frac{\partial \mu_T}{\partial w} = 0 \quad , \quad \frac{\partial \mu_T}{\partial \dot{\theta}} = 0 \tag{B-62}$$

$$\frac{\partial \nu_T}{\partial u} = \frac{1}{(\Omega R)_T}\left[-\sin\alpha + \left(\frac{\partial \epsilon}{\partial V} + \frac{\partial \epsilon_T}{\partial V}\right)V + (\epsilon + \epsilon_T)\right] \tag{B-63}$$

$$\frac{\partial v_T}{\partial w} = \frac{1}{(\Omega R)_T}\left[-1 + V\left(\frac{\partial \epsilon}{\partial w} + \frac{\partial \epsilon_T}{\partial w}\right)\right] \tag{B-64}$$

$$\frac{\partial v_T}{\partial \dot{\theta}} = \frac{1}{(\Omega R)_T}\, \ell_{TR} \tag{B-65}$$

$$\frac{\partial \epsilon_T}{\partial u} = \frac{-2C_{L_{\alpha_T}}}{\pi\, AR_T}\frac{\partial \epsilon}{\partial u} \tag{B-66}$$

$$\frac{\partial \epsilon_T}{\partial w} = \frac{-2C_{L_{\alpha_T}}}{\pi\, AR_T}\left(\frac{1}{V} - \frac{\partial \epsilon}{\partial w}\right) \tag{B-67}$$

The inplane force of the tail rotor and the pitching moment of the tail rotor about its hub are neglected.

HORIZONTAL TAIL EQUATIONS

The horizontal tail lift is expressed as

$$L_T = \tfrac{1}{2}\,\rho\, V^2\, S_T\, C_{L_{\alpha_T}}\left(\alpha + i_t - \epsilon + \frac{\dot{\theta}\ell_{HT}}{V}\right) \tag{B-68}$$

The derivatives of this expression are

$$\frac{\partial L_T}{\partial u} = \rho\, S_T\, C_{L_{\alpha_T}}\,(\alpha + i_t - \epsilon)\, V - \tfrac{1}{2}\,\rho\, V^2\, S_T\, C_{L_{\alpha_T}}\frac{\partial \epsilon}{\partial u} \tag{B-69}$$

$$\frac{\partial L_T}{\partial w} = \tfrac{1}{2}\,\rho\, V^2\, S_T\, C_{L_{\alpha_T}}\left(\frac{1}{V} - \frac{\partial \epsilon}{\partial w}\right) \tag{B-70}$$

$$\frac{\partial L_T}{\partial \dot{\theta}} = \tfrac{1}{2}\,\rho\, V\, S_T\, C_{L_{\alpha_T}}\,\ell_{HT} \tag{B-71}$$

where

$$\epsilon = \frac{2C_{L,S_{\alpha_e}}}{\pi\, AR}\left(1 - M_T^2\right)\frac{V_R}{V}\left(\alpha_o + \alpha_e\right) \tag{B-72}$$

$$\frac{\partial \epsilon}{\partial u} = \frac{2C_{L,S_{\alpha_e}}}{\pi\, AR}\left(1 - M_T^2\right)\left[\frac{V_R}{V}\frac{\partial \alpha_e}{\partial u} + \frac{\left(\frac{\partial V_R}{\partial u}V - V_R\right)}{V^2}\left(\alpha_o + \alpha_e\right)\right] \tag{B-73}$$

$$\frac{\partial \epsilon}{\partial w} = \frac{2C_{L,S_{\alpha_e}}}{\pi\, AR}\left(1 - M_T^2\right)\left[\frac{V_R}{V}\frac{\partial \alpha_e}{\partial w} + \frac{1}{V}\frac{\partial V_R}{\partial V}\right] \tag{B-74}$$

The drag of the horizontal tail is neglected.

Unclassified

Security Classification

DOCUMENT CONTROL DATA - R&D

(Security classification of title, body of abstract and indexing annotation must be entered when the overall report is classified)

1 ORIGINATING ACTIVITY (Corporate author) Department of Aerospace and Mechanical Sciences Princeton University	2a REPORT SECURITY CLASSIFICATION Unclassified 2b GROUP

3 REPORT TITLE

An Analytical Study of Factors Influencing the Longitudinal Stability of Tilt-Wing VTOL Aircraft

4 DESCRIPTIVE NOTES (Type of report and inclusive dates)

5 AUTHOR(S) (Last name, first name, initial)

Beppu, G. and Curtiss, H. C., Jr.

6 REPORT DATE	7a TOTAL NO. OF PAGES	7b NO OF REFS
July 1966	105	22

8a CONTRACT OR GRANT NO DA 44-177-AMC-8(T) b. PROJECT NO. 1P125901A14233 c. d	9a ORIGINATOR'S REPORT NUMBER(S) USAAVLABS Technical Report 66-53 9b OTHER REPORT NO(S) (Any other numbers that may be assigned this report) Princeton Univ. Aero. & Mech. Sci. Report No. 756

10 AVAILABILITY/LIMITATION NOTICES

Distribution of this document is unlimited.

11 SUPPLEMENTARY NOTES	12 SPONSORING MILITARY ACTIVITY
	U. S. Army Aviation Materiel Laboratories Fort Eustis, Virginia

13 ABSTRACT

An analytical method for predicting the stability characteristics of tilt-wing VTOL aircraft in the transition speed range is presented. Sample calculations based on an assumed tilt-wing VTOL transport configuration of the XC-142A class with double-slotted flaps are given.

Particular emphasis is placed on the sensitivity of the results to various assumptions made in the analysis. The contributions of the various aircraft components and the aerodynamic interactions of the components to the stability derivatives are discussed, as well as the changes in the characteristic modes of motion of the vehicle that result from variations in the stability derivatives. The trim conditions of the vehicle are shown to be quite sensitive to the prediction of the flap characteristics.

A limited comparison of the calculated results with experimental data obtained from a dynamic model of the XC-142A, which is somewhat dissimilar from the assumed configuration, is presented. This comparison indicates that the trends of the stability derivatives are correctly predicted. The agreement between theory and experiment is good in hovering; however, as the wing incidence is reduced, the difference between theory and experiment becomes quite large.

DD FORM 1 JAN 64 1473

Unclassified

Security Classification

Unclassified

Security Classification

14 KEY WORDS	LINK A		LINK B		LINK C	
	ROLE	WT	ROLE	WT	ROLE	WT
stability, longitudinal						
airplanes, VTOL - stability						
airplanes, tilt-wing						
airplanes (XC-142A)						
trim						

INSTRUCTIONS

1. ORIGINATING ACTIVITY: Enter the name and address of the contractor, subcontractor, grantee, Department of Defense activity or other organization *(corporate author)* issuing the report.

2a. REPORT SECURITY CLASSIFICATION: Enter the overall security classification of the report. Indicate whether "Restricted Data" is included. Marking is to be in accordance with appropriate security regulations.

2b. GROUP: Automatic downgrading is specified in DoD Directive 5200.10 and Armed Forces Industrial Manual. Enter the group number. Also, when applicable, show that optional markings have been used for Group 3 and Group 4 as authorized.

3. REPORT TITLE: Enter the complete report title in all capital letters. Titles in all cases should be unclassified. If a meaningful title cannot be selected without classification, show title classification in all capitals in parenthesis immediately following the title.

4. DESCRIPTIVE NOTES: If appropriate, enter the type of report, e.g., interim, progress, summary, annual, or final. Give the inclusive dates when a specific reporting period is covered.

5. AUTHOR(S): Enter the name(s) of author(s) as shown on or in the report. Enter last name, first name, middle initial. If military, show rank and branch of service. The name of the principal author is an absolute minimum requirement.

6. REPORT DATE: Enter the date of the report as day, month, year; or month, year. If more than one date appears on the report, use date of publication.

7a. TOTAL NUMBER OF PAGES: The total page count should follow normal pagination procedures, i.e., enter the number of pages containing information.

7b. NUMBER OF REFERENCES: Enter the total number of references cited in the report.

8a. CONTRACT OR GRANT NUMBER: If appropriate, enter the applicable number of the contract or grant under which the report was written.

8b, 8c, & 8d. PROJECT NUMBER: Enter the appropriate military department identification, such as project number, subproject number, system numbers, task number, etc.

9a. ORIGINATOR'S REPORT NUMBER(S): Enter the official report number by which the document will be identified and controlled by the originating activity. This number must be unique to this report.

9b. OTHER REPORT NUMBER(S): If the report has been assigned any other report numbers *(either by the originator or by the sponsor)*, also enter this number(s).

10. AVAILABILITY/LIMITATION NOTICES: Enter any limitations on further dissemination of the report, other than those imposed by security classification, using standard statements such as:

(1) "Qualified requesters may obtain copies of this report from DDC."

(2) "Foreign announcement and dissemination of this report by DDC is not authorized."

(3) "U. S. Government agencies may obtain copies of this report directly from DDC. Other qualified DDC users shall request through _____."

(4) "U. S. military agencies may obtain copies of this report directly from DDC. Other qualified users shall request through _____."

(5) "All distribution of this report is controlled. Qualified DDC users shall request through _____."

If the report has been furnished to the Office of Technical Services, Department of Commerce, for sale to the public, indicate this fact and enter the price, if known.

11. SUPPLEMENTARY NOTES: Use for additional explanatory notes.

12. SPONSORING MILITARY ACTIVITY: Enter the name of the departmental project office or laboratory sponsoring *(paying for)* the research and development. Include address.

13. ABSTRACT: Enter an abstract giving a brief and factual summary of the document indicative of the report, even though it may also appear elsewhere in the body of the technical report. If additional space is required, a continuation sheet shall be attached.

It is highly desirable that the abstract of classified reports be unclassified. Each paragraph of the abstract shall end with an indication of the military security classification of the information in the paragraph, represented as *(TS)*, *(S)*, *(C)*, or *(U)*.

There is no limitation on the length of the abstract. However, the suggested length is from 150 to 225 words.

14. KEY WORDS: Key words are technically meaningful terms or short phrases that characterize a report and may be used as index entries for cataloging the report. Key words must be selected so that no security classification is required. Identifiers, such as equipment model designation, trade name, military project code name, geographic location, may be used as key words but will be followed by an indication of technical context. The assignment of links, rules, and weights is optional.

Unclassified

Security Classification

49 16-66